Creld1 controls T cell homeostasis in mouse and human

Dissertation

zur

Erlangung des Doktorgrades (Dr. rer. nat.)

der

Mathematisch-Naturwissenschaftlichen Fakultät

der

Rheinischen Friedrich-Wilhelms-Universität Bonn

vorgelegt von

Lorenzo Bonaguro

aus

Thiene (Italien)

Bonn (10, 2019)

Angefertigt mit Genehmigung der Mathematisch-Naturwissenschaftliche Fakultät
der Rheinischen Friedrich-Wilhelms-Universität Bonn

Erstgutachter: Prof. Dr. Joachim Schultze
Zweitgutachter: Dr. Marc Beyer

Tag der Promotion: 27.03.2020
Erscheinungsjahr: 2020

I Index

…meravigliato da luoghi meno comuni e più feroci

Amico fragile – Fabrizio de André

II Abstract

Cysteine-rich with EGF-like domains 1 (Creld1) was recently found to be fundamental for the VEGF-mediated activation of NFATc1 during heart development. Creld1 complete KO in mice is lethal due to developmental problems during heart formation. Due to the broad expression of Creld1 across almost all cell types and tissues, I wanted to identify additional roles this protein might have in other cellular contexts. In this thesis, I could show how Creld1 functions as a modulator in both the canonical and non-canonical Wnt signalling pathway using an overexpression cell culture system and a conditional KO mouse model for Creld1 in T lymphocytes (*CD4^{Cre}; Creld1$^{flox/flox}$*). Furthermore, I could show how Creld1 acts as a plasma membrane protein through its cytosol-facing C-terminus, physically interacting with Wnt signalling components, upstream of β-Catenin and NFAT activation but downstream of Wnt binding to the Frizzled receptor. These data were confirmed in Creld1 KO CD4$^+$ T cells where a general downregulation of both canonical and non-canonical Wnt signalling was observed in homeostasis. Both, *ex vivo* and *in vivo*, Creld1 promote viability in CD4$^+$ T cells showing, in a conditional KO model, a dramatic increase of apoptotic cell death *ex vivo* and a marked reduction of total cell number in one-year-old animals *in vivo*. Furthermore, Creld1 depletion in CD4$^+$ T cells also affects main T cell effector functions showing an imbalanced activation kinetic and a differential proliferative capacity in accordance with current models of Wnt signalling as modulators of CD4$^+$ T cell homeostasis. Transcriptomic analysis of Creld1-deficient CD4$^+$ T cells further confirmed the cell-intrinsic defect in cell homeostasis and Wnt signalling activation and allowed the definition of a transcriptional footprint of Creld1 in T cells. This transcriptional signature was then shown to be conserved in human CD4$^+$ T cells when individual with low *CRELD1* expression were compared to high expressing ones showing a conserved role of *CRELD1* in human CD4$^+$ T cells. CRELD1^{low} transcriptional analysis also recapitulated the main phenotype found in the murine mouse model with a general down-regulation of Wnt signalling hallmark genes and an obvious apoptotic signature. The CRELD1-dependent transcriptional regulation was then shown to be conserved also in other immune

cells and even visible in total PBMCs. Interestingly, I correlated changes in CRELD1 expression to the process of immunosenescence in accordance with the phenotype of one-year-old mice. Taken together, this work suggests Creld1 as an important regulator of the Wnt signalling pathway in both mouse and human preventing the process of senescence of immune cells and highlighting this protein as a possible target in the treatment of age-related diseases.

III List of abbreviations

AMP	anti-microbial peptide
APC	antigen presenting cell
AVSD	atria-ventricular septal defect
BCA	bicinchoninic acid
Bcl	B cell lymphoma
BCR	B cell receptor
BSA	bovine serum albumin
CAN	chronic allograph nephropathy
cbEGF	calcium binding epidermal growth factor
CD	cluster of differentiation
CFP	cyan fluorescent protein
CFSE	carboxyfluorescein succinimidyl ester
CK	casein kinase
CLP	common lymphoid progenitor
CMP	common myeloid progenitor
COPD	chronic obstructive pulmonary disease
CsA	cyclosporin A
DAG	diacylglycerol
DAMP	damage-associated molecular pattern
DC	dendritic cell
DN	double negative
DNA	deoxyribonucleic acid
DP	double positive
ECAR	extracellular acidification rate
ECL	substrate for enhanced chemiluminescence
EGF	epidermal growth factor

ER	endoplasmic reticulum
FACS	fluorescence-activated cell sorting
FC	flow cytometry
FGF	fibroblast growth factor
FPP	fluorescence protease protection
GF	growth factor
GFP	green fluorescent protein
GMP	granulocytes-monocytes progenitor
GSEA	gene set enrichment analysis
GSK	glycogen synthase kinase
HRP	horseradish peroxidase
HSC	hematopoietic stem cells
IFNγ	interferon gamma
Ig	immunoglobulin
IL	interleukin
ILC	innate lymphoid cells
IP3	inositol triphosphate
JIA	juvenile idiopathic arthritis
KO	knock-out
LB	lysogeny broth
LEF	lymphoid enhancer-binding factor
LRP	low density lipoprotein receptor-related protein
MACS	magnet-activated cell sorting
MEP	megakaryocytes-erythrocytes progenitor
MHCI/II	major histocompatibility complex class I/II
NFAT	nuclear factor of activated T cells
NK	natural killer cells
nTreg	natural regulatory T cell

PAMP	pathogen-associated molecular pattern
PCR	polymerase chain reaction
PDI	protein disulphide activity
PDL	programmed death ligand
PFA	paraformaldehyde
PLC	phospholipases C
PMA	phorbol 12-myristate 13-acetate
PMSF	phenylmethylsulfonylfluoride
PRR	pattern recognition receptor
PRR	pattern recognition receptor
PVDF	polyvinylidene fluoride
RBCLB	red blood cell lysis buffer
RFP	red fluorescent protein
RIPA	radioimmunoprecipitation assay buffer
RNA	ribonucleic acid
RT	room temperature
SDS	sodium dodecyl-sulphate
SERCA	sarco/endoplasmic reticulum Ca2+-ATPase
SP	single positive
TCF	T cell factor
TCR	T cell receptor
TGF	transforming growth factor
Th	T helper cell
TLR	toll-like receptor
Trm	Tissue-resident memory T cell
VEGF	vascular-endothelial growth factor
VEGFR	vascular-endothelial growth factor receptor
WHO	world health organization

WT	wild-type
YFP	yellow fluorescent protein
β-ME	β-mercapto ethanol

IV Index of Figures

V Index of tables

VI Index of supplementary schematics

1 Introduction

1.1 The immune system

Humans, like all vertebrates, are constantly exposed to external microorganisms which can potentially cause disease, nevertheless, most of the time we are able to efficiently clear the infection and restore normal homeostasis. This vital function is mainly accomplished by the immune system, a complex network of cellular, chemical and mechanical mediators evolved and adapted to protect the organism from every challenge that can jeopardise its integrity and function. Unlike other organ systems in the human body, the immune system must have the potential to be activated when needed and consequently inactivated when the possible threat has been resolved (Murphy, K. & Weaver, 2016). The implication of this mechanism is that it must be kept under very strict control in order to maintain this balance between activation and unresponsiveness. Perturbations of this mechanism have pathological consequences for example an excessive or uncontrolled response can lead to autoimmunity or anaphylaxis whereas silencing or insufficient response is associated with cancer or chronic infection (Eberl, 2016; Hu, Ott and Wu, 2018).

In defence against potentially pathogenic agents not only specialized cells of the immune system take part in the protection of the organism. In fact, the first layer of defence is composed of mechanical barriers such as the epithelial cells of the skin or the endothelial mucous membranes of the respiratory tract or gastrointestinal system. These layers act as an initial mechanical protection that prevents the intrusion of microorganisms (Murphy, K. & Weaver, 2016).

Most pathogens are normally blocked by this first layer of defence, but when infection does occur, specialized cells of the immune system and their chemical mediators are promptly activated. This type of response can in turn be divided into innate immunity; a rapid response but with limited specificity towards pathogens (Buchmann, 2014; Gasteiger *et al.*, 2017) and adaptive immunity, normally initiated after the initial innate response and characterized by a

greater specificity for the pathogens as well allowing for the development of long-term immune memory (Murphy, K. & Weaver, 2016).

Most cellular components of the immune system derive from a common pool of pluripotent stem cells in the bone marrow named hematopoietic stem cells (HSCs) (Laurenti and Göttgens, 2018). Cutting-edge research in the early 2000s described HSCs as a homogeneous population able to first differentiate into the common lymphoid- and myeloid-progenitors (CLP and CMP respectively) loosing self-renewal and differentiation capabilities (Miyamoto *et al.*, 2002). CLP in the bone marrow and in the thymus respectively will give raise to B and T cells, the main component of the adaptive immune response (Rothenberg, 2014; Jensen, Strid and Sigvardsson, 2016); CLP can also differentiate into NK and ILCs (Geiger and Sun, 2016; Zook and Kee, 2016), which are lymphoid cell components of the innate immune system. CMPs, the myeloid progenitors, will further differentiate into MEP, the progenitors for erythrocytes and megakaryocytes and GMPs that will further differentiate into monocytes, eosinophils, neutrophils and DCs (Görgens *et al.*, 2013; Weiskopf *et al.*, 2016). The last 15 years of immunological research highly focused on clarifying these processes in more detail, with the development of single-cell transcriptomic techniques greatly advancing our knowledge on how the process of differentiation does not rely on discrete states of differentiation but instead can be described as a continuum differentiation processes from the HSC progenitors following several possible differentiation trajectories (Zhang *et al.*, 2018; Bassler *et al.*, 2019).

1.1.1 *The innate immune system*

The innate immune system is the most ancient component of the immune system and can be found in all vertebrates (Gasteiger *et al.*, 2017). The innate response is initiated by specialized myeloid and lymphoid cells. Those cells express specific receptors generally referred to as pattern recognition receptors (PRRs). One example of this class of molecules are the toll-like receptors (TLRs) able to recognize specific molecular patterns, distinctive of potentially harmful intruders such as pathogen- or danger-associated molecular patterns (PAMPs or

DAMPs) (Takeuchi and Akira, 2010). The activation of these PRRs by the binding of specific ligands leads to the activation of the innate immune response. This type of response takes place quickly and leads to either cell-dependent mechanisms (such as phagocytosis and cytotoxicity) or the secretion of important soluble mediators, such as antimicrobial peptides (AMPs), complement components as well as cytokines and chemokines (Takeuchi and Akira, 2010).

The main mediators of the innate immune response are mononuclear phagocytes, neutrophils, ILCs and NK cells, macrophages and dendritic cells (Murphy, K. & Weaver, 2016). Those different cell types are able to use different strategies to eliminate pathogens, phagocytes can directly engulf and degrade the pathogens by the recognition of specific PAMPs on the surface (phagocytosis), NK cells on the other hand can recognize specific pathogen-associated patterns (PAMPs) and release cytotoxic granules leading to the death of pathogen- or virus-infected cells. Another fundamental component of the innate response are professional antigen presenting cells (APCs) such as dendritic cells (DCs); these cells have phagocytic capabilities but more importantly, they are able to present small pathogen-derived peptides by MHC molecules on their cell surface and migrate to the secondary lymphoid organs (e.g. spleen and peripheral lymph nodes) where they can activate the cross talk between the innate and the adaptive immune response (Murphy, K. & Weaver, 2016).

The innate immune response is traditionally defined as a quick immunological response with a restricted spectrum of specificities; it is also traditionally described as lacking memory features, with memory mainly being associated with the adaptive immune system. However, this dogma has recently been challenged with the introduction of the concept of “trained immunity” in the myeloid compartment (Arts, Joosten and Netea, 2016; Netea *et al.*, 2016; Netea and van der Meer, 2017) and the potential to acquire memory for natural killer (NK) (O’Sullivan, Sun and Lanier, 2015) and innate lymphoid cells (ILCs) (O’Sullivan, Sun and Lanier, 2015).

1.1.2 *The adaptive immune system*

The adaptive immune response is triggered by the presentation of antigen-specific peptides on the surface of antigen presenting cells to T cells (Murphy, K. & Weaver, 2016). This type of response is slower than the innate response but has the ability to both be highly specific against a certain pathogen and lead to a lifelong immunological memory. B and T cells are the main components of the adaptive immune system generally referred to as lymphocytes. Both T and B cells acquire their high specificity against specific pathogens by randomised rearrangement of a genomic locus coding for the T or B cell receptors (TCR, BCR, respectively) (Murphy, K. & Weaver, 2016). Evolutionary highly controlled, this recombination process can lead to the generation of T or B cell clones (defined as expressing the same T or B cell receptor). Each clone will be able to bind to a specific exogenous peptide bound to MHC I or II molecules; nevertheless, stochastically some TCR or BCR clones will be able to recognize self-antigens. These self-reactive B or T cell clones must either be removed or tolerised to avoid anti-self immune responses (O'Sullivan, Sun and Lanier, 2015). The bone marrow and the thymus are the main organs of maturation of B and T cell respectively in which a tight control of the correct rearrangement of the B or T cell receptor takes place (Murphy, K. & Weaver, 2016). During maturation in the thymus, T cells also differentiate into $CD4^+$ or $CD8^+$. These two cell types can recognize different MHC molecules and have a different effector function. $CD4^+$ T cells or T helper cells have the crucial function to orchestrate the cross-activation of several cell types in response to immune stimulation and activation. $CD8^+$ T cells, or cytotoxic T cells, mainly have the role of recognizing infected cells and release cytotoxic granules as described previously for NK cells (Murphy, K. & Weaver, 2016).

B cells express the BCR on the surface of the plasma membrane. This receptor can be secreted in the form of antibodies upon B cell activation and class-switching. Antibodies are highly specialised molecules and are key components of the humoral immune response. Antibodies are generally able to recognize pathogens with high specificity and affinity, binding the cell surface of pathogens, allow them to be recognised by other components of the immune

system (Murphy, K. & Weaver, 2016). For example, antibodies bound to specific pathogens can initiate the process of opsonisation mediated by professional phagocytes.

A key feature of the adaptive immune system, generally used to distinguish it from the adaptive response, is the ability of both B and T cells to develop a long-term memory (De Silva and Klein, 2015; Kurosaki, Kometani and Ise, 2015; Nutt *et al.*, 2015). During an infection, specific T or B cell clones will expand and at least some of these cells will differentiate into memory cells; in case of a re-exposure to the same pathogen, these memory cells can trigger an adaptive immune response much faster than during the first exposure normally avoiding any pathological manifestation for the host (Murphy, K. & Weaver, 2016).

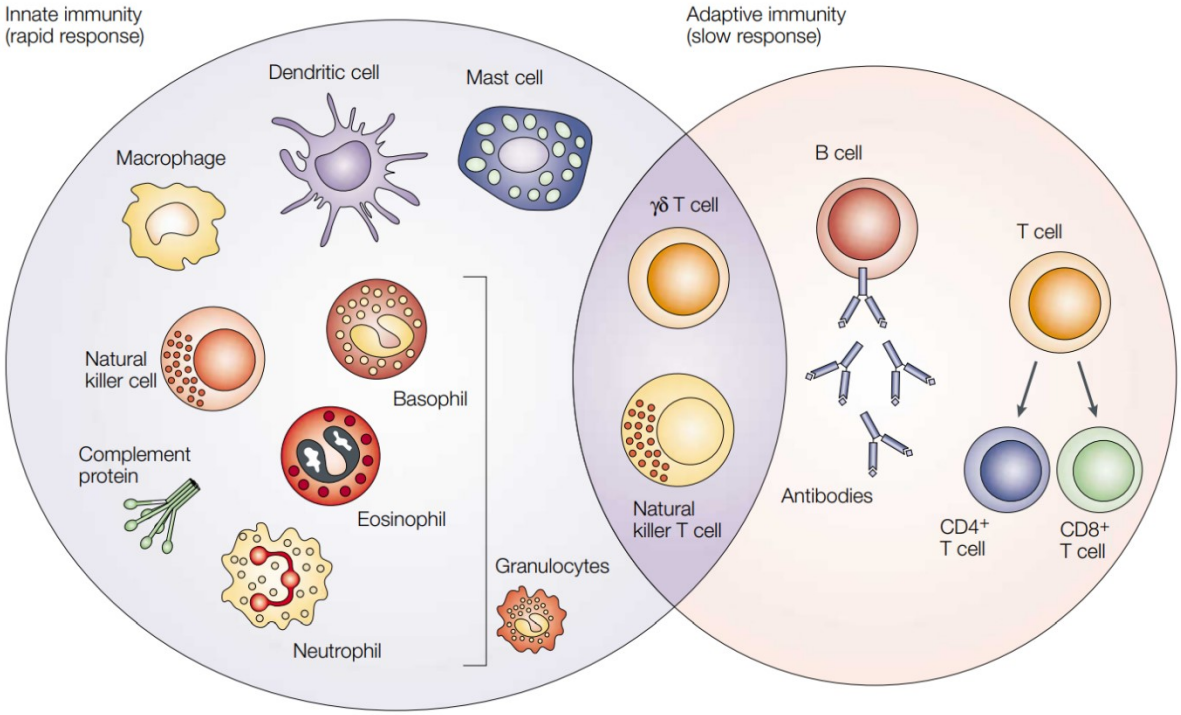

Figure 1.1 The innate and adaptive immune system

The innate immune system is the first line of defence of the immune system, it is composed of soluble mediators (complement proteins) and several cellular components classified as granulocytes (basophils, neutrophils and eosinophils), monocytes, macrophages, dendritic cells mast cells and ILCs. The innate immune system provides a quick and aspecific response to pathogens; it can also activate the adaptive immune system. The adaptive response is slower but provides high specificity and cellular memory, composed of B and T cells ($CD4^+$ and $CD8^+$), γδ T cells and NK T cells. The latter have cytotoxic function and provide an interface between innate and adaptive immunity (Figure taken from Dranoff, 2004).

1.1.3 *T cell development in the thymus*

As described above, $CD4^+$ and $CD8^+$ T cells have a helper and cytotoxic function respectively in the adaptive immune response. Both cell types arise from a common lymphoid progenitor developed in the bone marrow and consequently migrate to the thymus (Germain, 2002). The expression at the cell surface of either CD4 or CD8 is used to classify T cells into helper and cytotoxic and gives these cells the specificity for the binding to MHC class II and I molecules, respectively (Murphy, K. & Weaver, 2016). These two surface markers are also used to monitor the developmental stages of lymphocytes in the thymus.

CLP precursor cells generated in the bone marrow from a pool of HSCs migrate via the blood stream to the thymus. Upon entering the thymus, CLPs are committed to differentiate into T cells, losing the capabilities to differentiate into B or NK cells (Teh *et al.*, 1988; Baldwin *et al.*, 1999; Pui *et al.*, 1999) (**fig 1.2**). These cells are now defined as double negative T cells due to the lack of expression of either CD4 or CD8. These cells can then proceed through four developmental stages characterized by the expression of the surface markers CD25 and CD44 named DN-1 to DN-4 (DN1, $CD44^+CD25^-$; DN2, $CD44^+CD25^+$; DN3, $CD44^-CD25^+$; and DN4, $CD44^-CD25^-$) (Godfrey *et al.*, 1993). At this stage, the CMP progenitors can still give rise to both γδ T cells and αβ T cells (Robey and Fowlkes, 1994), it is only at the DN-3 stage that T cells recombine the β-TCR chain which forms an important component of both CD4 and CD8 T cells. A functional rearrangement of the TCR and a correct assembly with the CD3 complex is essential for adequate differentiation of T cells (Germain, 2002). During the DN-3 and DN-4 differentiation state, the T cell precursors rearrange also the α chain of the TCR and start expressing both CD8 and CD4 at the cellular surface (Robey and Fowlkes, 1994; Germain, 2002). These cells are now named double positive and generally compose the majority of thymocytes in both human and mice. Double positive T cells with newly-arranged TCRs not able to bind MHC complexes with sufficient affinity will not receive fundamental survival signalling leading to quick apoptosis of the cells (Merkenschlager *et al.*, 1997; Zerrahn, Held and Raulet, 1997). Due to the low probability of the TCR locus to rearrange into

a functional receptor, only 5-10% of the DP thymocytes will be able to bind MHC complexes. Within those cells, a small fraction can bind MHC complexes loaded with self-peptides with high affinity. These TCR clones need to be removed by apoptosis to avoid the generation of autoreactive circulating T cells (negative selection (Klein *et al.*, 2014; Takaba and Takayanagi, 2017). The small pool of cells with a successful TCR rearrangement that do bind with moderate affinity to the self-presenting MHC complex will now be committed to become $CD4^+$ or $CD8^+$ T cells based on the level of affinity to either MHC II or I molecules, respectively (positive selection) (Klein *et al.*, 2014; Takaba and Takayanagi, 2017). Nevertheless, the commitment of DP cells to become CD4 or CD8 single positive cells is still a matter of debate today (Germain, 2002; Krueger, Ziętara and Łyszkiewicz, 2017). Many molecular pathways have been identified to play a role in this process of successful maturation of thymocytes such as the NFAT (Nuclear factor of activated T cells) pathway, downstream of TCR engagement and the Wnt signalling pathway for the correct commitment and exclusive repression of the CD4 or CD8 transcriptional program (Macian, 2005; Kovalovsky *et al.*, 2009; Naito *et al.*, 2011; Ma *et al.*, 2012).

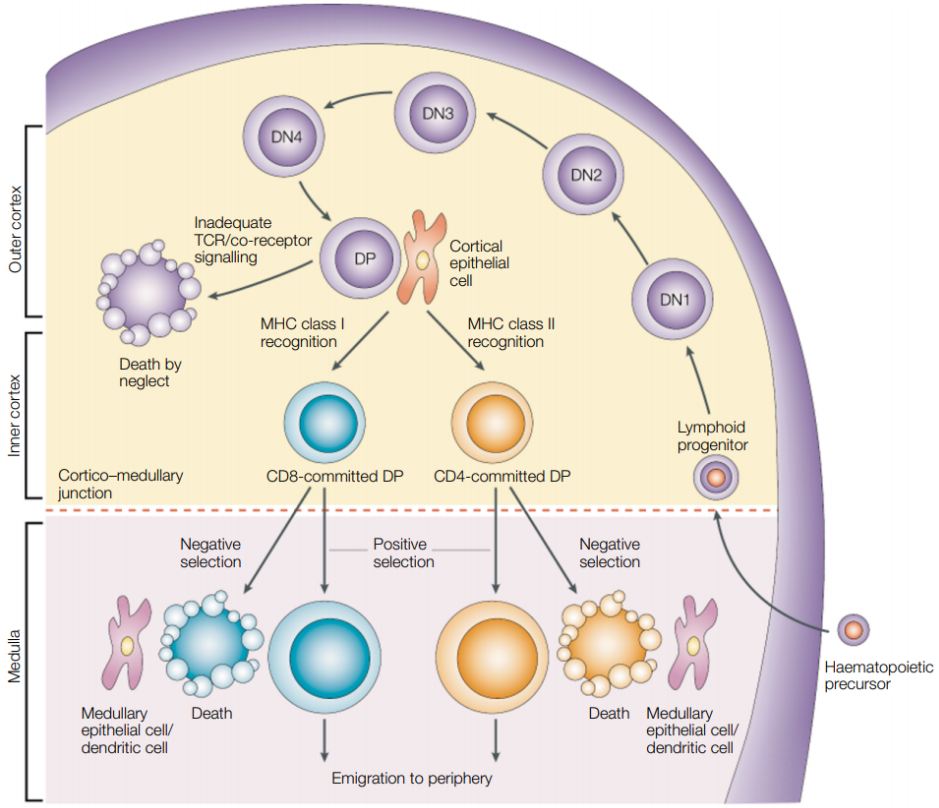

Figure 1.2 T cell development in the thymus is a tightly controlled process

Common lymphoid progenitors migrate from the bone marrow to the thymus where they are then committed to develop into T cells. The lymphoid progenitors enter the cortex where they go through four different double negative stages of development (DN1, CD44$^+$CD25$^-$; DN2, CD44$^+$CD25$^+$; DN3, CD44$^-$CD25$^+$; and DN4, CD44$^-$CD25$^-$). During this process, the rearrangement of the TCR β-chain takes place. Still in the cortex, DN4 cells rearrange the TCR α-chain and express both CD4 and CD8 (DP) whereas T cell clones are positively selected to be able to bind MHCII or I with moderate affinity and acquire a lineage commitment towards CD4 or CD8 T cells. Committed cells then migrate to the medulla where they face self-antigen loaded dendritic cells. Only TCR clones not able to bind this MHC complex will be selected and migrate to the periphery as single positive T cells. (Figure taken from Germain, 2002).

1.1.4 *CD4$^+$ T cell function and current mouse models*

CD4$^+$ T cells have a crucial role orchestrating the activation and the resolution of the adaptive immune response. These cells have a critical role, for example in inducing antibody production by B cells, or enhancing antimicrobial activity by macrophages recruiting granulocytes to the sites of infection. CD4$^+$ T cells can also orchestrate the suppression of the immune response by releasing anti-inflammatory mediators, avoiding excessive inflammation and tissue damage (Zhu and Paul, 2008).

Thymic CD4$^+$ T cells are in a so-called “naïve state” and migrate to the secondary lymphoid organs where a pool of cells is constantly maintained by turn-over from the thymus (Bourgeois

et al., 2008; Zhu and Paul, 2008). In the periphery, $CD4^+$ T cells are maintained without antigen stimulation by tonic TCR signalling (the engagement of the TCR with a self-presenting MHC complex) and homeostatic stimulation by IL-7 and IL-15 (Wiehagen *et al.*, 2010; Sprent and Surh, 2011). Several other survival TCR-independent mechanisms are also suggested to be active in these cells leading to a complex network of basal survival signals to the cells. Albeit, these additional pathways are not well understood.

Antigen unexperienced $CD4^+$ T cells are generally referred to as naïve, defined as $CD62L^+$, $CD25^-$ and $CD44^-$ making up the majority of the T cell population in secondary lymphoid organs in young healthy mice. The activation of naïve $CD4^+$ T cells by non-self-peptides loaded onto MHC class II molecules presented on the surface of APCs normally leads to the clonal expansion of a specific T cell clone and the differentiation of these cells into a specific functional subset (Zhu and Paul, 2008). Effector T cell subsets are defined by the spectrum of cytokines they produce and are specialized in the protection against a specific class of pathogens (Kaplan, Hufford and Olson, 2015). Effector T helper cells are divided into Th1, Th2, Th17 and iTregs based on the production of IFNγ, IL-4, IL-17 or IL-10, respectively. These subtypes are also characterized by the expression of hallmark transcription factors and therefore have a distinctive transcriptional program (Zhu and Paul, 2008; Kaplan, Hufford and Olson, 2015). This differential activation of naïve T cells upon activation allows an immune response that is tailored against the class of pathogen causing the infection. For example, Th1 cells are mostly involved in the defence against intracellular pathogens whereas Th2 cells are involved in the protection against multicellular parasites (Murphy, K. & Weaver, 2016). The different differentiation processes itself were also found to be mediated by a combination of cytokines, microenvironment and quality of the TCR stimulation leading to the activation of a specific transcriptional program. Once the infection is resolved, a pool of the activated T cells can acquire a memory phenotype and these cells have been shown to reside in secondary lymphoid organs and recirculate in the blood and tissues (Zhu and Paul, 2008; Murphy, K. & Weaver, 2016). Memory T cells can be distinguished from naïve $CD4^+$ cells by the expression of CD44 and the low expression of CD62L (Gerberick *et al.*, 1997). These cells can be quickly

re-activated and have a pre-defined set of cytokines that will be produced upon activation. Furthermore, it was recently shown that a small fraction of effector cells can differentiate into tissue-resident memory cells (Trm) (Mami-Chouaib and Tartour, 2019). These cells show an unusual behaviour since they do not travel back to the lymphoid organs and are instead confined to a single tissue. Consequently, these cells can activate an even quicker response to a re-exposure of a previously encountered pathogen. The single exception to this peripheral functional specialization of the CD4⁺ T cells are natural regulatory T cells (nTregs). Those cells acquire their characteristic immune modulatory function already during thymic development (Zhu and Paul, 2008) (**fig 1.3**).

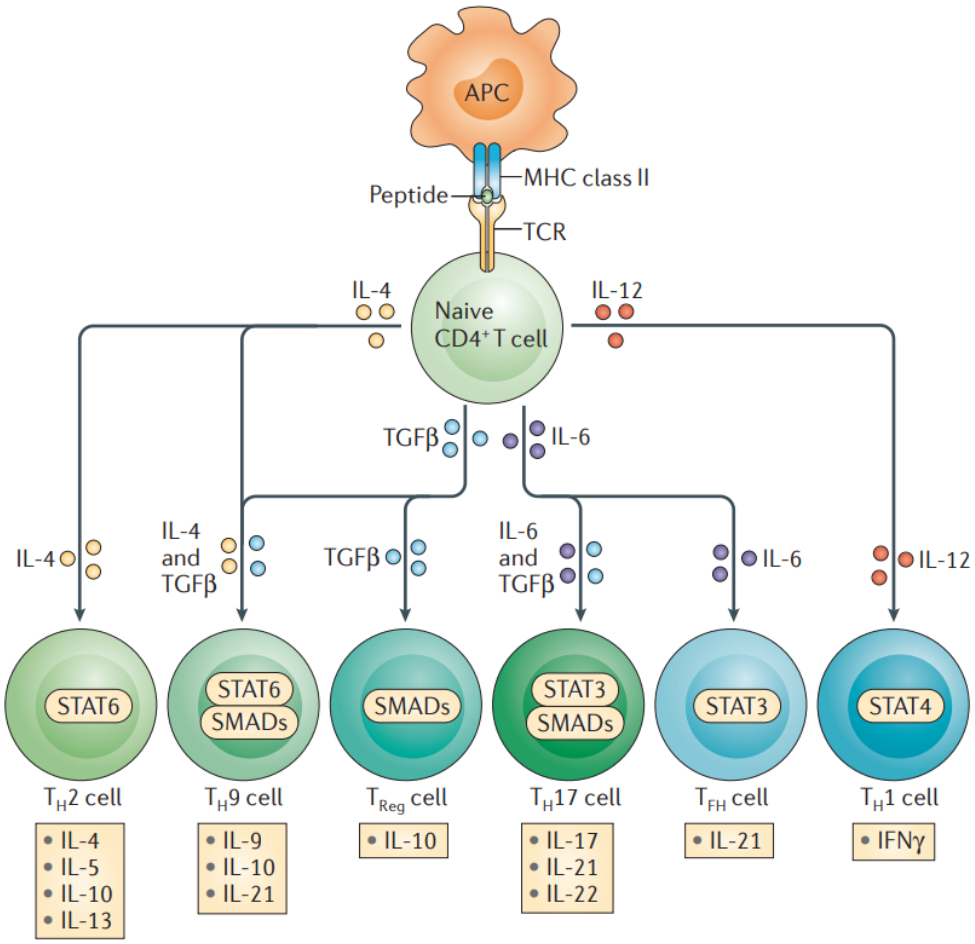

Figure 1.3 CD4⁺ T cell differentiation is mediated by cytokines in the environment

Even though the strength of TCR engagement with the MHC-II on APCs and the quality of the co-stimulation were shown to play a role in the differentiation process of naïve CD4+ T cells; the mix of cytokines in the microenvironment plays a key role in this process. As shown, different cytokines can activate different intracellular pathways and transcriptional programs leading to the generation of functionally differentiated effector CD4⁺ T cell subsets. Each T cell subtype is then characterized by the pattern of cytokines secreted in response to stimulation (Figure taken from Kaplan, Hufford and Olson, 2015).

Due to the central role of helper T cells in the orchestration of the appropriate immune response, the study of $CD4^+$ T cell biology has gained considerable attention in the last 20 years. To understand $CD4^+$ T cell molecular biology, several strategies have been developed. Numerous strategies have been used to investigate the role of specific genes in T cell biology, the most common technique is the use of the Cre/LoxP system to generate conditional KO models. Specific Cre lines can be used at different stages of thymic development for example Lck-Cre or CD4-Cre target $CD4^+$ and $CD8^+$ T cells during early and late thymic development respectively. In these mouse models, a specific gene (genetically engineered to include loxP sites to be recombined by a Cre recombinase enzyme) can be deleted in CD4 expressing cells, mainly T cells, to study its function. With the recent advent of inducible Cre lines (CD4-Cre/ERT2), the recombination can be induced by pharmacological treatment, allowing the study and the function of a specific gene in the periphery and excluding any developmental effect in the thymus.

1.1.5 *Pathological consequences of T cell dysregulation*

Molecular processes of T cell activation and repression are normally kept under tight control in the organism, since variation of this equilibrium in both directions can lead to severe pathological consequences. Excessive and uncontrolled T cell activation often leads to the development of allergic or autoimmune disease. Indeed, for example, Th2 cells are involved in allergic asthma (Lambrecht, Hammad and Fahy, 2019) and Th17 cells were shown to have a central role in the development of several other autoimmune diseases such as rheumatoid arthritis (Kotake *et al.*, 2017). While the role of T cells in mediating several autoinflammatory diseases is long under investigation, it is only in the last decade that ground breaking research could show the fundamental role of the lymphoid compartment in the tumour microenvironment, where immune-modulating drugs (PDL1 blocking antibodies) are already having a strong impact in the clinics. This predominant role was globally recognized till the point to add the immune modulatory capabilities of cancer cells as a hallmark for metastatic

invasiveness in the recent update of the famous “hallmark of cancer” review (Hanahan and Weinberg, 2011; Fouad and Aanei, 2017). If fact, primary or acquired immunodeficiency patients have an increased risk of developing tumours. Competent immune responses can indeed identify tumour-specific antigens on the surface of cancer cells and trigger both innate and adaptive immune responses (Dunn *et al.*, 2002). Tumour cells often develop molecular mechanisms to maintain an equilibrium with the immune response (Malladi *et al.*, 2016) eventually leading to the tumour escaping the immune response (Fouad and Aanei, 2017; Noguchi *et al.*, 2017; Jiang *et al.*, 2019). Taken together it is clear that even if infectious diseases are not anymore one of the most widespread causes of death in the developed world, the study of the molecular mechanisms that underpin immunological responses are still of great importance for human health.

1.2 Cell homeostasis

Each single cell in a multi-cellular organism is governed by an incredibly complex network of molecular pathways, each of which contribute to cellular homeostasis and function. Basic molecular processes such as cell survival, activation, proliferation and differentiation must be tightly regulated often by the interplay of several molecular mechanisms (Borggrefe *et al.*, 2016). From single cells to complex organs, molecular mediators like Wnt, EGF, FGF, VEGF, insulin or insulin-like GFs are fundamental to maintain homeostasis and balance in complex organisms (Clevers, 2006; Pollak, 2008; Matsumoto and Ema, 2014; Zeng and Harris, 2014; Brewer, Mazot and Soriano, 2016; Ushach and Zlotnik, 2016). Often the impairment of these pathways results in an incredible variety of pathological states such as cancer, metabolic disease, chronic inflammatory conditions or neurodegenerative disease (Hamilton, 2008; Goel and Mercurio, 2013; Dashkevich *et al.*, 2016; Libro, Bramanti and Mazzon, 2016; Ma and Hottiger, 2016; Meikle and Summers, 2017; Zhan, Rindtorff and Boutros, 2017; Shim and Madsen, 2018). Thousands of years of evolution lead to the development of several molecular mechanism to tightly control the balance of those pathways and prevent pathological

deviations (Clevers and Nusse, 2012; Liang *et al.*, 2019; Mukai, Fujita and Morita, 2019). Medical research in the last century greatly improved our knowledge on the function and molecular regulation of single pathways thanks to naturally occurring mutations or animal models. Despite that, still not much is understood about the crosstalk of the reciprocal regulation of single pathways in the complex network.

A clear example of this intricate network of events is the activation of the NFAT (Nuclear factor of activated T cells) family of transcription factors, NFAT was first identified as a transcription factor activated downstream of tyrosine kinase receptors, such as VEGFR, and ZAP70 which is part of the TCR complex (Macian, 2005). For a long time, NFAT activation was directly connected only to the activation of those receptors. Recently it was shown that the activation of this transcription factor is also one of the main molecular processes downstream of Wnt signalling induced by triggering Frizzled receptors through G protein activation (non-canonical Wnt signalling) showing how different molecular pathways can interplay to fine tune the regulation of similar downstream molecular processes (De, 2011).

1.3 The Wnt signalling pathway

Wnt1 was first identified 30 years ago in *Drosophila melanogaster* (Wingless) and in mouse (Int-1) (Nusse and Varmus, 1982). It was found that Wnt was important in the control of segment polarity both in Drosophila and Xenopus (Nusse and Varmus, 1982). A few years later, a more detailed view of this molecular pathway became apparent with the identification of Wnt as a lipid-modified secreted protein that was able to bind the Frizzled receptor and co-receptor LRP to activate β-Catenin and the TCF/LEF complex that eventually leads to gene transcription (Nusse and Clevers, 2017). This complex molecular mechanism is now known as the canonical Wnt signalling pathway. In recent years, the spectrum of downstream events mediated by Wnt binding to its receptor was further expanded with the discovery of two new pathways; the non-canonical Wnt/calcium and planar cell polarity pathway (Yang and Mlodzik, 2015). Additionally, over the past few years, several mutations in key components of the Wnt

signalling pathway have been linked to a broad variety of pathologies ranging from tumorigenesis (Zhan, Rindtorff and Boutros, 2017) to type II diabetes showing the broad relevance of this molecular pathway (Nusse and Clevers, 2017). At the cellular level, Wnt/β-Catenin signalling is crucial for the regulation of proliferation, differentiation, fate specification and apoptosis during development as well as playing a role in maintaining tissues homeostasis (Nusse and Clevers, 2017).

1.3.1 *Canonical Wnt signalling pathway*

Conventionally, canonical Wnt signalling is described as a bimodal process divided by the presence or absence of Wnt at the cell surface. In absence of Wnt (inactive Wnt signalling), β-Catenin is phosphorylated by the destruction complex which contains the scaffold proteins Axin and APC and the kinases CK1 and GSK3 which is responsible of the phosphorylation of β-Catenin. The phosphorylation of β-Catenin is a signal to the cell machinery to proceed with ubiquitination and consequently degradation of the protein leading to the repression of TCF/LEF target genes. On the other hand, the activation of the pathway is mediated by the binding of secreted Wnt to the Frizzled (Fzd) receptor and the co-receptor LRP5/6 leading to the phosphorylation of LRP by CK1 and the recruitment of Dishevelled (Dvl). The stabilization of this complex at the inner part of the plasma membrane ultimately leads to the inhibition of the destruction complex and consequently to the increase in level of β-Catenin. Free β-Catenin can now translocate to the nucleus and form an active complex with LEF and TCF leading to the activation of target gene transcription (**fig 1.4**) (Staal, Luis and Tiemessen, 2008; Nusse and Clevers, 2017; Zhan, Rindtorff and Boutros, 2017).

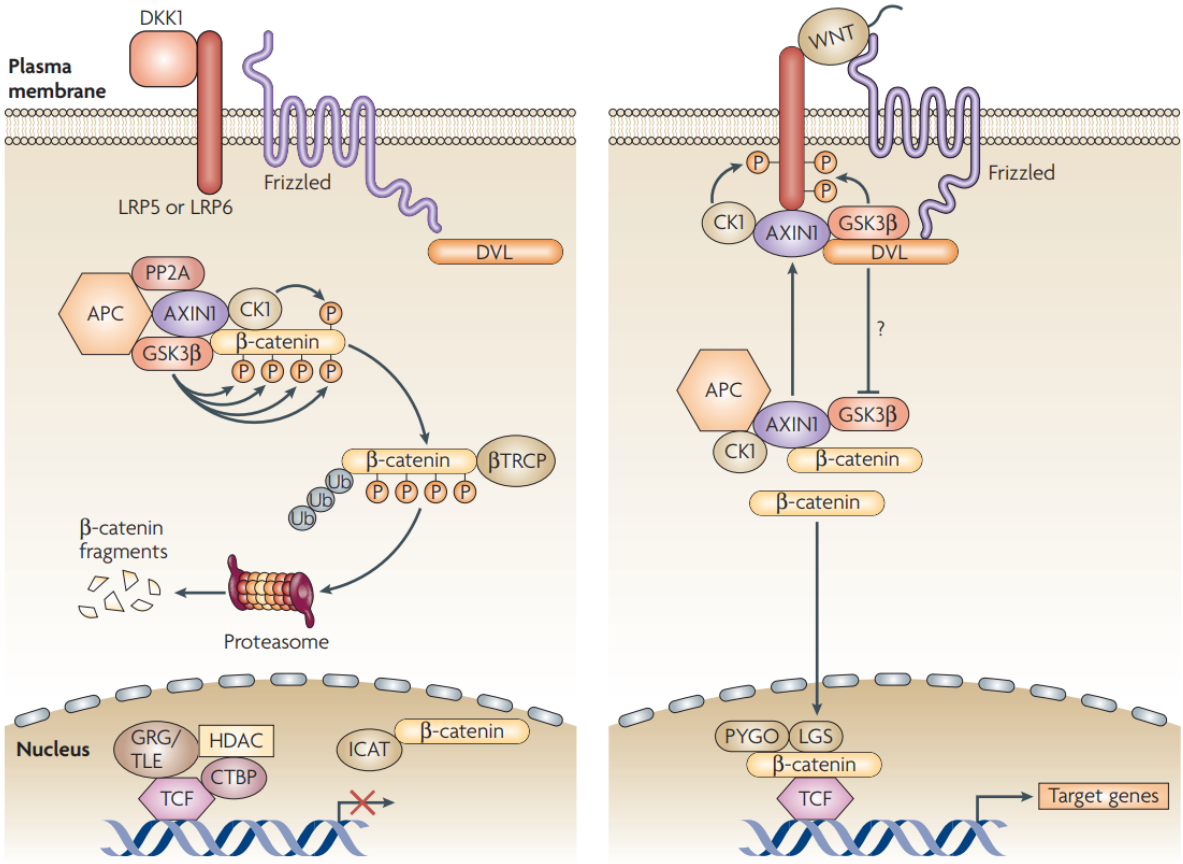

Figure 1.4 Canonical WNT signalling regulates β-catenin activation

In absence of WNT binding to the Frizzled receptor (a), β-catenin is phosphorylated by the kinases CK1 and GSK3 and consequently ubiquitinated and degraded. The protein complex in which CK1 and GSK3 are acting on β-catenin is called the destruction complex and also includes the anchor proteins AXIN and APC. In the nucleus, in absence of β-catenin, TCF is bound to several repressor proteins limiting the expression of target genes. When WNT is available for binding to Frizzled and the co-receptor LRP, LRP itself is phosphorylated by CK1 and AXIN is recruited at the plasma membrane disrupting the destruction complex. In this context, β-catenin degradation is inhibited and the concentration of the transcription factor rapidly increases in both the cytosol and nucleus. Nuclear β-catenin can now bind to TCF and LEF and promote the expression of target genes. (Figure taken from Staal, Luis and Tiemessen, 2008).

1.3.2 *Non-canonical Wnt/calcium signalling*

As described for the canonical Wnt signalling pathway, the non-canonical Wnt/calcium signalling is initiated by the binding of a lipid-modified Wnt molecule to the Frizzled receptor (Staal, Luis and Tiemessen, 2008). As a G protein-coupled receptor, Frizzled activates phospholipases C (PLC) leading to an increase in the cytosolic levels of DAG (diacylglycerol) and IP_3 (inositol triphosphate). This increase in levels of IP_3 stimulates the release of calcium from ER stores leading to Calcineurin activation and consequent activation of NFAT, a process

described below in more detail (De, 2011). The cross-talk between canonical and non-canonical Wnt-calcium signalling remains elusive with some reports suggesting the combination of Wnt5a and Frizzled 2-3-4-6 (Yang and Mlodzik, 2015) and 5 (Yang and Mlodzik, 2015) can lead to exclusive activation of the non-canonical pathway. Molecular studies examining the interplay between the two pathways showed that both canonical and non-canonical Wnt signalling can be activated in a coupled manner (Thrasivoulou, Millar and Ahmed, 2013) proposing that de-polarization of the nuclear membrane by calcium release might be required for efficient translocation of β-Catenin to the nucleus (**fig1.5**).

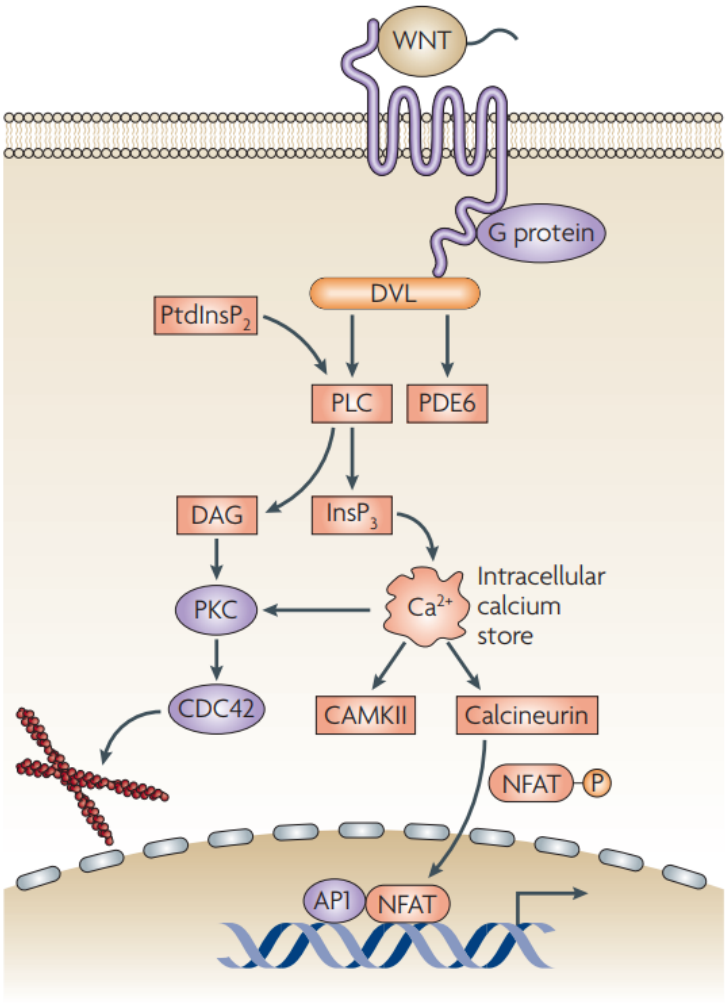

Figure 1.5 Non-canonical WNT signalling regulates calcium influx and NFAT activation

Non-canonical WNT-Ca^{2+} signalling involves, downstream WNT binding of the Frizzled receptor, the activation of Frizzled-associated G proteins. This signalling acts on PLC leading to the cleavage of PtdInsP2 in DAG and InsP3 leading to a transient increment of cytosolic calcium. Free calcium will then trigger Calcineurin activation via Calmodulin consequently leading to NFAT dephosphorylation. NFAT can then migrate to the nucleus where, in a complex with AP1, regulates target genes. (Figure taken from Staal, Luis and Tiemessen, 2008).

1.3.3 *Wnt signalling in T cell development and function*

As expected from the general relevance of Wnt signalling in cell homeostasis, this pathway was also shown to be active in $CD4^+$ and $CD8^+$ T lymphocytes. Despite its well-established role in thymic development (Ma *et al.*, 2012; Yu *et al.*, 2012; Steinke *et al.*, 2014; Johnson *et al.*, 2018), its potential role in peripheral T cell functions is still poorly understood. In T cell development, modulation of the Wnt signalling pathway impacts thymic maturation. Single KO for TCF1 leads to a moderate block at the single positive stage of thymic development in an age dependent manner (Schilham *et al.*, 1998; Emmanuel *et al.*, 2018). Only when both, TCF1 and LEF7, are deleted from murine lymphocytes does the phenotype escalate leading to a strong block at the single positive stage and reduced cellularity in the periphery (Schilham *et al.*, 1998). To finally connect TCF/LEF activation to Wnt signalling activation, it was shown that overexpression of soluble Frizzled, as decoy receptor, could inhibit thymocyte differentiation (Staal *et al.*, 2001). Furthermore, high levels of DKK, a natural inhibitor of Wnt signalling, was sufficient to block T cell maturation at the DN1 or DN3 stages of development depending on the Cre promoter used (Xu *et al.*, 2003). Recently, the role of TCF1 and LEF1 was further characterized showing how Tcf7 (murine orthologue of TCF1) KO cells do not only affect thymic development but also predispose mice to the development of lymphoblastic lymphomas (Yu *et al.*, 2012). At the molecular levels, it was also shown that TCF1 and LEF1 could act upstream of Th-POK (Th inducing POZ-Kruppel factor), an important factor in T helper cell commitment, promoting differentiation into $CD4^+$ T cells while concurrently silencing Runx3 to prevent CD4 expression in $CD8^+$ T cells (Steinke *et al.*, 2014).

In mature $CD4^+$ T cells, Wnt signalling was shown to play a role in the differentiation process from the naïve to effector state (van Loosdregt and Coffer, 2018). Wnt was also shown to promote Th2 differentiation (Yu *et al.*, 2009; Notani *et al.*, 2010) and inhibit Th17 differentiation (Ma *et al.*, 2011; Yu *et al.*, 2011) by direct inhibition of the *IL17* locus. Nevertheless, the possible implications of Wnt signalling in homeostatic T cell maintenance remain elusive.

1.4 The NFAT family of transcription factors

First identified more than three decades ago, nuclear factor of activated T cells (NFAT), was shown to be an inducible DNA-binding protein that regulates the *IL-2* promoter (Shaw *et al.*, 1988). Five members of the NFAT family of transcription factor have been identified, four of which were shown to be activated by Calcineurin-mediated dephosphorylation (Okamura *et al.*, 2000). At the molecular level, NFAT is activated by Calcineurin-mediated dephosphorylation and consequently migrates to the nucleus where it can form a complex with members of the AP-1 family (JUN or FOS) of transcription factors and regulate gene transcription (**fig 1.6**) (Macian, 2005). All members of the NFAT family of transcription factors (NFAT1 [NFATc2], NFAT2 [NFATc1], NFAT3 [NFATc3] and NFAT4 [NFATc4]) are regulated in a calcium-Calcineurin dependent manner with the exception of NFAT5 (TonEBP) which is activated in response to osmotic stress in a Calcineurin independent manner (**fig 1.6**).

Despite the NFAT family of transcription factors being first identified in T cells (Shaw *et al.*, 1988), it is now clear that it also functions in other immune cells such as dendritic cells (DCs), B cells, megakaryocytes and macrophages (Crist, Sprague and Ratliff, 2008; Shukla *et al.*, 2009; Zanoni *et al.*, 2009). Furthermore, NFAT has been shown to be crucial for several developmental processes in the nervous system, heart, blood vessels, kidneys, as well as in bone maintenance and haematopoiesis (Graef, Chen and Crabtree, 2001; Crabtree and Olson, 2002; Hogan *et al.*, 2003; Kiani *et al.*, 2004; Macian, 2005).

1.4.1 *NFAT signalling in T cells*

In human and murine T cells, only four members of the NFAT family are expressed (NFATc1, NFATc2, NFATc4 and NFAT5) and their roles has been investigated in the last years individually or in combination taking advantage of available KO mouse models (Xanthoudakis *et al.*, 1996; Ann M Ranger *et al.*, 1998; Oukka *et al.*, 1998; Yoshida *et al.*, 1998; Peng *et al.*, 2001; Monticelli and Rao, 2002; Rengarajan, Tang and Glimcher, 2002; Pachulec, Neitzke-Montinelli and Viola, 2016). Studies of single deletions of each member of the family did not

show any dramatic phenotype in mice with the exception of NFATc1 where the global KO resulted in developmental lethality due to cardiac developmental problems (A M Ranger *et al.*, 1998). The mild phenotype of the single KO for the NFAT family members could be explained by the high sequence homology that the proteins share, especially in the DNA binding region postulating a possible compensatory effect (Macian, 2005) considering also that all members are known to be activated downstream of TCR stimulation. Only when multiple members are deleted, does a phenotype accelerate, for example the deletion of both NFATc1 and c2 lead to severely impaired T cell functions with defects arising in cytokine production and cytolytic activity. Notably, NFATc4 is the only member of the NFAT family which expression is markedly increased during T cell development. Indeed, KO studies for this family member showed severe reduction in single positive cells in the thymus due to an increased apoptotic rate at the double positive stage.

More recently it was shown that different NFAT family members have the capacity to polarize naïve $CD4^+$ T cells into a specific subset (Lee, Kim and Choi, 2018). For example, it was shown that conditional KO of NFATc1 in T cells leads to a decreased differentiation rate into Th2 subsets (A. M. Ranger *et al.*, 1998) and protects mice from the development of experimental asthma (Koch, Reppert and Finotto, 2015).

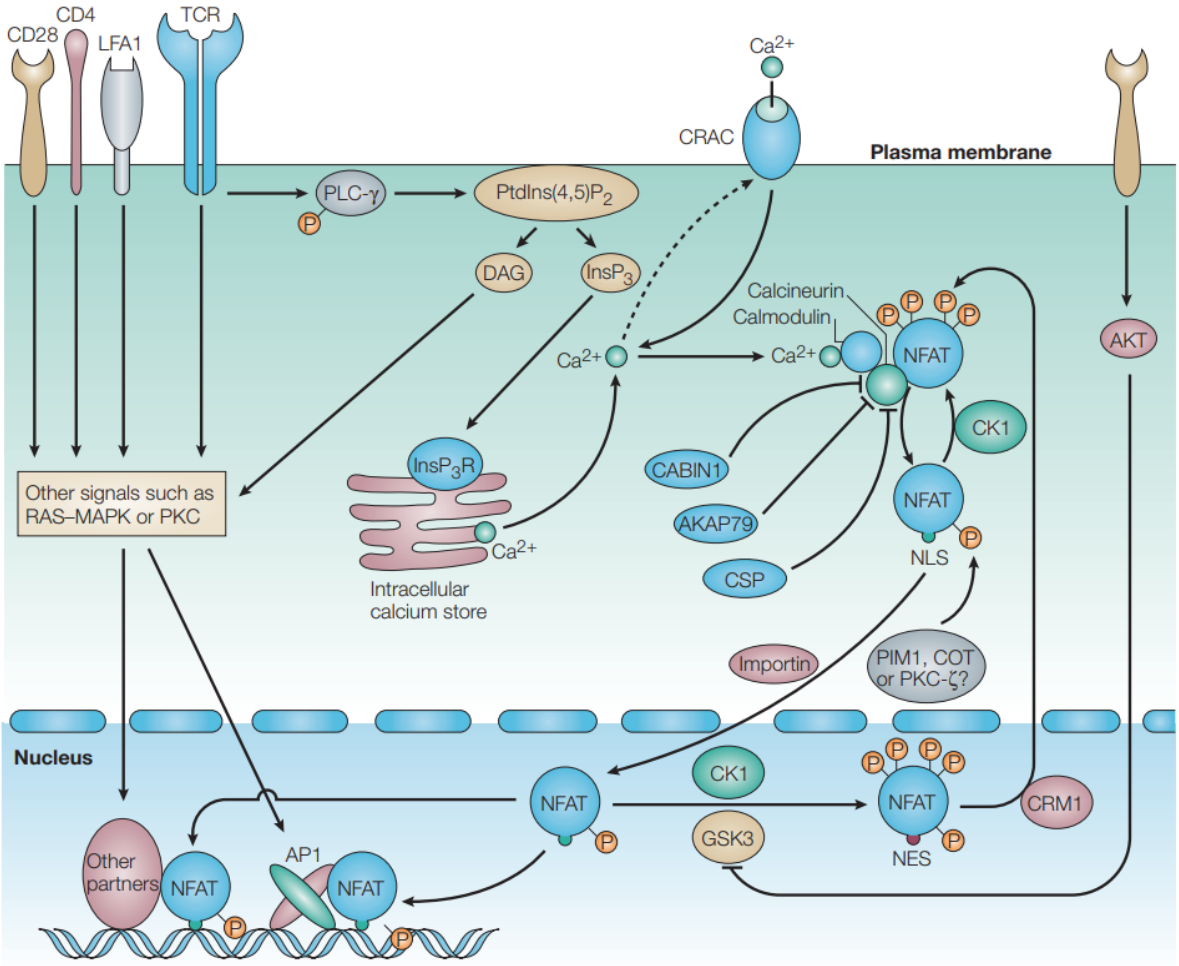

Figure 1.6 NFAT family of transcription factors is activated downstream of TCR stimulation

Engagement of the TCR from the MHCI/II of an APC triggers a wide variety of downstream events within T cells. The TCR complex act as tyrosine kinase leading to the activation of the PLC-γ. This lipase is able to hydrolyse the PtdInsP2 in DAG and InsP3. Both of these (either both of these or these two) byproducts have an important function in the TCR pathway but especially InsP3 leads to the release of calcium from intracellular stores (ER) that then will lead, in a positive feedback loop, to the opening of the calcium channel CRAC at the plasma membrane. This series of events will lead to an increased concentration of calcium in the cytosol able to activate Calcineurin in a Calmodulin-calcium dependent manner. Activated Calcineurin can dephosphorylate NFAT exposing the nuclear localization sites previously masked from the phospho-group. NFAT can now translocate to the nucleus via Importin where, cooperatively with the AP1 transcription factor will regulate the expression of a broad variety of genes such as IL-2 or RCAN3. (Figure taken from Macian, 2005a).

1.5 Cellular senescence and aging

Aging can be defined as a gradual decline of the organism occurring heterogeneously across different organs. Loss of the normal organ functionality and thus aging has been shown to be a risk factor for several age-related diseases (Niccoli and Partridge, 2012; Kim, Cho and Yoo, 2017) such as cardiovascular diseases, dementia, osteoporosis, osteoarthritis, cancer, type II diabetes, idiopathic pulmonary fibrosis and glaucoma (Raisz, 1988; Querfurth and LaFerla, 2010; Gunasekaran and Gannon, 2011; Niccoli and Partridge, 2012).

At the molecular level, aging has been shown to be tightly associated with cellular senescence. This cellular state was initially described as a proliferative stop and exit from the cell cycle caused by cellular stress, DNA damage, telomere shortening and mitochondrial dysfunction (López-Otín *et al.*, 2013). More recently, it was found that perturbation of paracrine stimuli such as growth factors could induce cellular senescence, for example Wnt signalling was shown to be fundamental to prevent senescence both *in vitro* and *in vivo* (Ye *et al.*, 2007; Hoffmeyer *et al.*, 2012). SFRP1, a soluble receptor for Wnt, was able to sequester the ligand and consequently inhibit the Wnt signalling pathway and mediate cellular senescence *in vivo* and *in vitro* highlighting how activation of β-Catenin target genes is required to prevent cellular senescence (Elzi *et al.*, 2012). This shows how not only cell intrinsic events are responsible for induction of senescence and consequently aging but also the microenvironment of the cell, and especially the right combination of survival signalling, are vital to prevent cellular senescence.

The immune system is not unaffected by the process of aging and cellular senescence. This process is characterized by several changes in the capacity of the body to correctly respond to infection or to exert a proper anti-tumour response, collectively termed immunosenescence (Fulop *et al.*, 2017; Nikolich-Žugich, 2018). Immunosenescence is generally characterized by drastic changes in cellular frequencies such as reduction in the ratio between naïve and memory T cells (Fulop *et al.*, 2017; Alpert *et al.*, 2019) with a concomitant impairment in the adaptive response (Fulop *et al.*, 2017).

Recently, some of these changes affecting the immune system during aging have been deeply characterized in a longitudinal study (IMM-AGE) (Alpert *et al.*, 2019). In this publication, Alpert and colleagues could show how monitoring single individuals over time highlighted profound changes in the composition of the immune system over the course of several years such as the reduction of the ratio between naïve and memory $CD4^+$ and $CD8^+$ T cells and the increment in the number of circulating monocytes (Alpert *et al.*, 2019).

Despite these hallmark changes in the composition of the immune system having been highlighted previously, in this recent publication, it appears clear that each individual follows a common trajectory in the aging of the immune system. Furthermore, the process of aging of the immune system appears not to be highly correlated with age of the donors emphasising how genetics, environment and anamnesis have a profound effect on the “age” of the immune system.

1.6 Creld1 as a novel modulator of NFAT signalling involved in AVSD

In humans, the gene *Cysteine rich with EGF-like domain 1* (*CRELD1*) was first identified in 2002 and mapped to human chromosome 3 (Rupp *et al.*, 2002). The gene was first described as a matricellular protein due to the predicted presence of two EGF-like and two EGF-calcium binding domains (Rupp *et al.*, 2002). In addition to these already known domains, CRELD1 was found to also contain a highly conserved domain of unknown function called here the WE domain due to the presence of a repetitive sequence rich in tryptophan (W) and glutamic acid (E). This domain was predicted to have a possible role in protein-protein interactions. Indeed, predictive structural biology showed how CRELD1 contains two transmembrane domains and a signal peptide predicting U-shaped insertion in the cellular membrane (Rupp *et al.*, 2002). More recently, another homologous member of the CRELD1 family of proteins was identified, named CRELD2 (Maslen *et al.*, 2006). This protein was shown to share most of the structural features with CRELD1, but interestingly differs by the absence of a transmembrane domain

predicting an extracellular localization. Orthologues for both CRELD1 and CRELD2 can be identified in all vertebrates. In *Drosophila melanogaster* and *C. elegans*, only one CRELD orthologue has been identified (dCRELD1 and crld-1 respectively), however this gene was shown to be transcribed into two distinct splicing variants (dCRELD1A and dCRELD1B) predicted to be structurally similar to CRELD1 and CRELD2, respectively (NCBI - Gene).

For several years after its first identification, any function of CRELD1 remained widely obscure. Several mutations in the CRELD1 gene locus have been associated with increased susceptibility to atrio-ventricular septal defects (AVSDs) especially in patients with trisomy of chromosome 21 (Down Syndrome) (Robinson *et al.*, 2003; Zatyka *et al.*, 2005; Asim *et al.*, 2018). Only recently, the study of a knockout (KO) mouse model for Creld1 revealed its importance in heart development. In fact, it was shown that homozygous KO animals die at day 12.5 of embryonic development (E12.5) due to aberrant heart development. This developmental problem was finally correlated with the ability of Creld1 to regulate the activation of the Calcineurin/NFAT pathway both *in vivo* and *in vitro* (**fig 1.7,** Mass et al. 2014). Recently, genetic studies on *C. elegans* proposed how crld-1 protein could have disulphide isomerase (PDI) activity in the ER regulating maturation and localization or the ionotropic acetylcholine receptors (D'Alessandro *et al.*, 2018). Nevertheless, the molecular mechanisms explaining functions of Creld1 remain widely unrevealed.

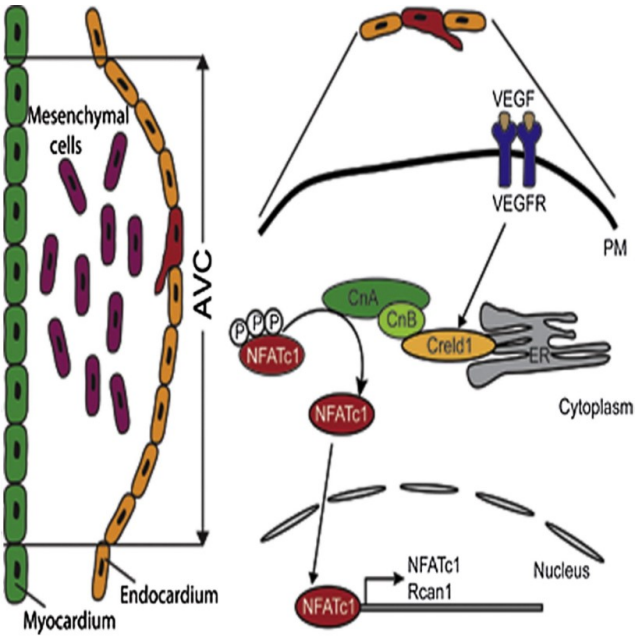

Figure 1.7 Creld1 is important for cardiac development regulating NFATc1 activation

Creld1 is fundamental for correct heart development. Creld1 KO animals die during embryogenesis due to incorrect formation of heart valves. This phenotype was mechanistically connected to the ability of Creld1 to regulate Calcineurin activation downstream of VEGF stimulation in the endocardium (Figure taken from Mass et al.*, 2014).*

2 Aim of the thesis

Several decades of scientific research have aimed to decipher the complex molecular machinery involved in T cell biology. Despite an extensive characterization of the biological processes involved in T cell activation and differentiation in response to antigen presentation, just a few molecular pathways have been linked to homeostatic maintenance of the pool of non-antigen experienced T cells or memory T cells in a non-inflammatory context (IL-7/IL-15; tonic TCR stimulation). Recent literature showed how molecular processes involved in cellular maintenance of other cell types could also be involved in T cell homeostasis. Moreover, the relationship between different molecular processes cooperating in a highly interconnected network in T cell biology has not yet been fully characterized. Advances in our knowledge about underlying processes in T cell maintenance could provide medical and pharmaceutical approaches in the treatment of immune-related diseases such as those mechanisms linked to immunosenescence. This dysfunctional state is common in elderly and characterized by a significant reduction in the number of circulating T cells and in the ability of those cells to respond to stimulation appropriately. Consequently, the individual is exposed to many potential threats that lead to age-related diseases, which – as a consequence – put a significant burden on health care systems.

Creld1 was recently described to function in the modulation of NFAT activation. The NFAT family of transcription factors is crucial in the regulation of T cell physiology and involved, together with several others, in the maintenance of a healthy immune system.

Therefore, the aim of this thesis is to provide more insight into the molecular mechanisms regulated by Creld1 both *in vivo* and *in vitro* with a focus on $CD4^+$ T cell homeostasis by using a CD4-Cre mouse line to generate a conditional KO of Creld1 in $CD4^+$ T cells.

3 Materials

3.1 General laboratory consumables and equipment

3.1.1 *Consumables*

Product	*Company*
1.5/2 ml reaction tubes	Eppendorf
Agilent Seahorse XF96 Cell Culture Microplates	Agilent
Agilent Seahorse XF96 Extracellular Flux Assay Kits	Agilent
Cell culture dish (10 cm)	BD Falcon
Cell culture plates (6-well, 12-well, 24-well, 96-well flat bottom)	BD Falcon
Cell culture plates (96-well round bottom)	Sarstedt
Cell strainers (70µM, 100µM)	BD Falcon
Disposal autclave bags	Roth
Flow cytometry tubes	Sarstedt
General laboratory equipment	Faust, Schutt
IBI-treated 8-well plates	Ibidi
nitrocellulose membrane	Hybond N+, Amersham
Parafilm	American National Cam
PCR reaction tubes	Sarstedt
Plastic wares	Greiner
Reaction tubes (15 ml, 50 ml)	Greiner
Reagent reservoirs	Greiner
Serological pipettes	Sarstedt
Sterile filters	Whatman
Syringe	Inject disposable 5 ml Braun
White half-size 96-well plate for luciferase	Costar
X-ray films	Fuji MedicalX-Ray Film Super RX
Consumables	Company

Table 1 List of consumables used in this thesis

3.1.2 ***Equipment***

Equipment	*Company*
Autoclave	H+P Varioklav Dampfsterilisator EP-2
Bacteria incubator	Innova 44 New Brunswick scientific
Balances	Kern & Sohn 440-35A Kern & Sohn ABJ-NM Kern & Sohn EW-N
Cell counting chamber	La Fontaine via Labotec - improved neubauer
Cell culture incubator	Binder CB 150
Centrifuges	5415R/5424 Eppendorf Avanti J26 XP Beckman Coulter Rotina 420R
Confocal Microscope	Zeiss LSM710
Developer Machine	Curix 60 AGFA
Electro pipet	Accu Jet
Flow Cytomyter	BD bioscience LSRII BD bioscience Symphony BD bioscience Celesta
Fluorescence microscope	Olympus SZX 12
Inverted light microscope	Zeiss Stemi 2000
Laminar flow bench	BDK laminar flow
Microwave	Panasonic NN-E235M
PCR machine	C1000 Thermal Cycler Biorad
Photometer	Nano Drop 2000 PeqLab Tape Station Agilent
Plate Reader	Fluostar Omega (BMG labtech) Tecan infinite M200
Power supply	Biorad Power pac 3000
Real Time PCR machine	Roche lightcycler
Thermo block	Eppendorf
Transilluminator	BioView transilluminator UST-30M
Vortex	Vortex Genie2
Water bath	Julabo SW22
Western blot system	Biorad Mini Trans-Blot

Table 2 List of equipment used in this thesis

3.2 Reagents and kits

Product	Company
2-Log DNA ladder, 1 kb DNA ladder	NEB
2-Propanol >99.5%	Roth
Albumin Bovine Fraction V	Roth
Annexin V-FITC Kit	Trevigen
BCA protein assay	Pierce
Bioplex cytokine multiplexing	Biorad
BrefeldinA solution (1000x)	eBioscience
Cell stimulation cocktail	eBioscience
CFSE	Biolegend
CountBright absolute counting beads	Life technologies
Cyclosporin A	Sigma-Aldrich
Digitonin	Invitrogen
DMEM	Gibco
Dual-Glo	Promega
Dulbecco modified PBS	Gibco
ECL Western Blotting Substrate	Pierce
Ethanol	Roth
Ethanol absolute for molecular biology	Sigma-Aldrich
Ethylenediaminetetraacetic acid (EDTA)	Sigma-Aldrich
FACS Clean	BD Bioscience
FACS Rinse	BD Bioscience
HBSS	Gibco
Histofix (4% PFA)	Roth
IMDM	Gibco
Lipofectamine 2000	Thermo Scientific
LIVE/DEAD Fixable near-IR/yellow	Thermofisher
Luciferase Assay Kit	Promega
MagniSort Mouse CD4 T cell enrichment kit	Thermo Scientific
Methanol-free PFA	Pierce
milk powder	Roth
Monensin solution (1000x)	eBioscience
Nucleic Acid & Protein Purification, NucleoBond, PC100	Macherey & Nagel
NucleoSpin RNA/Protein	Macherey & Nagel
PCR Nucleotide mix	Roche
OneComp/UltraComp compensation beads	Invitrogen
Penicillin-Streptomycin	Gibco
Poly-L-lysine	Sigma-Aldrich

Precision Plus Protein All Blue Standards	Biorad
Protease Inhibitor cOmplete cocktail tablets	Roche
QIAzol Lysis Reagent	Qiagen
QuantiTect, Reverse Transcription Kit	Quiagen
RFP-trap	Chromotek
RNAeasy micro kit	Quiagen
Seahorse assay medium (RPMI)	Agilent
SYBR Safe DNA stain	Invitrogen
Thapsigargin	Sigma-Aldrich
Triton X-100	Roth
TurboFect	Thermo Scientific
Trypsin	Gibco

Table 3 List of reagents and kits used in this thesis

3.3 Buffers

Buffer	*Composition*
Agarose	1% agar-agar in TAE
Ammonium persulfate (APS)	10% APS
Alkaline lysis solution I	50mM glucose, 20mM Tris-Cl, 10mM EDTA
Alkaline lysis solution II	0.2N NaOH, 1% SDS
Alkaline lysis solution III	60 ml 5M potassium acetate, 11.5 ml acetic acid, 28.5 ml H2O
Ampicillin (1000x)	50mg/ml
Intestinal digestion solution I	5mM DTT in HBSS, 2% FCS, Penicillin 100 U/ml, Streptomycin 100ug/ml
Intestinal digestion solution II	5 mM EDTA in HBSS, 2% FCS, Penicillin 100 U/ml, Streptomycin 100 µg/ml
Intestinal digestion solution III	HBSS, 10 mM HEPES, Penicillin 100 U/ml, Streptomycin 100 µg/ml
KHM buffer	110 mM KOAc, 2 mM MgCl2 , 20 mM HEPES (pH 7.2)
Laird buffer	0.1 M Tris (pH 8.0), 0.2 % SDS, 0.2 M NaCl, 5mM EDTA
MACS buffer	0.5% BSA, 2mM EDTA in PBS
PBS (20x)	2.6 M NaCl, 140 mM Na2 HPO 4 , 60 mM NaH 2 PO 4
PFA	4% PFA in PBS
Proteinase K stock solution (20 °C)	20 mg/ml in DEPC
Red blood cells lysis buffer	155 mM NH4Cl , 12 mM NaHCO 3 , 0.1 mM EDTA
RIPA Co-IP	10 mM Tris/Cl pH 7.5; 150 mM NaCl; 0.5 mM EDTA; 0.5% NP-40
RIPA WB	10 mM Tris/Cl pH 7.5; 150 mM NaCl; 0,5 mM EDTA; 0,1% SDS; 1% Triton X-100; 1% Deoxycholate
SDS	10% SDS
SDS-PAGE loading buffer (5x)	100 mM Tris, 3% SDS, 10% Glycerol, 0.1% Bromphenol blue, 2 % β-Mercaptoethanol (pH 6.8)
SDS-PAGE running buffer (10x)	250 mM Tris/HCl, 1.92 M Glycine, 1 % SDS

TAE buffer	40 mM Tris-Acetate (pH 8.0), 1 mM EDTA
TBST	0.01 M Tris/HC l (pH 7.5), 0 15 M NaCl, 0.05 % Tween 20
Transferring buffer	25 mM Tris, 150 mM Glycine, 10 Methanol
WB blocking solution	5% milk powder in TBST
WB loading buffer	Lysis buffer 20 mM Tris/HCl (pH 7.5), 200 mM NaCl,20 mM EDTA, 2 % SDS

Table 4 List of buffers used in this thesis with exact composition

3.4 Recombinant proteins

Enzyme	*Company*
GoTaq	Promega
Phusion Polymerase	NEB
Antarctic Phosphatase	NEB
Proteinase K	Sigma Aldrich
Restriction enzymes	NEB
RNAse A	Sigma Aldrich
T4 DNA ligase	NEB
Trypsin	Sigma Aldrich

Table 5 List of recombinant proteins used in this thesis

3.5 Antibodies

3.5.1 *Immunohistochemistry*

Specificity	*Clone*	*Company*
Anti-Creld1 goat (Polyclonal)	polyclonal	R&D
Anti-Goat Alexa Fluor 488	polyclonal	Invitrogen
Anti-Goat Alexa Fluor 647	polyclonal	Invitrogen

Table 6 List of immunohistochemistry antibodies used in this thesis

3.5.2 *Flow cytometry and FACS*

Specificity	*Clone*	*Company*
Anti-CD4 PerCp5.5 (RM4-5)	RM4-5	Biolegend
Anti-CD4 APC-Cy7 (RM4-5)	RM4-5	eBioscience
Anti-CD4 BV650 (RM4-5)	RM4-5	Biolegend
Anti-CD3 BV510 (17A2)	17A2	Biolegend
Anti-IFNγ PE-Cy7 (XMG1.2)	XMG1.2	eBioscience
Anti-IL4 APC (11B11)	11B11	eBioscience

Anti-IL17 PE (eBio17B7)	eBio17B7	eBioscience
Anti-IL9 APC (RM9A4)	RM9A4	Biolegend
Anti-Tbet efluor660	eBio4B10	eBioscience
Anti-GATA3 PE-CF594	L50-823	BD
Anti-RORγt APC	AFKJS-9	eBioscience
Anti-FoxP3 Efluor450	FjK-16s	eBioscience
Anti-CD25 Alexa Fluor 647	PC61	Biolegend
Anti-CD44 Pacific Blue	IM7	Biolegend
Anti-CD62L APC-Cy7	MEL-14	eBioscience
Anti-CD69 BV 510	H1.2F3	Biolegend
Anti-KLRG1 PE-Cy7	2F1	eBioscience
Anti-Bcl2 Alexa Fluor 647	BCL/10C4	Biolegend
Anti-clCaspase3 Alexa Fluor 488	D175	Cell Signalling
Anti-Fas FITC	SA367H8	Biolegend
Anti-FasL PE	MFL3	Biolegend

Table 7 List of antibodies used for flow cytometry or FACS

3.5.3 ***Western blot***

Specificity	*Clone*	*Company*
Anti-β-Actin	AC-15	Novus Biologicals
Anti-β-Catenin	6B3	Cell Signalling
Anti-RFP	5F8	ChromoTek
Anti-Rabbit IgG, HRP-linked	polyclonal	Cell Signalling
Anti-Mouse IgG, HRP-linked	polyclonal	Cell Signalling

Table 8 List of Western blot antibodies

3.6 DNA plasmids

Plasmid	*Source*
CFP-CD3δ	H. Lorenz, National Institutes of Health, Mary land
CD3δ-YFP	H. Lorenz, National Institutes of Health, Mary land
Creld1-RFP	E. Mass
Human β-Catenin-GFP	Addgene (#71367)
M50 Super 8x TOPFlash	Addgene (#12456)
M51 Super 8x FOPFlash (TOPFlash mutant)	Addgene (#12457)
mRFP in pYFP-C1	L. Bonaguro
NFATc1-GFP	E. Olson, University of Texas Southwestern Medical Center, Dallas
pMJ Green	AG Willecke, Bonn

pYFP-C1	AG Hoch
RFP-Creld1	L. Bonaguro
RFP-Creld1 C309S	L. Bonaguro
RFP-Creld1 E414K	L. Bonaguro
RFP-Creld1 P162A	L. Bonaguro
RFP-Creld1 R107H	L. Bonaguro
RFP-Creld1 R329H	L. Bonaguro
RFP-Creld1 sol. C	L. Bonaguro
RFP-Creld1 T311I	L. Bonaguro
RFP-Creld1 ΔC1	L. Bonaguro
RFP-Creld1 ΔC2	L. Bonaguro
RFP-Creld1 ΔEGF	L. Bonaguro
RFP-Creld1 ΔEGF-like	L. Bonaguro
RFP-Creld1 ΔN	L. Bonaguro
RFP-Creld1 ΔWE	L. Bonaguro

Table 9 List of plasmids used in this thesis

3.7 Primers

3.7.1 *Cloning primers*

Name	*Sequence*
EcoRI_Creld1_-SP_F	GTC-GAATTCCCCTCTCCTCCTCCCCATC
AgeI_Kozak_mRFP_F	ATTACCGGTAACATG-GCCTCCTCCGAGG
AgeI_Kozak_mRFP_F	ATTACCGGTAACATGGCCTCCTCCGAGG
AgeI_RFP-Creld1-dCT_F	GCTACCGGTAACATGGCTCCACTGCC
AgeI_RFP-Creld1-dCT_F	GCTACCGGTAACATGGCTCCACTGCC
Creld1 1st TM_SalI_R	ACTGTCGACTTACAAGTCACCCTTGGCAGC
Creld1_mut_stop_KpnI_R	ATTGGTACCTTATCTACCCTTGATGAAGCCCT
Creld1_mut_stop_KpnI_R	ATTGGTACCTTATCTACCCTTGATGAAGCCCT
Creld1_-SP_SalI_R	ACCGTCGACTTATCTACCCTTGATGAAGCCC
Creld1_-SP_SalI_R	ACCGTCGACTTATCTACCCTTGATGAAGCCC
Creld1_-SP_SalI_R	ACCGTCGACTTATCTACCCTTGATGAAGCCC
Creld1_-SP_SalI_R	ACCGTCGACTTATCTACCCTTGATGAAGCCC
EcoNI_Creld1_mut_F	CGGCCTGGGAGGAAGAGAA
EcoRI_Creld1_-SP_F	GTCGAATTCCCCTCTCCTCCTCCCCATC
EcoRI_Creld1TM_F	GTCGAATTCGTCCCGGAGTCGGC

mCreld1 2TM_mRFP_F	TCCACCGGCGCCGCCAAGGGTGACTTGGT
mRFP_mCreld12TM_R	ACCAAGTCACCCTTGGC-GGCGCCGGTGGA
RFP-Creld1-dCT_SalI-ST	GCCGTCGACTTATGACAACCAGTACCCAGTC

Table 10 List of oligonucleotides used for cloning

3.7.2 *Genotyping primers*

Mouse line	*Forward primer*	*Reverse primer*
Creld1flox	TTTCTACATCCCTTGCCTGC	ACTCTCCTACTGCTACATCC
CD4Cre	**CD4-Cre** CCCAACCAACAAGAGCTC **Ctrl** -CCTGAGCTGTCCTTAGAAAGTTGCTAG	**CD4-Cre** CCCAGAAATGCCAGATTACG **Ctrl** GGGGTTCATGTCCATGGGCCAC
ROSA26	**1-**CCCCGTAATGCAGAAGAAGA **2-**AAGGGAGCTGCAGTGGAGTA	**1-**CGTAGTAGTAGCCGGGCAGT **2-**CCGAAAATCTGTGGGAAGT
NFAT-luc	CAAATCACAGAATCGTCGTATGCAG	TGGCGAAGAAGGAGAATAGGGTTGC

Table 11 List of primers used for genotyping PCRs

3.7.3 *qRT-PCR primers*

Target	*Fw*	*Rev*	*Taq-man probe (Roche)*
Tbp	GGACTACATTAATGGTGGAGAGC	AGAATCGAGCCCGTGGTT	38
Creld1	GAACCATCCGGGACAACTT	CTCCAGCACCTCCACCAG	69

Table 12 List of primers used for qRT-PCR

3.8 Bacterial strains

Strain	*Genotype*
DH5a	F-end A1 deo R (φ80 lacZ ΔM15) rec A1 gyr A (N al r) thi 1-hsd R17 (rK --, m K ++) sup E44 re lA1 Δ(lac ZYA arg F)U169

Table 13 Bacterial strain used in this thesis

3.9 Cell lines

Line	*Source*
NIH-3T3	Thomas Magin, U Leipzig

Table 14 Cell lines used in this thesis

3.10 Media

3.10.1 ***Bacterial culture***

Medium	*Composition*
LB-medium	10 g NaCl, 10 g tryptophan, 5 g yeast extract in 1 l aqua bidest (pH 7. 0)
LB-ampicillin medium	LB medium with 50 µg/ml ampicillin
LB-kanamycin medium	LB medium with 25 µ g/ml kanamycin
LB-ampicillin agar	LB medium with 20 g agar and 50 µg/ml ampicillin
LB-kanamycin agar	LB medium with 20 g agar and 25 µg/ml kanamycin

Table 15 Composition of media used for bacterial culture

3.10.2 ***Murine cell culture***

Use	*Composition*
NIH-3T3	10 % FBS, 1 % Penicillin/Streptomycin in DMEM
Primary lymphocytes	10 % FBS, 1 % Penicillin/Streptomycin in RPMI or IMDM MORE
Seahorse assay	2mM L-glutamine, 1mM Na-Pyruvate, 10mM Glucose, pH 7.4

Table 16 Composition of media used for culture of murine cells

3.11 Animals

Mice were carried under SPF condition with a 12 hours light/dark cycles and food and water *ab libitum*. Conditional *Creld1*$^{fl/fl}$ mice were generated from *Creld1*$^{tm1a(EUCOMM)Wtsi)}$ ES cells from the EUCOMM consortium (C57BL/6N background) via injection into blastocysts from B6 albino mice and backcrossed to *C57BL/6JRcc*. Transgenic mice were crossed to *delete-Flp* mice (king gift of Prof. Willecke) to remove the FRT-flanked selection cassette. *CD4*^{Cre} mice were a kind gift of Prof. Wunderlich (Univerity of Cologne). *NFAT-luc* mice (*B6;FVB-Tg(Myh6/NFAT-luc)1Jmol/J*) were a king gift of Prof. Ritter (University of Würzburg) and *Rosa26*$^{stop\text{-}tdTomato}$ animals were kindly provided by Prof. Wachten (University of Bonn).

3.12 Software

Software	*Distributor*
GraphPad Prism v.5	GraphPad
Microsoft Excel 2016	Microsoft
R 3.4.3	r-project
R Studio	R Studio
CRAN packages (several)	CRAN
Bioconductor Packages (several)	Bioconductor
Agilent Seahorse Wave Software	Agilent
ZEN (black edition)	ZEISS

Table 17 Software used for data analysis

4 Methods

4.1 Nucleic acid isolation and purification

4.1.1 *DNA extraction from mouse tissue*

Tail snips or ear punches from 3-week-old mice were used for genotyping purposes. Tissue was incubated in 400 µl of Laird buffer at 55°C over-night in a water bath or alternatively for 3-4 hours in a shaking thermo-block to allow for complete tissue dissociation. 500 µl of pure isopropanol was then added to precipitate the DNA. After centrifugation at 16,000 g for 10 minutes, the DNA was washed with 1 ml of 70% ethanol. To facilitate complete recovery, the DNA was centrifuged once more for 5 minutes and the pellet was air dried prior to resuspension in double distilled water (ddH2O) for analytical use. To facilitate resuspension of the DNA, the solution was heated for 30 minutes at 55°C.

4.1.2 *Plasmid DNA extraction from transformed bacteria*

For analytical purposes, single bacterial colonies were inoculated in antibiotic-supplemented LB medium and incubated over night at 37°C vigorously shaking (250 rpm). The following day 1.5 ml of bacterial culture was transferred to a reaction tube and centrifuged at 16,000 g for 30 seconds in a pre-cooled centrifuge (4°C). Pelleted bacteria were resuspended in 100 µl of ice-cold Alkaline lysis solution I. 200 µl of Alkaline lysis solution II was added to dissociate the bacterial membrane by drastic pH change, the reaction tube was then carefully mixed avoiding shear stress (e.g. vortexing). The alkaline pH was then neutralized by addition of 150 µl of Alkaline lysis solution III and incubated on ice for up to 5 minutes. The bacterial lysate was then centrifuged for 5 minutes at 16000g in a cooled centrifuge and 400 µl of supernatant was then mixed with 800 µl of absolute analytical ethanol to ease the precipitation of nucleic acids. Precipitated nucleic acids were then collected by centrifugation for 5 minutes at 16000g. DNA pellets were then washed once with 70% ethanol and centrifuged again prior to desiccation.

The pellet was then resuspended in 100 µl of ddH2O and used for plasmid validation or stored at -20°C.

For preparative purposes, plasmid DNA was purified using the Macherey & Nagel NucleoSpin Plasmid Kit according to manufactures instructions to archive high yield and low contamination of RNA or pyrogenic compounds. DNA was then used for transient transfection in eukaryotic cells.

4.1.3 *DNA clean-up*

Plasmid DNA or DNA fragments deriving from enzymatic reactions (polymerase chain reaction or restriction enzyme digestion) or gel electrophoresis band separation were purified using the Machery & Nagel Nucleospin Extract II Kit according to manufacturer's instructions.

4.1.4 *RNA isolation*

To purify RNA from cell lines, primary cells or tissues, QUIAZOL lysis reagent was used. Cells were incubated for 5 minutes with the appropriate volume of lysis reagent and shortly vortexed to facilitate dissociation of the material. Lysed cells were either processed immediately or stored at -80°C. QUIAZOL was then added with 1:5 volumes of chloroform and then shaken for 15 seconds and incubated for 3 minutes at RT. The solution was then centrifuged at 12000g for 10 minutes keeping a constant temperature of 4°C. The aqueous phase was collected and the RNA was precipitated with 1 volume of isopropanol. To improve RNA precipitation, the solution is incubated at -20°C for a minimum of 3 hours (maximum over-night) and centrifuged again. RNA pellets were then washed with 500 µl of 80% ethanol and centrifuged for 5 minutes. The pellet was then air-dried and resuspended in nuclease-free water. RNA purification for RNA sequencing experiments was purified using the QUIAGEN RNAeasy MinElute kit according to manufacturer instructions.

4.1.5 *Assessment of DNA and RNA quality*

DNA and RNA purity as well as concentration was determined using the Nanodrop instrument, absorbance ratios 260/280 and 260/230 which can give an indication of contamination from proteins or phenols/carbohydrates respectively. 1 µl of RNA or DNA diluted in nuclease free water was used for the measurement. RNA concentration and quality for RNA-seq experiment was determined via TapeStation according to manufacturer's instructions.

4.1.6 *cDNA library preparation for qRT-PCR and RNA-seq*

Previously purified RNA was reverse transcribed using the QuantiTect Reverse Transcription Kit (QIAGEN) including a pre-treatment with DNase to remove contamination of genomic DNA. 500 µg of total RNA was used as input for the reaction in a final volume of 10 µl. cDNA was then diluted to 50 µl with nuclease-free H_20. RNA-seq libraries were prepared accordingly to the TruSEQ protocol.

4.1.7 *Electrophoresis of DNA fragments*

DNA electrophoresis was carried out with 1% or 1.5% agarose solution depending on the size of the fragment of interest. Electrophoresis-grade agarose was diluted in 1x TAE buffer and boiled for complete solubilisation. SYBR Safe was then added to the agarose solution. Once the gel solidified, it was placed in a gel electrophoresis chamber filled with 0.5x TAE buffer. DNA sample and size reference ladders were mixed with DNA loading buffer and loaded on to the gel. Electrophoresis was then carried out with a constant voltage of 60 to 100 V. Resolved DNA fragments were then analysed by UV trans-illumination.

4.2 Cloning and preparation of mammalian expression vectors

4.2.1 *DNA enzymatic digestion and de-phosphorylation*

Backbone expression vectors or PCR products were enzymatically digested with NEB restriction endonucleases. Total PCR product or 2-5 µg of plasmid DNA were incubated in a final volume of 25 µl containing the appropriate reaction buffer (depending on the enzyme combinations) and 0.5 µl of each enzyme. The reaction was incubated for 3-4 hours at 37°C. Backbone vectors were then directly de-phosphorylated with Antarctic phosphatase (NEB) for an additional 30 minutes at 37°C to prevent re-ligation. DNA fragments were then purified by gel electrophoresis before further processing.

4.2.2 *DNA ligation*

To achieve ligation of DNA fragments and the plasmid backbone, different ratios were tested and optimized for each combination used. Ligation reactions were carried out with 1 µl of T4 DNA ligase in a final volume of 15 µl. The ligase was directly used for transformation of competent bacteria after overnight incubation at 16°C.

4.2.3 *Transformation of chemocompetent bacteria*

To transform ligated DNA into DH5α *E. coli*, competent cells were allowed first to thaw on ice and added with 10 µl of the ligase reaction. Bacteria were then incubated on ice for 30-45 minutes and heat shocked at 42°C for 60-90 seconds. After heat shock, bacteria were allowed to rest for 2 additional minutes on ice before 1 ml of LB medium was added and incubated at 37°C for 45 minutes while shaking at 250 rpm to allow production of antibiotic resistance. Cells were then plated on antibiotic-supplemented plates and incubated over-night at 37°C. Single colonies were picked and further grown for validation.

4.2.4 *DNA sequencing*

Newly generated expression vectors were always double-validated via restriction digestion and sequencing. Sequencing was carried out by GATC. Sequencing results were aligned with the predicted sequence generated *in silico*. Possible mismatches were further validated using sequencing chromatograms to identify possible technical mistakes in the sequencing results.

4.2.5 *Generation of the constructs for in vitro protein expression*

RFP-Creld1 expression vectors were cloned by amplification of the coding sequence of mCreld1, excluding the predicted signal peptide by overhang-PCR using a cDNA template and artificially adding the restriction sites EcoRI and SalI at the 5' and 3' of the coding sequence respectively. The newly added restriction sites were used to clone the coding sequence into the pEYFP-C1 backbone vector. The YFP tag was consequently replaced with a Creld1 signal peptide in front of an mRFP tag generating an in-frame sequence coding for N-terminally RFP-tagged Creld1. The signal peptide-RFP sequence was generated *in vitro* as a gBlock (by IDT) and cloned using the AgeI and EcoRI restriction sites. The deletion mutant for the extracellular domain of Creld1 (*RFP-Creld1-ΔN*) was generated by PCR amplification of the 3' region of Creld1 coding for the transmembrane and intracellular domains. The PCR product was then cloned into the RFP-Creld1 backbone as replacement of the original coding sequence using the SalI and EcoRI restriction sites. The deletion mutants for the intracellular domain of Creld1 (*RFP-Creld1-ΔC1 and RFP-Creld1-ΔC2*) were cloned by amplification of a truncated variant of Creld1 and consequently replaced in the RFP-Creld1 backbone using the SalI and EcoRI restriction sites, a stop codon was artificially added to allow correct translation of the proteins. Finally, the soluble Creld1 cytosolic domain (RFP-Creld1-solCt) was cloned as an overlapping PCR between the mRFP-tag and Creld1 intracellular domain and cloned into the pEYFP-C1 backbone removing the YFP tag.

4.3 Polymerase Chain Reaction (PCR)

4.3.1 *High-fidelity amplification of DNA fragments*

DNA fragments used for the generation of expression vectors were amplified with Phusion High Fidelity DNA polymerase to avoid point mutations being introduced by the polymerase reaction. Each different reaction was optimized accordingly to the following table:

Component	*Amount for each reaction*
Nuclease-free water	To 20 µl
5x Phusion High Fidelity buffer	4 µl
10 mM dNTPs	0.4 µl
10 µM Forward primer	1 µl
10 µM Reverse primer	1 µl
Template DNA	50-100 ng
Phusion DNA polymerase	0.2 µl

The reaction was then carried out using the following program:

Step	*Temperature*	*Time*
Initial denaturation	98°C	1 min
Denaturation	98°C	10 sec
Annealing	45-72°C	30 sec
Amplification	72°C	30 sec per Kb
		Repeat 30-35x
Final extension	72°C	5 min
Hold	4°C	--

Table 18 General protocol for high fidelity amplification of DNA fragments

Each reaction was then analysed on an agarose gel and specific bands were purified as described above.

4.3.2 *Genotyping PCR*

DNA extracted from mouse tails or ear punches was used to identify the genotype of the mouse used for all experiments. For each reaction, positive and negative controls were also used.

4.3.2.1 Creld1 flox

Protocol

Component	Amount for each reaction
Nuclease-free water	9.63 µl
5x GoTaq buffer	3 µl
10 mM dNTPs	0.3 µl
10 µM EU5 primer	0.75 µl
10 µM EU6 primer	0.75 µl
Template DNA	0.5 µl
GoTaq	0.07 µl

Program

Step	Temperature	Time
Initial denaturation	95°C	3 min
Denaturation	95°C	15 sec
Annealing	61°C	20 sec
Amplification	72°C	25 sec
		Repeat 39x
Final extension	72°C	3 min
Hold	12°C	--

Table 19 Protocol used for genotyping PCR of Creld1 flox animals

4.3.2.2 CD4-Cre

Protocol

Component	Amount for each reaction
Nuclease-free water	14.45 µl
5x GoTaq buffer	4 µl
10 mM dNTPs	0.2 µl
50 µM CD4-Cre_F primer	0.2 µl
50 µM CD4-Cre_R primer	0.2 µl
100 µM Creld2-WT_F primer	0.1 µl
100 µM Creld2_R primer	0.1 µl
Template DNA	0.5 µl
GoTaq	0.07 µl

Program

Step	Temperature	Time
Initial denaturation	95°C	2 min
Denaturation	95°C	30 sec
Annealing	58°C	20 sec
Amplification	72°C	45 sec
		Repeat 39x
Final extension	72°C	5 min
Hold	12°C	--

Table 20 Protocol used for genotyping PCR of CD4 Cre animals

4.3.2.3 tgROSA

Protocol

Component	Amount for each reaction
Nuclease-free water	17.8 µl
5x GoTaq buffer	5 µl
10 mM dNTPs	0.2 µl
10 µM ROSA_F1 primer	0.2 µl
10 µM ROSA_F2 primer	0.2 µl
10 µM ROSA_R1 primer	0.2 µl
10 µM ROSA_R2 primer	0.2 µl
Template DNA	1 µl
GoTaq	0.2 µl

Program

Step	Temperature	Time
Initial denaturation	95°C	3 min
Denaturation	95°C	15 sec
Annealing	61°C	15 sec
Amplification	72°C	25 sec
		Repeat 35x
Final extension	72°C	3 min
Hold	12°C	--

Table 21 Protocol used for genotyping PCR of tgROSA animals

4.3.2.4 NFAT-luc

Protocol

Component	Amount for each reaction
Nuclease-free water	To 20 µl
5x GoTaq buffer	4 µl
10 mM dNTPs	0.4 µl
100 µM NFAT-luc_F primer	0.1 µl
100 µM NFAT-luc_R primer	0.1 µl
Template DNA	0.5 µl
GoTaq	0.1 µl

Program

Step	Temperature	Time
Initial denaturation	95°C	3 min
Denaturation	95°C	10 sec
Annealing	53°C	15 sec
Amplification	72°C	30 sec
		Repeat 35x
Final extension	72°C	5 min
Hold	12°C	--

Table 22 Protocol used for genotyping PCR of NFAT luc animals

4.3.3 *qRT-PCR*

cDNA was generated from 100 ng of isolated total RNA using the Transcriptor First Strand cDNA synthesis kit (Roche). qRT-PCR was then performed using the LightCycler TaqMan master mix kit (Roche) according to manufacturer instructions. Expression was normalized on the housekeeping gene *Tbp* and displayed as fold-change over control.

4.4 Protein Biochemistry

4.4.1 *Protein extraction*

For total protein extraction for co-immunoprecipitation experiments, cells were lysed in RIPA buffer. RIPA buffer was prepared according to the downstream-use of the protein extract, for protein detection using Western blot, RIPA was prepared with Triton X-100 and for co-

immunoprecipitation NP-40 was used to preserve protein-protein interactions. Lysis buffer was freshly added with protease inhibitor mix and PMSF to inhibit protease activity and prevent protein degradation. For electrophoresis of the protein content, protein lysates were further processed by ultrasonication (3x 30 seconds on ice) to allow permeabilization and protein extraction from the nucleus. Samples were then centrifuged for 15 minutes at 16000 g to remove the membrane precipitate that could interfere with western blotting. Samples were then stored at -80°C or added with 5x gel loading buffer to a final concentration of 1x with 2% β-mercaptoethanol and heated for 5 min at 98°C to degrade secondary and tertiary structures and reduce the disulphide bonds.

4.4.2 *Quantification of protein concentration*

Bicinchoninic acid (BCA) was used to quantify total protein content in the lysate. Reactions were carried out according to the manufacturer instruction (BCA Protein Assay - Pirece). Briefly, a standard curve was obtained by preparing serial dilutions of BSA (bovine serum albumin) in the same buffer used for cell lysis. Each reaction was carried out in a final volume of 200 µl. The reaction was incubated for 30 min a 37°C after which the absorbance at 562 nm was measured. Using linear regression of the values obtained with the standard curve, the absolute protein concentration was calculated.

4.4.3 *SDS-PAGE and Western blot*

Protein separation was carried out using poly-acrylamide gels under denaturing conditions to allow, in the presence of an electric field, the separation of a mixture of proteins according to their molecular weights. SDS (sodium dodecylsulphate) was added to evenly distribute positive charges to the proteins. Different concentrations of acrylamide can be used to generate gel matrices with different pore sizes to better resolve proteins with higher molecular weights (low acrylamide concentration) or low molecular weight (high acrylamide concentration). Each gel was manually prepared freshly before the separation. Gels were composed of 2 phases, a stacking gel with lower acrylamide concertation (4%) allowing

stacking of the protein and a running phase with higher acrylamide concentration (10%) to resolve the protein content according to the molecular weight. Gel electrophoresis was carried out in SDS-running buffer first at 60 V for 30 minutes in the stacking phase and later at 100 V. Each gel was loaded with 5-10 µg of total protein from each sample.

Western blot was used to identify and quantity proteins of interest. SDS-PAGE separated proteins were transferred to a PVDF membrane previously activated for 1 minute in methanol. The membrane was then placed on top of the acrylamide gel and between two layers of Whatman paper. Protein transfer was carried out in transfer buffer for 1 hour at 100V. Due to the salt composition of the buffer and to prevent overheating of the membrane, the transfer was carried out at 4°C. Efficient transfer of the protein ladder was used as a readout of the success of the procedure. After protein transfer all protein-free spots on the membrane were saturated with 5% milk in TBST for 1 hour at room temperature. The primary antibody was then incubated with the membrane over-night at 4°C to allow specific binding of the protein of interest. The membrane was then washed 3 times with TBST for 10 minutes each and consequently incubated with the secondary antibody. Secondary antibodies used were conjugated with HRP (horseradish peroxidase) and selected to react against the species in which the primary antibody was developed. Secondary antibody was incubated for 1 hour at room temperature after which the membrane was washed other 3 times for 10 min with TBST. ECL was then added on the membrane reacting with the HRP enzyme conjugated with the secondary antibody. This reaction could then be detected using an X-ray film allowing the precise position and intensity of the signal. After film development, relative protein amounts were quantified using ImageJ and normalized to a housekeeping protein (β-Actin).

4.4.4 *Co-immunoprecipitation and mass spectrometry*

Previously transfected murine 3T3 fibroblasts were washed with 1 ml of ice-cold PBS and scraped to mechanically detach the cells from the plate without the use of enzymatic digestion. Cell suspensions were then processed according to the RFP-Trap MA protocol. Briefly; cell suspensions were centrifuged for 3 minutes at 500 g and resuspended in 200 µl of ice-cold

lysis buffer supplemented with PMSF and protease inhibitors. Cell lysis was carried out for 30 minutes on ice gently mixing every 10 minutes. Cell lysates were then centrifuged for 10 minutes at 20000 g in a chilled centrifuge, only the supernatant was collected and diluted with 300 µl of dilution buffer. Simultaneously, for each reaction, 25 µl of RFP-trap was washed twice in ice-cold dilution buffer and then added to the protein lysates. The lysates were then incubated for 1 hour at 4°C while shaking. After incubation beads where magnetically separated and washed 3 times with dilution buffer. Finally, the beads were resuspended in 100 µl of 5% SDS in PBS and heated for 5 minutes at 98°C to denature the protein and releasing them from the beads. Proteins were then reduced (5 mM DTT, 30 min at 56°C), alkylated (40 mM CAA, 60 min at 25°C) and processed using SP3 (Höhne *et al.*, 2018).Trypsin was added in a 1:50 ratio and proteins were digested at 37°C for 16 hours. Peptides were recovered and stored at -20°C prior to MS measurement. Protein mixtures were then analysed on a Q Extractive Plus Orbitrap mass spectrometer coupled with a pre-fractionation EASY nLC 12000 UPLC. Raw mass spectrometry data was processed with the MaxQuant software using standard settings and using the mouse proteome as a reference for protein identification. LFQ (label-free quantification) was enabled and used as quantitative measurement of protein content in the different conditions. Missing values were imputed using the R tool imputeLCMD, imputed table was used for the principal component analysis and fold change calculation (mass spectrometry and initial protein quantification and missing values imputation were done in collaboration with CECAD – Cologne). Significantly enriched proteins were then used to filter the BioPlex2 dataset including all first edges and all nodes to include secondary interactions. Filtered proteins were used for the generation of the network on interactions including additional CRELD1 interactors form the BioPlex2 dataset itself. Protein lists were then used for KEGG and GSEA.

4.4.5 ***Cytokine measurements***

Serum cytokines were quantified using a murine Luminex Bio-Plex of 23 analytes. Cryo-preserved serum was diluted 1:2 with assay diluent and processed according to

manufacturer's instructions (performed by Falk lab, MHH, Hannover). Experimental values too low to be quantified with the used standard curve were set to the minimal amount captured by the assay. Values were then log_2 transformed for visualization.

4.5 Confocal microscopy

Confocal microscopy images were taken using a laser scanning microscope LSM 710 DuoScan. Images were acquired with optimal resolution based on objective/detector combination at 8-bit colour depth. Laser power was set to avoid oversaturation of the signal and a detection range was chosen to prevent spill-over of other fluorescent dyes. All fixed stainings were imaged within 2-3 hours post fixation to prevent sample degradation. Images were acquired with Zen 2010 software and analysed using ImageJ.

4.6 Cell culture

Immortalized murine fibroblasts (NIH-3T3) were cultured in DMEM medium supplemented with 10% foetal calf serum and 1% penicillin/streptomycin, primary murine T cells were cultured in IMDM supplemented with foetal calf serum (10%), penicillin/streptomycin (1%), L-glutamine (1%), HEPES (5mM), natrium-pyruvate (0.5 mM) and β-mercaptoethanol (55 µM). Cells were kept at 37°C with 5% CO_2.

4.6.1 *Transient transfection of NIH-3T3 cells*

NIH-3T3 cells were used for transient transfection of recombinant proteins. Cells were transfected directly after seeding prior to attachment to the plastic with either Lipofectamine 2000 or Turbofect as transfection reagents. Transfection mix was prepared in OPTIMEM mixing plasmid DNA and transfection reagents at a ratio of 1:4 (Lipofectamine 2000) or 1:2 (TurboFect) DNA: reagents were incubated for 30 minutes at room temperature. Transfection mix was then added in a drop-wise manner. Trubofect transfection was used exclusively for the preparation of the mass spectrometry samples.

4.6.2 *NFAT-GFP localization and Creld1 membrane staining*

For the qualitative assessment of NFATc1 localization, NIH-3T3 cells were transfected with NFATc1-GFP in combination with different RFP-Creld1 constructs. Briefly, cells were seeded and directly transfected on ibidi µ-slides (8 wells, ibiTreat) and incubated for 24 hours to allow the expression of the recombinant proteins. Cells were then fixed for 4 minutes with 4% methanol-free PFA and analysed by confocal microscopy. NFATc1 localization was manually determined following the localization of the GFP-tag in co-transfected cells and classified as "nuclear", "cytosolic" or "nuclear/cytosolic" when residual signal was still present at the cytosol. Creld1 extracellular staining was performed by short fixation of the cells (as described above) and staining with α-Creld1 antibody (1:400 in TBS + 1% BSA) under non-permeabilizing conditions for 2 hours at room temperature. After washing in staining buffer, cells were incubated with the correct secondary antibody (α-goat Alexa488 conjugated 1:500 or Alexa647 conjugated 1:500). membrane transport inhibitor (Brefeldin A) or thapsigargin (1 µM) was also added 4 hours or 45 minutes respectively before initial fixation of the cells.

4.6.3 *Fluorescence protease protection assay*

CD3δ-CFP and YFP-CD3δ constructs were kindly provided by Holger Lorenz (ZMBH, Heidelberg). The assay was performed on an 8-well µ slide (ibidi) and live-imaged on an LSM 710 DuoScan confocal microscope according to Lorenz et al. (Lorenz *et al.*, 2006). Briefly, cells were seeded at 30,000 cells per well and directly transfected with 100 ng of each DNA plasmid; 24 hours post-transfection, cells were washed twice with KHM buffer and treated with 20 µM digitonin for 3 minutes to permeabilize the plasma membrane. Efficient plasma membrane permeabilization was assessed by free diffusion of soluble proteins after treatment. After permeabilization, cells were incubated with a final concentration of 5mM of trypsin and incubated for 9 additional minutes to allow digestion of cytosol-exposed fluorescent proteins. Cells were finally treated with Triton X-100 to allow trypsin to digest peptides inside sub-cellular compartments (Lorenz *et al.*, 2006). For each of the steps, a control protein was used;

plasma membrane permeabilization was controlled with a soluble YFP (pEYFP), trypsin activity prior and after Triton X-100 treatment was controlled with CD3δ-CFP and YFP-CD3δ respectively, tagging CD3δ in the cytosol facing and ER-lumen facing termini. Confocal imaging was performed throughout the procedure taking a picture every 30 seconds. Fluorescence intensity was then quantified using ImageJ and normalized to the fluorescence level before the digitonin treatment.

4.6.4 *In vitro T cell differentiation and rescue experiment*

Naïve $CD4^+$ T cells ($CD3^+CD4^+CD25^-CD44^{low}CD62L^{high}$) were purified by FACS (fluorescence activated cell sorting) after pre-enrichment for CD4+ T cells using MACS negative selection. Naïve T cells were stimulated with plate-bound α-CD3 (3µg/ml) and soluble α-CD28 (1µg/ml) activating antibodies. Cells were differentiated for 5 days with a cocktail of cytokines and cytokine blocking antibodies. Th_0 cells were incubated with only supplement of α-IFNγ and α-IL-4 blocking antibodies (2 µg/ml), Th_1 cells were supplemented with IL-12 (10 ng/ml) and α-IL-4 (2 µg/ml), Th_2 with IL-4 (10 ng/ml) and α-IFNγ (2 µg/ml), Th_9 with α -IFNγ (2µg/ml), IL-4 (10 ng/ml) and TGFβ (0.3 µg/ml), iTregs with α-IL-4 and α-IFNγ, TGFβ (2 ng/ml), IL-2 (100 U/ml) and retinoic acid (2.5 nM) and Th_{17} with α -IL-4 and α-IFNγ (2 µg/ml), IL-6 (20 ng/ml), and TGFβ (0.3 µg/ml). Th_9 cells, unlike the other subtype, were differentiated on IgG-coated plates with soluble α-CD3 (0.25 µg/ml) and soluble α-CD28 (1 µg/ml). Th_0, Th_2 and Th_9 cells were rested on day 3 and 4 in round bottom plates with 100U/ml IL-2 and re-exposed to the respective differentiation medium at day 4. After differentiation, cells were stimulated for 4 hours with PMA and ionomycin in the presence of inhibitors of protein secretion (Brefeldin A and Monensin) prior to intracellular staining and flow cytometry.

Rescue experiment was performed with MACS purified $CD4^+$ T cells treated ex-vivo for 24 hours with rmIL-7 (1 ng/ml), IL-7/IL-15 (1 and 10 ng/ml respectively) Wnt3a (40 ng/ml) or BI-5521 (30 nM).

4.6.5 *Metabolic analysis of activated T cells*

Metabolic changes in $CD4^+$ T cells upon TCR stimulation were measured using the Seahorse XFe96 analyser. $CD4^+$ T cells were purified magnetically by negative selection (MACS) and seeded on poly-L-lysine coated Seahorse cell culture plates at a concentration of 300,000 cells per well. Cells were then incubated for 1 hour at 37°C without controlled CO_2 levels before starting the measurement. Baseline ECAR (extra cellular acidification rate) was measured for 32 minutes (4 cycles) before injection of soluble α-CD3 (3 µg/ml) and α-CD28 (1 µg/ml) antibodies. After stimulation, ECAR was measured for 2 hours and 40 minutes (20 cycles). Each cycle was defined as 3 minutes of mixing and 5 minutes of measurement. To normalize for the possible difference in total cell numbers in each well, crystal violet staining was performed. Briefly, cells were fixed with 100 µl of 4% PFA for 5 minutes and then stained with 100 µl of 0.05% crystal violet staining for 30 minutes. After staining, cells were washed twice with H_2O and left to air-dry. Crystal violet was then resuspended with 200 µl of methanol and the absorbance was measured at 590 nm.

4.6.6 *Luciferase assay*

NFAT-luc transgenic $CD4^+$ T cells were purified by MACS sorting and used to assess the activation levels of the NFAT family of transcription factors. Pooled $CD4^+$ T cells from the spleen and peripheral lymph nodes were seeded at a concentration of 1 million/well and stimulated with plate-bound α-CD3 (3 µg/ml) and soluble α-CD28 (1 µg/ml) activating antibodies also in combination with Cyclosporin A (CsA). As a negative control, cells were incubated in pure medium and as positive control, PMA and ionomycin were added to the medium. After 1, 2 or 3 days of treatment cells were washed in PBS and counted. Firefly luciferase intensity was measured with the Luciferase Assay System (Promega) accordingly to manufacturer's manual on a MicroLumatPlus plate reader (Berthold). Luciferase intensity was subtracted of the plate background, normalized on the total cell number, and shown as fold change over control.

4.6.7 *CFSE staining*

Cells were labelled with Carboxyfluorescein succinimidyl ester (CFSE) to monitor the proliferation over time, labelling was performed at a final concentration of 0.5 µM for 8 minutes. 100,000 sorted conventional $CD4^+$ T cells ($CD4^+CD25^-$) were stimulated with α-CD3/ α-CD28-conjugated beads in a ratio of 1:3 beads/cell. After 3 days of stimulation, the samples were entirely acquired by flow cytometry. To calculate precisely the total cell number the stimulating beads were used as a reference since a known number of beads was added to each sample. For Creld1-induced proliferation, cells were CFSE labelled and consequently transfected with different Creld1 constructs as described above. CFSE dilution was then measured after 24, 48 and 72 hours after transfection. Cells were also measured at day 0 both with and without CFSE labelling and used as a reference point for the calculation of the number of cellular divisions using the following equation:

$div_{num} = log_2\left(\frac{\tilde{M}_{day0}-\tilde{M}_{unstained}}{\tilde{M}_{dayX}-\tilde{M}_{unstained}}\right)$ assuming a dilution factor of 2 at each cellular division.

4.7 Flow cytometry and cell sorting

4.7.1 *Cell preparation from complex organs or cell culture plates*

Preparation of cells from the spleen and peripheral lymph nodes was done by mechanical digestion of the tissue trough a 100 µm strainer using a syringe plunger. Cell suspension was then moved to a collection tube and the strainer was washed twice with ice-cold PBS. Lymph nodes were now directly processed for flow cytometry. The spleen, in contrast was first treated with red blood cell lysis buffer (RBCLB) to remove the erythrocytes from the cell suspension. For each spleen, 1 ml of room-temperature RBCLB was added and the tube was shook for 2 minutes manually before washing with 40 ml of ice-cold PBS. Complex organs, such as the colon and small intestine were processed as follows to prepare a single cell suspension. Colon and small intestine were first cleaned. The Peyer's patches were removed and the organ was

cut longitudinally. The organ was then cut into pieces of approximately 1 cm and stored in digestion buffer 1 (DB1) and incubated at 37°C for 20 min to allow removal of the mucosal tissue. Tissue was then moved to digestion buffer 2 and incubated at 37°C for 15 min to remove the epithelial cell. This process was repeated 3 times. Finally, a last incubation in DB3 for 10 minutes was used to allow the clean-up from serum and EDTA. The tissue was then moved to a 6-well plate and treated with DNAse and liberase to finally digest the tissue. The enzymatic digestion was carried out for 45 minutes and the cell suspension was then washed and processed for flow cytometry. NIH-3T3 were treated with trypsin to prepare a single cell suspension; after 2 or 3 minutes enzymatically separated cells were washed twice with PBS and analysed.

4.7.2 *MACS and FACS purification*

$CD4^+$ T cells were purified either by MACS (magnet-activated cell sorting) or FACS (fluorescence-activated cell sorting). MACS sorting was performed according to manufacturer´s instructions. Briefly, a single cell suspension in MACS buffer was first concentrated to 100 million cells/ml, 3.4 µl/0.1 ml of antibody mix was then added and incubated 10 minutes at room temperature. Cells were then washed with 10 ml of MACS buffer and resuspended at the original volume after 5 minutes of centrifugation (400g). Streptavidin magnetic beads were then added and, after 5 minutes, the cells were loaded on a LS MACS column. Flow-through of enriched $CD4^+$ T cells were collected and used for experiments or FACS sorting. For the purification of Naïve $CD4^+$ T cells, MACS-enriched $CD4^+$ T cells were stained with fluorescently labelled antibodies for 30 min in MACS buffer at 4°C. Cells were then FACS sorted on a BD FACS AriaIII. Cells were sorted with a 70 µm nozzle into cooled glass FACS tubes filled with 1 ml of FCS.

4.7.3 *Flow cytometry*

A single cell suspension was stained extracellularly with fluorescently labelled antibodies for 30 minutes at 4°C in PBS with blocking antibodies against the Fc receptors (α-CD16, α-CD32).

Creld1 staining was performed in two steps, first cells were incubated with α-Creld1 (1:200) antibody for 2 hours at 4°C in MACS buffer followed by secondary antibody (anti-goat Alexa 488 1:400) for 45 minutes at room temperature. If no intracellular staining was needed cells were directly analysed. For intracellular staining, cells were first fixed for 10 minutes in 4% PFA (methanol-free) and washed twice with PermBuffer (FoxP3 Fix/Perm Kit) and then stained for intracellular proteins for 30 minutes at room temperature in PermBuffer. If nuclear proteins (e.g, transcription factors) were stained, the cell suspension was fixed with FixBuffer (FoxP3 Fix/Perm Kit) for 1 hour and stained for 30 minutes with antibody mix at room temperature. Finally, two washing steps (1x PermBuffer, 1x PBS) were used to remove all the unbound antibody and to change buffer to PBS before flow cytometric analysis. If both intracellular and nuclear protein were detected, the two staining procedures were performed consequently. Fluorescently labelled cells were recorded on a BD LSRII configured with violet, blue, yellow/green and red lasers.

4.8 Bioinformatic analysis

4.8.1 *RNA-seq analysis*

The Illumia FASTQ output file was pseudo-aligned using the Kallisto tool set. Counts were then processed according to the DEseq2 pipeline and finally rlog-transformed for visualization. Differentially expressed genes with $p<0.01$ for each comparison were used as input for CoCena2 co-expression analysis, correlated genes ($p<0.05$, cor>808) were used for network and clustering analysis. Transcription factor CoCena2 analysis was performed on all expressed transcription factors filtering for correlation>0.888 with $p<0.05$. For each identified CoCena2 module, GSEA was calculated based on the gene contributing to each module. RNA-seq analysis was done in collaboration with Jonas Schulte-Schrepping and Dr. Thomas Ulas (GSE133863).

4.8.2 ***Analysis of publicly available human transcriptomic data***

4.8.2.1 Analysis of the CEDAR dataset

The uncorrected CEDAR database was downloaded from the CEDAR web portal. Transcriptome data were filtered to include only healthy donors and corrected for experimental batch, sex and smoking habits using the batch correction tool provided in the limma pipeline (R). CRELD1 expression was then binned on the 5^{th} and 95^{th} defining the two groups $CRELD1^{low}$ and $CRELD1^{high}$ respectively. The transcriptome of the two groups was compared according to the limma pipeline comparing $CRELD1^{low}$- $CRELD1^{high}$. Ranked gene lists from the comparison were used for GSEA of selected pathways. Gene set variation analysis (GSVA) was also performed for the cKO down and cKO up signature. Each cell type analysed was independently binned and analysed as described above.

4.8.2.2 Analysis of the ImmVar dataset

Expression data from the ImmVar study were downloaded from the GEO as pre-processed data and no further correction was carried out. CRELD1 expression was then used for the binning on the on the 5^{th} and 95^{th} defining the two groups $CRELD1^{low}$ and $CRELD1^{high}$ respectively and analysed as described for the CEDAR dataset. Also in this case, each cell type was independently binned for the analysis.

4.8.2.3 Analysis of PBMC sample collection

Collection of Affymetrix expression profiles from Herresthal et al. 2019 was corrected for the study using the batch correction tool provided in the limma pipeline. First, the dataset was filtered for only health donors and used as previously described for the CEDAR dataset. For the comparison between heathy and disease donors, all healthy samples were compared with specific disease samples. Between the two groups, CRELD1 expression was evaluated and GSEA was performed for selected gene sets in the comparison of disease-healthy.

4.8.2.4 Analysis of the 500FG dataset

Raw RNA-seq counts were fist rlog transformed and corrected for sex using the batch correction tool provided by the limma pipeline (R). Donors were then binned using CRELD1 expression on the 10th (CRELLD1^{low}) and 90th (CRELD1^{high}) percentiles. As previous comparison between the transcriptome of the two groups was used for GSEA and evaluation of single genes. Using the same grouping, the two absolute cell counts were analysed and population and cytokine secretion were compared.

4.9 Quantification and statistical analysis

Detailed description of the statistical analysis of each experiment can be found in the figure legends. “n” number indicated the number of biological replicates derived from one or more technical replicates. Statistical significance was determined using an unpaired two-tailed Student’s t test or one-way ANOVA, $p<0.05$ was considered significant ($p<0.05$ *, $p<0.01$ **, $p<0.001$ ***, $p<0.0001$ ****). GraphPad Prism 5, R 3.5.1 and Microsoft Excel 2016 were used for the analysis.

5 Results

5.1 Generation and validation of a CD4$^+$ T cell-specific conditional knock-out mouse model for Creld1

Creld1 was recently identified as a crucial regulator of the NFAT pathway during heart development (Mass *et al.*, 2014). Considering the importance of the NFAT transcription factor family in CD4$^+$ T cells, and that Creld1 is expressed throughout all adult tissues, it was of interest to study the possible involvement of Creld1 in some of the key biological functions of CD4$^+$ T cells.

Due to the embryonic lethality observed in Creld1 complete knock-out (KO) mice, a conditional KO model of Creld1 in CD4$^+$ T lymphocytes was generated. Creld1^{flox} mice (EUCOMM) were crossed with CD4^{Cre} animals (**fig 5.1 A**). These mice carry the Cre recombinase under the control of the CD4 promoter, so the recombinase will be expressed in all CD4 expressing cells leading to the selective rearrangement of the *Creld1* genomic locus in lymphocytes. As shown previously (Lee *et al.*, 2001), CD4^{Cre} mice will lead to efficient recombination of a target locus in the late double negative stage of T cell development. The recombination will then be close to 100% in the double positive developmental stage (CD4$^+$/CD8$^+$).

Creld1^{flox} mice carry two LoxP sites in cis arrangement and oriented in the same direction between exon three and exon six. The recombination of the locus mediated by Cre recombinase will lead to the deletion of the four exons between the loxP sites. As a result of this genomic rearrangement, a frame shift occurs in the coding sequence of *Creld1*, leading to a premature stop codon (**fig 5.1 A/B**). Concerning the remaining protein (**fig 5.1 B**), it was shown not to be functional. When Cre is expressed ubiquitously (pgk-Cre) in the background of Creld1$^{flox/flox}$ mice, these mice phenocopy the complete KO of Creld1 (personal communication with Dr. E. Mass).

In this study CD4^{Cre}; Creld1$^{flox/flox}$ mice were compared with Creld1$^{flox/flox}$ or Creld1$^{flox/+}$ animals, referred to as control (**fig 5.1 C**)

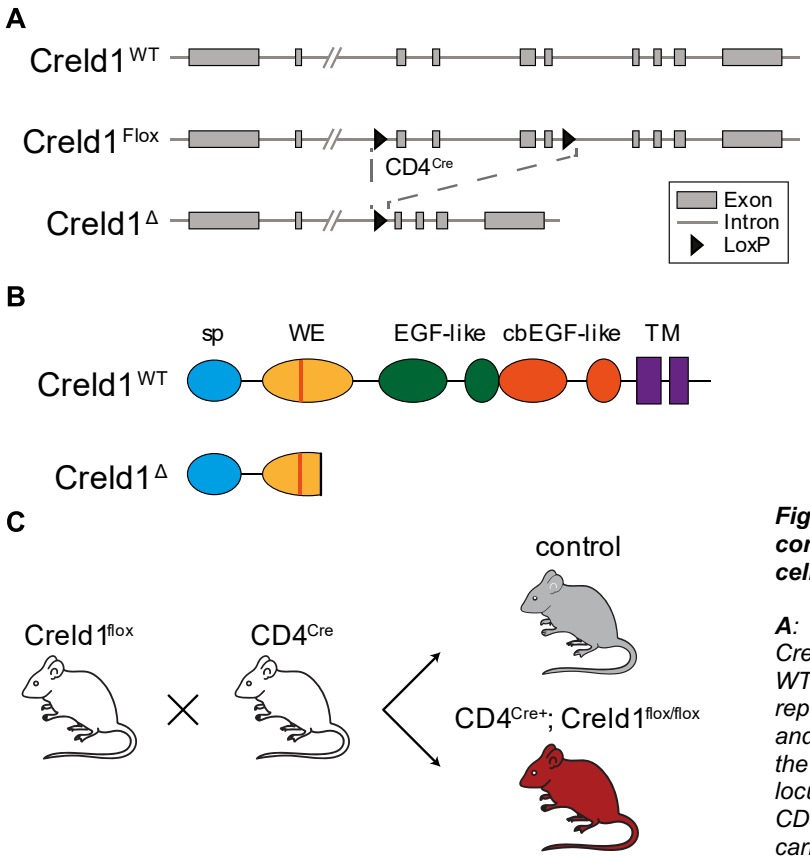

Figure 5.1 Generation of a conditional KO for Creld1 in CD4 T cells

***A**: schematic representation of the Creld1 genomic region comparing the WT with the flox locus. **B**: schematic representation of CRELD1 WT protein and the truncated version produced by the rearrangement of the genomic locus. To study the role of Creld1 in CD4+ cells $CD4^{Cre}$;$Creld1^{flox/flox}$ mice carrying both Creld1 mutated alleles were compared to control animals (**C**).*

5.1.1 *Validation of $CD4^{Cre}$ recombination efficiency*

To confirm the capability of $CD4^{Cre}$ to effectively recombine a genomic region, $CD4^{Cre}$ animals were crossed with $Rosa26^{stop\text{-}tdTomato}$ animals (**fig 5.2 A**). These mice contain the coding sequence for the tdTomato reporter preceded by a stop codon flanked by two loxP sites in the Rosa26 locus. In this setting, the mice will express the fluorescent tdTomato reporter only after efficient recombination and have been used to validate the recombination efficiency in major T cell populations.

Spleens from *$CD4^{Cre}$; $Rosa26^{stop\text{-}tdTomato}$* or control animals (wild type or $Rosa26^{stop\text{-}tdTomato}$) were harvested, homogenized and stained with fluorescently labelled antibodies. The cell suspension was then analysed by flow cytometry to identify the percentage of cells, for each specific populations of T lymphocytes, in which an efficient recombination of the floxed site occurred; thus, expressing the reporter gene tdTomato.

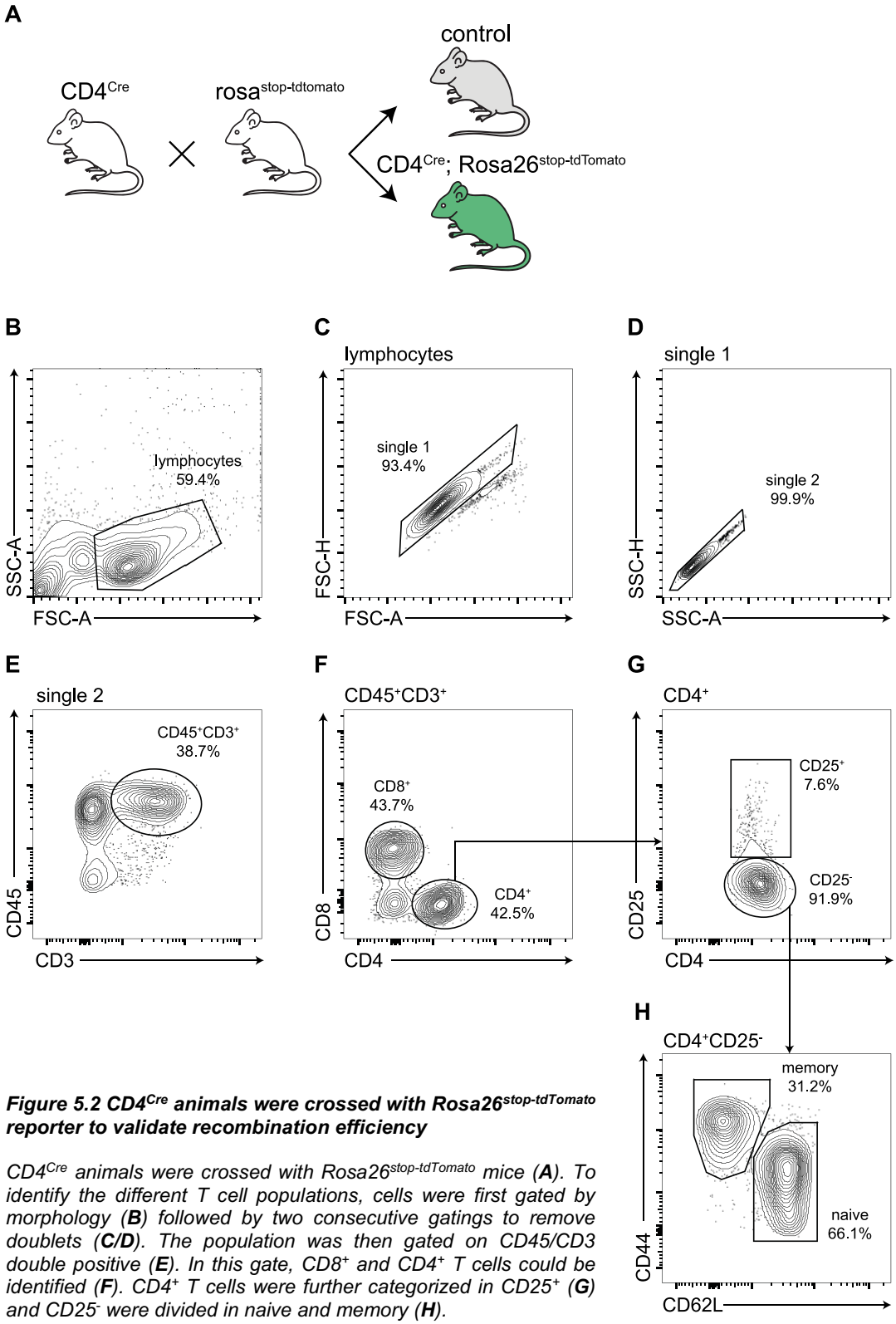

Figure 5.2 CD4^{Cre} animals were crossed with Rosa26$^{stop\text{-}tdTomato}$ reporter to validate recombination efficiency

*CD4^{Cre} animals were crossed with Rosa26$^{stop\text{-}tdTomato}$ mice (**A**). To identify the different T cell populations, cells were first gated by morphology (**B**) followed by two consecutive gatings to remove doublets (**C/D**). The population was then gated on CD45/CD3 double positive (**E**). In this gate, CD8^{+} and CD4^{+} T cells could be identified (**F**). CD4^{+} T cells were further categorized in CD25^{+} (**G**) and CD25^{-} were divided in naive and memory (**H**).*

The strategy used to identify specific cell populations involved first the selection of cells based on morphology (**fig 5.2 B**), thus removing all debris derived from dead cells; and doublets were then eliminated with two consecutive gates (**fig 5.2 C/D**). Lymphocytes were then

selected according to the co-expression of CD45 and CD3 (**fig 5.2 E**). $CD4^+$ and $CD8^+$ T cells were then defined based on the expression of either CD4 or CD8 at the cell membrane (**fig 5.2 F**). $CD4^+$ T lymphocytes were further divided into $CD25^+$ according to CD25 expression (a mixture of Tregs and effector $CD4^+$ T cells - **fig 5.2 G**) and, in the population not expressing CD25, naïve ($CD44^{low}$ and $CD62L^{high}$) and memory ($CD44^{high}$ and $CD62L^{low}$) $CD4^+$ T cells were identified (**fig 5.2 H**). For each identified population, the percentage of cells expressing the tdTomato reporter was quantified in both *$CD4^{Cre}$; $Rosa26^{stop\text{-}tdTomato}$* or controls (**fig 5.3 A/B**). It was clearly evident that the recombination was very efficient, in fact we can observe a percentage of tdTomato expressing cells greater than 97% in all the animals analysed and in all the populations identified even in for $CD8^+$ lymphocytes (**fig 5.3 A/B**). Indeed, $CD8^+$ T cells undergoes a developmental stage where both CD4 and CD8 are expressed (DP) in which the recombination of the locus takes place.

In contrast, in all animals used as controls, no cells expressing tdTomato have been identified (**fig 5.3 A/B**).

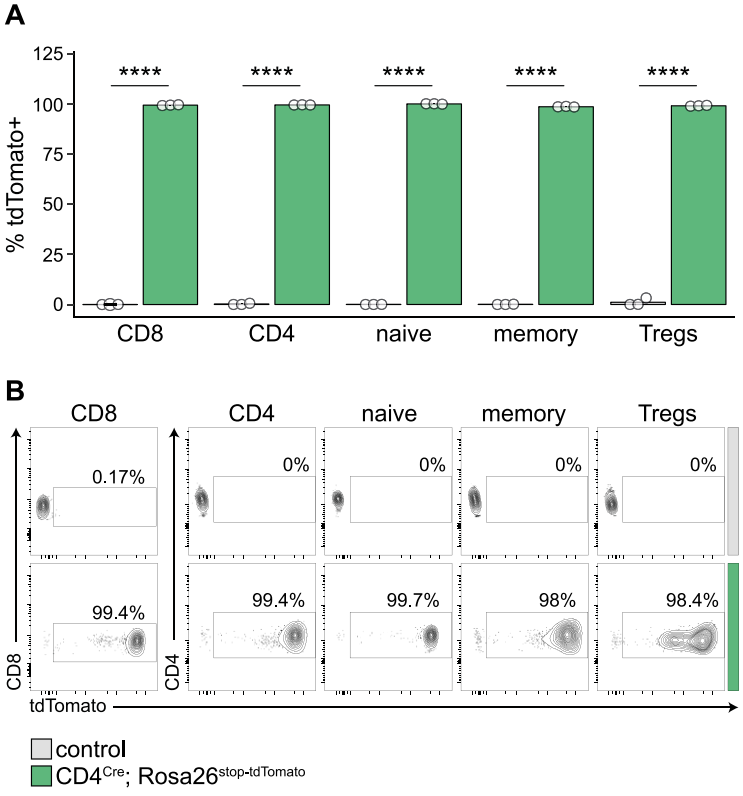

Figure 5.3 $CD4^{Cre}$ mouse line efficiently recombines in T cells

*Percentage of tdTomato-positive cells in spleen is shown for the main T cell populations analysed by flow cytometry from control or $Rosa26^{stop\text{-}tdTomato}$-derived cells (n=3). Cell were gated on single cells/$CD45^+$/$CD3^+$ Exemplary flow cytometry plot (**B**) and summary statistics (**A**) is shown. Statistical significance was tested by unpaired t-test (**** p<0.0001).*

So far, only the ability of the $CD4^{Cre}$ line to specifically target the cell population subject of this study were tested. As a next step, we tested whether Creld1 expression can be deleted in the $CD4^+$ T cell compartment with this KO strategy. For this purpose, spleens from *$CD4^{Cre}$; $Creld1^{flox/flox}$* or control animals were collected and stained with fluorescently labelled antibodies. Naïve $CD4^+$ cells were then sorted according to their expression of cell markers as described above ($CD3^+CD4^+CD25^-CD44^{low}CD62L^{high}$). *Creld1* expression was analysed in the purified cell population by qRT-PCR with primers capable of amplifying only the wild-type (WT) transcript (**fig 5.4 A**) showing no signal in naïve $CD4^+$ cells from conditional KO animals.

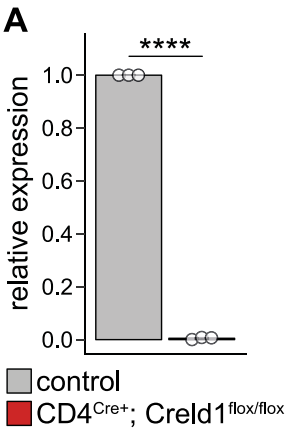

Figure 5.4 Creld1 genomic locus can be efficiently recombined in $CD4^+$ T cells

A**: Creld1 expression in sorted $CD4^+$ T cells by qRT-PCR normalized on Tbp, expression is shown as fold change over control (n=3). Statistical significance was tested by unpaired t-test (* p<0.0001).*

These findings clearly show that recombination is also effective in the *Creld1* locus making this animal model suitable to studying the role of Creld1 in $CD4^+$ T lymphocytes.

5.2 Characterization of the immune status of young conditional Creld1 KO mice

First, CD4-specific conditional KO mice were analysed to assess whether the development of $CD4^+$ T lymphocytes occurred normally and whether these cells were typically distributed across the body in adult mice. For this purpose, 12 to 14-week-old mice were analysed for the correct development of T lymphocytes in the thymus, and their distribution in the secondary lymphoid organs and peripheral tissues.

5.2.1 *$CD4^{Cre}$; $Creld1^{flox/flox}$ show minor macroscopic differences*

First, the mice were analysed at macroscopic level. Total body weight was unaltered in *$CD4^{Cre}$; $Creld1^{flox/flox}$* mice compared to control mice from the same litter. The body weight of each mouse was then used to normalize the weight of each organ analysed (**fig 5.5 A**). The weight of the spleen appeared slightly decreased in conditional KO mice (**fig 5.5 B**) while for liver and kidney no differences were found either in weight (**fig 5.5 C/D**) or appearance (data not shown). Interestingly, in both, the colon and the small intestine, the length appeared slightly increased in *$CD4^{Cre}$; $Creld1^{flox/flox}$* mice (**fig 5.5 E/F**).

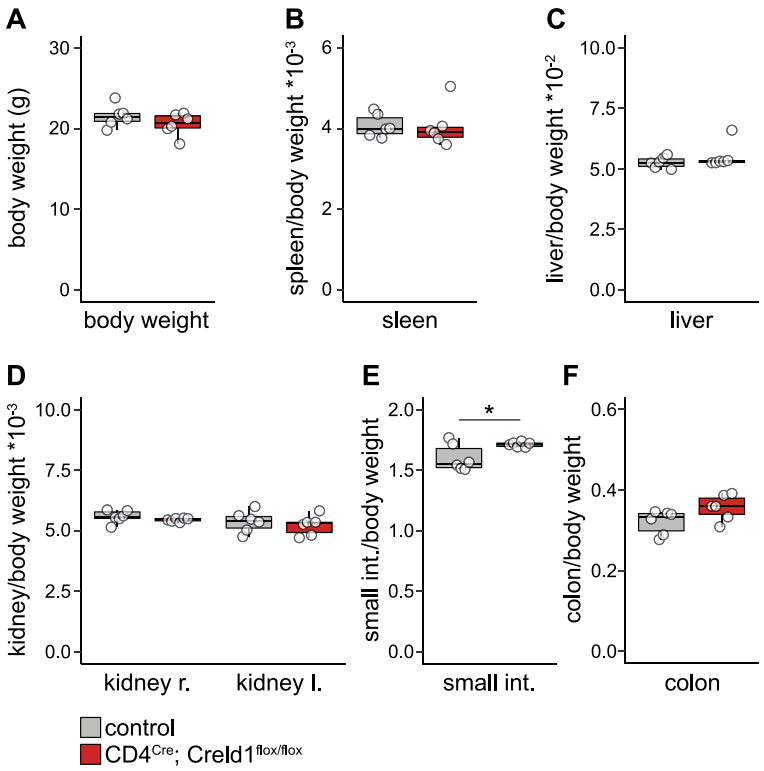

Figure 5.5 CD4^{Cre}; Creld1$^{flox/flox}$ mice do not show majour macroscopic difference

*Analysis of physical parameters of 12-week old control and CD4^{Cre}; Creld1$^{flox/flox}$ animals. Body weight (**A**), normalized weight of spleen (**B**), liver (**C**), right and left kidney (**D**), length of small intestine (**E**) and colon (**F**) are shown (n=6). Statistical significance was tested by unpaired t-test (* p<0.05).*

5.2.2 *Thymic T cell development is unchanged in CD4^{Cre}; Creld1$^{flox/flox}$ mice*

As described previously, T cell precursors in the thymus undergo four different developmental stages starting from the double negative stage before they start to express both, CD4 and CD8, to finally commit to one of these two T cell subtypes.

To analyse the development of T cells in control and *CD4^{Cre}; Creld1$^{flox/flox}$* animals, the thymus from both genotypes was harvested and manually homogenized. Single cell suspensions were then stained with fluorescently labelled antibodies and analysed by flow cytometry. The gating strategy used to identify the different T cell populations in the thymus involved at first the selection of cells by morphology (**fig 5.6 A**), followed by two consecutive gates aimed to remove the doublets (**fig 5.6 B/C**). At this stage, all CD45-expressing cells were selected (**fig 5.6 D**) and in this population the expression pattern of CD4 and CD8 was analysed (**fig 5.6 E**). Here the cells can be divided into double negative (DN – CD4$^-$CD8$^-$), the first developmental stage in the thymus, double positive (DP – CD4$^+$CD8$^+$) the second developmental stage, and two single positive stages (either CD4$^+$ or CD8+). Double negative

cells can be further subdivided into four groups based on the expression of the two surface markers CD25 and CD44 (**fig 5.6 F**).

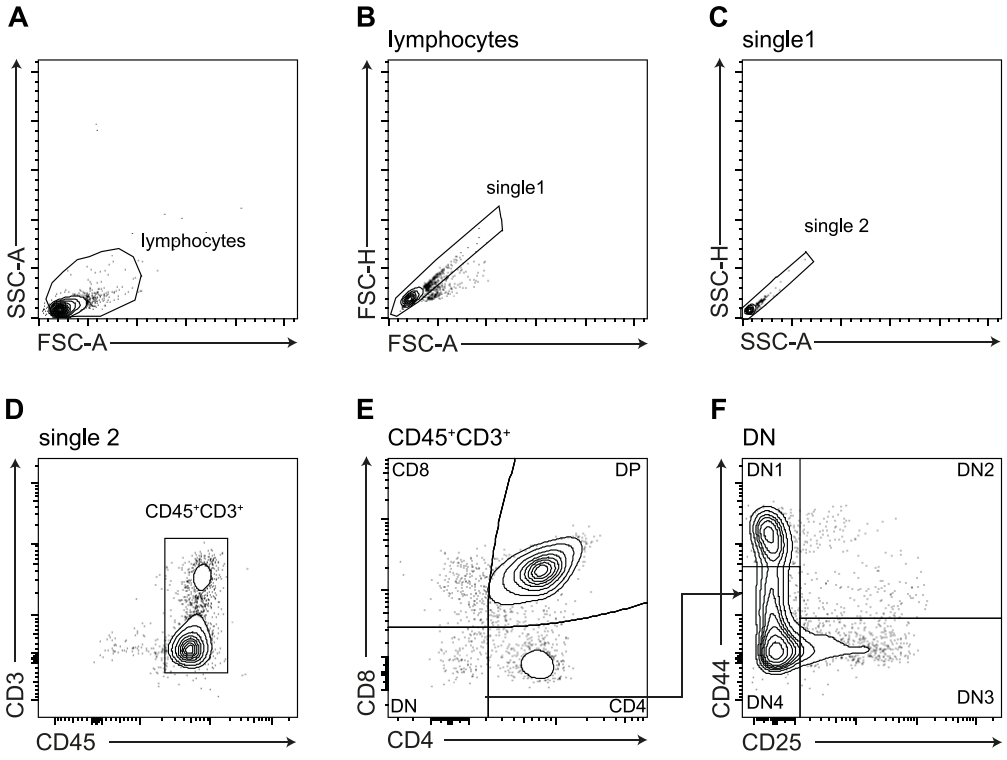

Figure 5.6 Gating strategy used to identify thymic cell populations

***A**: living cells gate; **B/C**: gating for the removal of doublets in the sample. **D**: thymocytes selection by the expression of CD45 and CD3. T cells were then separated in DN, DP ad SP by the expression of CD4 and CD8 (**E**). DN stratification into DN1 to DN4 (**F**).*

For each of the above-mentioned cell populations, the percentage relative to the parent gate and the absolute cell number was quantified (respectively **fig 5.7 A/B** and **C/D**). This analysis clearly shows that development in the thymus takes place normally in *CD4^{Cre}; Creld1$^{flox/flox}$* animals since no difference was identified in both relative percentages and absolute cell numbers in any of the populations analysed. Although we would expect an effect on T cell development in the KO of Creld1 since this process is highly regulated by the NFAT transcription factor family this result has not come unexpected. As mentioned above, the rearrangement of the genomic locus mediated by the CD4^{Cre} recombinase will take place only in the late DN4 stage so until that stage both control and *CD4^{Cre}; Creld1$^{flox/flox}$* cells will be genetically identical. Starting from the late DN4 stage to the DP stage the Cre recombinase

will be expressed and the rearrangement of the locus will lead to the production of a non-functional, truncated version of Creld1. Considering the low expression levels of Creld1 and the predicted relatively long half-life (>30h, ProtParam algorithm, ExPaSy) residual protein might be available up to early single positive stages thereby masking a possible role of Creld1 in T cell development.

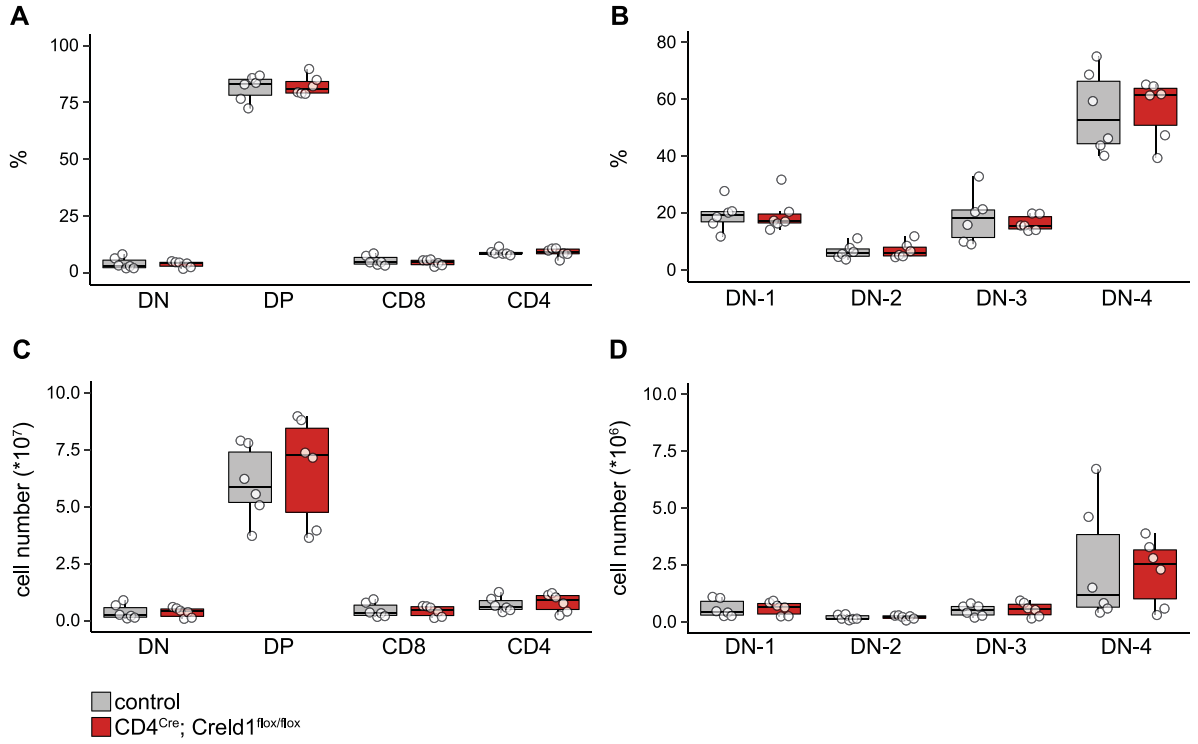

Figure 5.7 T cells develop normally in the thymus of CD4^{Cre}; Creld1$^{flox/flox}$ mice

*Thymic T cell development from 12 weeks old control and CD4^{Cre}; Creld1$^{flox/flox}$ mice was analysed by flow cytometry. **A/B**: Percentage and total cell number (**C/D**) for double negative cells (DN - CD8$^-$/CD4$^-$), double positive (DP – CD8$^+$/CD4$^+$), CD8 and CD4 T cells (**A/C**). **B/D**: Double negative developmental stages defining DN-1 (CD44$^+$/CD25$^-$), DN-2 (CD44$^+$/CD25$^+$), DN-3 (CD44$^-$CD25$^+$), DN-4 (CD44$^-$/CD25$^-$) (n=6). Statistical significance was tested by unpaired t-test (* p<0.05, ** p<0.01, *** p<0.001, **** p<0.0001).*

5.2.3 *Secondary lymphoid organs are normally populated in CD4^{Cre}; Creld1$^{flox/flox}$ mice*

Fully developed single positive T cells migrate from the thymus to the secondary lymphoid organs such as the spleen and the lymph nodes and spread throughout the body. To assess the homeostatic state of the lymphoid compartment in *CD4^{Cre}; Creld1$^{flox/flox}$* mice, secondary lymphoid organs were analysed for distribution of the main T cell populations.

Spleen, peripheral lymph nodes (a pool of inguinal and brachial lymph nodes) and mesenteric lymph nodes were analysed. As shown if figure 5.8, cells were fist gated by morphology (**fig 5.8 A**), doublets were removed with two consecutive gates (**fig 5.8 B/C**) and lymphocytes were selected as CD3$^+$ cells (**fig 5.8 D**). Lymphocytes were first separated in CD4$^+$ and CD8$^+$ T cells by the expression of the specific lineage marker (**fig 5.8 E**). CD4$^+$ T cells were then further divided into Tregs defined as positive for both CD25 and Foxp3, the hallmark transcription factor of these cells (**fig 5.8 F**). CD25$^-$ cells were subdivided into naïve and memory CD4$^+$ T cells according to the expression pattern of the markers CD44 and CD62L (**fig 5.8 G/H**).

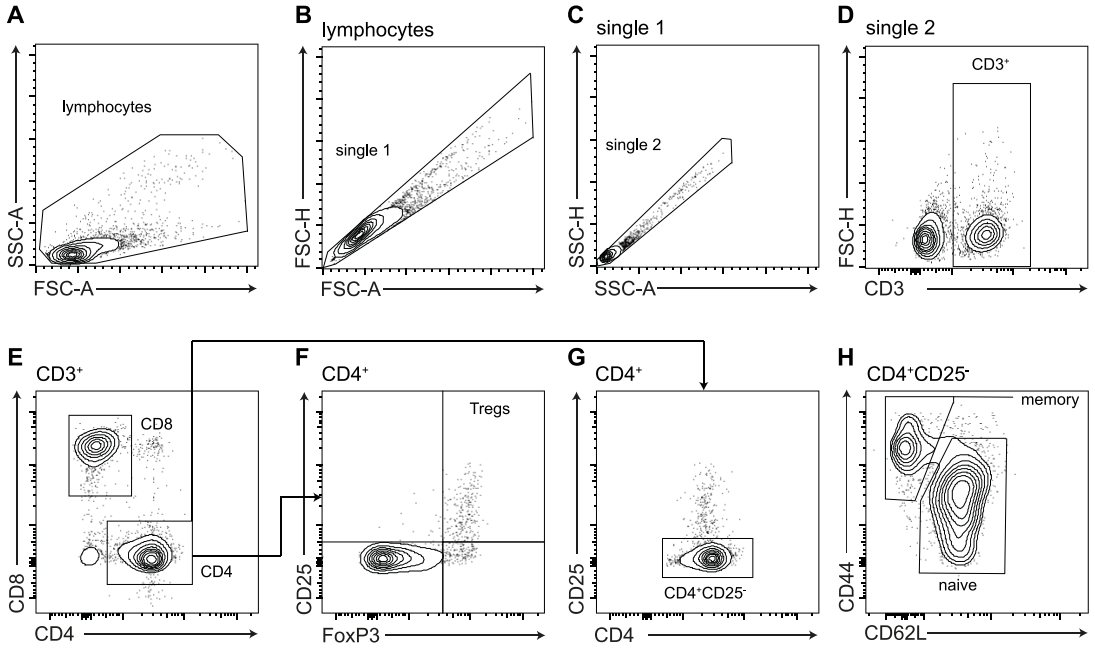

Figure 5.8 Gating strategy used to identify T cell populations in secondary lymphoid organs

***A**: Living cell gate; **B/C**: Gating for the removal of doublets in the sample **D**: Total lymphocytes were selected by the expression of CD3 at the cellular surface. **E**: Identification of $CD4^+$ and $CD8^+$ T cells. Within the $CD4^+$ population Tregs were identified by co-expression of CD25 and FoxP3 (**F**) and Tconv were defined as $CD4^+$ but $CD25^-$ cells. (**G**). **H**: Identification of naïve and memory T cells.*

For each cell population identified the total cell number and the percentage relative to the parent gate were calculated. No difference was apparent between control and *$CD4^{Cre}$; $Creld1^{flox/flox}$* animals in the spleen (**fig 5.9 A/B**), peripheral lymph nodes (**fig 5.9 C/D**) and mesenteric lymph nodes (**fig 5.9 E/F**). This result demonstrated that lymphocytes migrate to the secondary lymphoid organs populating them similarly to control animals. It therefore appears that Creld1 is not required for the development and organization of lymphocytes in young animals.

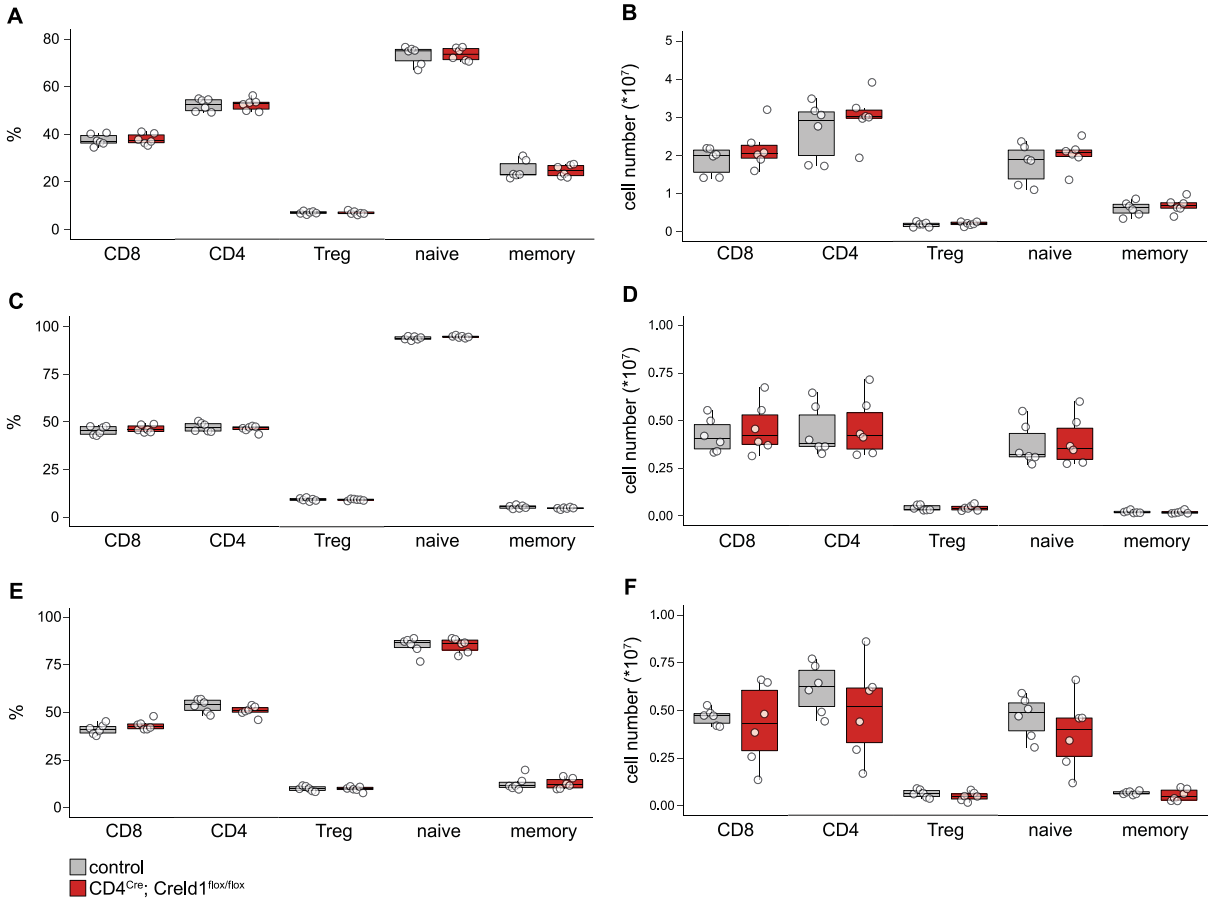

Figure 5.9 T cells populate the secondary lymphoid organs normally in CD4^{Cre}; Creld1$^{flox/flox}$ mice

*Secondary lymphoid organs from 12 week old control and CD4^{Cre}; Creld1$^{flox/flox}$ mice were analysed by flow cytometry. Spleen (**A/B**), peripheral lymph nodes (**C/D**) and mesenteric lymph nodes (**E/F**) were analysed for both relative percentage (**A/C/E**) and total cell number of different T cell populations (**B/D/F**) (n=6). Statistical significance was tested by unpaired t-test (* p<0.05, ** p<0.01, *** p<0.001, **** p<0.0001).*

5.2.4 *Peripheral tissues are normally colonised in CD4^{Cre}; Creld1$^{flox/flox}$ mice*

For the analysis of the lymphoid cells colonising peripheral tissues, such as colon and small intestine, lymphocytes were isolated from these organs and analysed by flow cytometry.

Due to the complexity of the organs analysed, the gating strategy had to be adjusted to correctly identify the cells of interest. First, dead cells were excluded using a live/dead fluorescent dye (**fig 5.10 A**), living cells were further selected by expression of CD45 isolating all immune cells (**fig 5.10 B**). At this point cells were gated by morphology (**fig 5.10 C**) and singlets were selected with two consecutive gates (**fig 5.10 D/E**). T lymphocytes were then selected by expression of both CD45 and CD3 (**fig 5.10 F**). In this gate CD4$^+$ and CD8$^+$ T cells

could be identified based on the expression of either CD4 or CD8 respectively (**fig 5.10G**). $CD4^+$ T cells were further divided into T_{regs} based on the expression of Foxp3 (**fig 5.10H**).

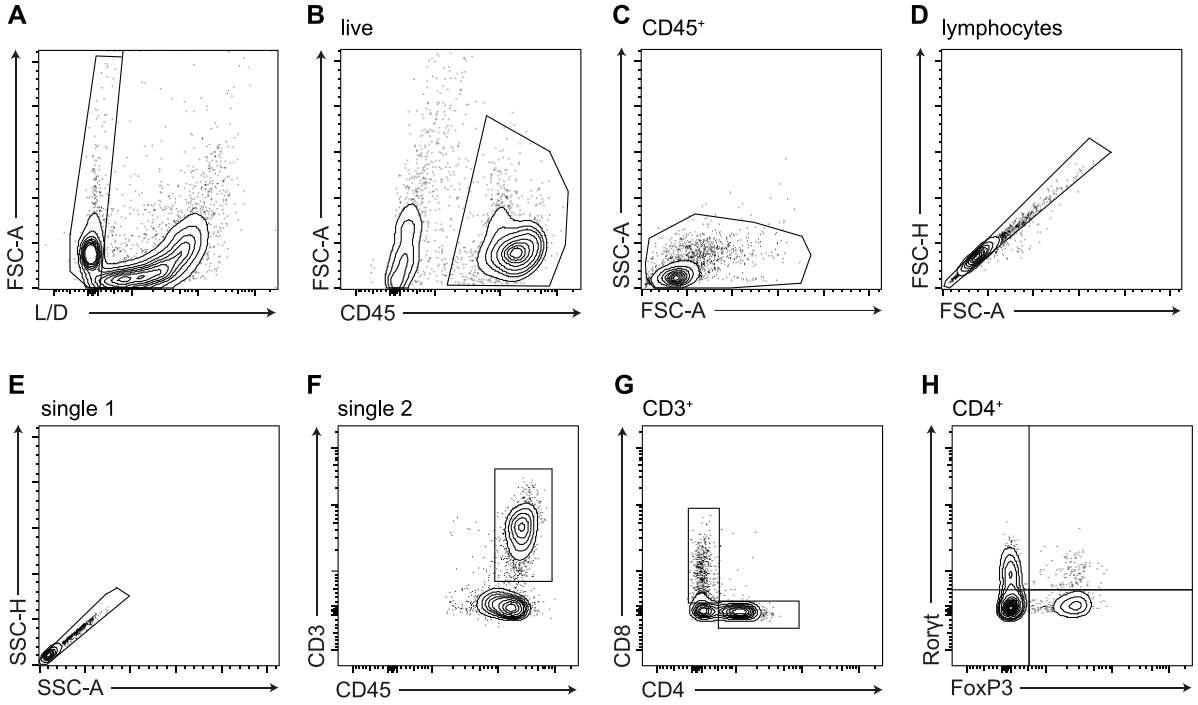

Figure 5.10 Gating strategy used to identify T cell populations in peripheral tissues

***A**: living cells gate. **B**:immune cell selection by expression of CD45. **B**: morphology gate on immune cells. **D/E**: removal of doublets using forward and side scatter respectively. Lymphocytes were selected by the co-expression of CD45 and CD3 (**F**). In this gate helper and cytotoxic T cells were selected by the expression of either CD4 or CD8 (**G**). $CD4^+$ Tregs were then defined as $CD4^+$ $FoxP3^+$ cells (**H**).*

In accordance with the cell distribution in the secondary lymphoid organs, the distribution of the different T cell populations was generally unchanged in control and *$CD4^{Cre}$; $Creld1^{flox/flox}$* animals at 12 weeks of age in both the small intestine and colon (**fig 5.11 A/B** and **C/D** respectively). Nevertheless, interestingly in both, the small intestine and the colon, $CD4^+$ T cells and Treg total numbers tended to be lower in $Creld1^{flox/flox}$ animals compared to controls. This might suggest a less efficient migration of T cells into the peripheral organs or a reduced viability of the cells populating these organs.

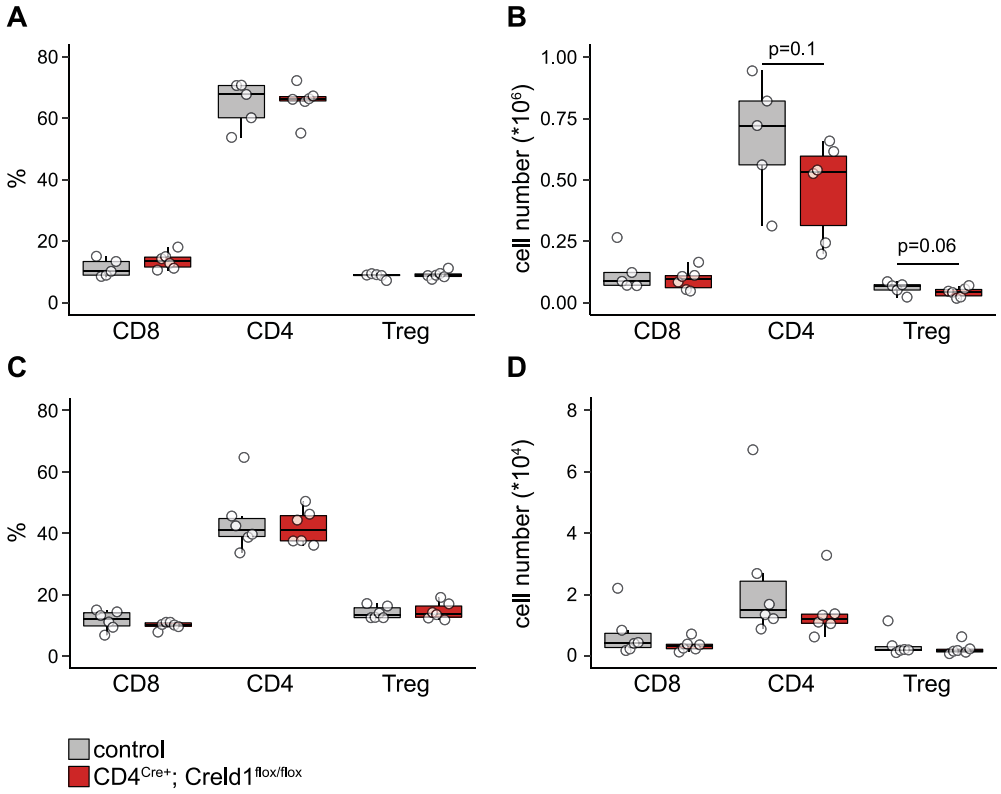

Figure 5.11 T cells populate the peripheral tissues in CD4^{Cre}; Creld1$^{flox/flox}$ mice normally

*Lymphocytes from 12 weeks old control and CD4^{Cre}; Creld1$^{flox/flox}$ mice were analysed in peripheral tissues by flow cytometry. **A/C**: percentage. **B/C**: total cell number in small intestine (**A/B**) and colon (**C/D**) (n=6). Statistical significance was tested by unpaired t-test (* p<0.05, ** p<0.01, *** p<0.001, **** p<0.0001).*

5.2.5 *T cell differentiate normally in young CD4^{Cre}; Creld1$^{flox/flox}$ mice*

As introduced previously (see section 1.1.4), antigen-experienced naïve T cells are epigenetically programmed to produce a specific pattern of cytokines targeted to a specific type of T cell response. T cells from 12-week-old mice derived from both, secondary lymphoid organs and tissues, were stimulated with PMA and Ionomycin to induce cytokine production in combination with inhibitors of protein secretion. Cells were then stained with fluorescently labelled antibodies including intracellular staining for hallmark cytokines. Cells were then analysed by flow cytometry allowing the identification of the different T cell subgroups.

CD4$^+$ T cells were identified in lymphoid organs and tissues as described before (**fig 5.8** and **5.10**) and categorized by the expression of specific cytokines. After conventional gating to CD4$^+$ lymphocytes, IL-2 positive cells were identified by the expression of the cytokine IL-2 (**fig 5.12 A**). Th1 (T helper 1) cells are generally defined as IFNγ/TNFα double positive cells

(**fig 5.12 B**). Another physiopathologically relevant subgroup are Th17 cells due to their involvement in several autoimmune diseases, these cells can be divided into conventional Th17 cells (IL-17$^+$) and pathogenic Th17 (IL17$^+$IFNγ$^+$) (**fig 5.12 C**).

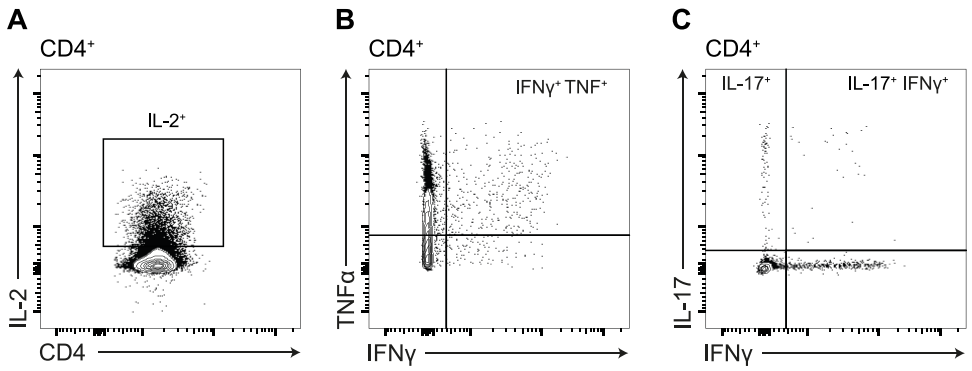

Figure 5.12 Identification of differentiated T cells in CD4^{Cre}; Creld1$^{flox/flox}$ mice

***A**: IL2-producing T cells. **B**: Th1 cells (TNFα$^+$ and IFNγ$^+$). **C**: Th17 (IL17$^+$ IFNγ$^-$) pathogenic Th17 as IL17$^+$ IFNγ$^+$ (**C**).*

All populations identified by the cytokine expression profiles were quantified in the spleen, peripheral lymph nodes, mesenteric lymph nodes, small intestine and colon in 12-week-old control and *CD4^{Cre}; Creld1$^{flox/flox}$* animals. No significant differences were found in the differentiation for IL-2-producing cells (**fig 5.13 A**), Th1 cells (**fig 5.13 B**) nor for Th17 and pathogenic Th17 cells (**fig 5.13 C** and **D** respectively). Only a modest increase in the percentage of Th1, Th17 and pathogenic Th17 cells were found in the spleen of Creld1-deficient mice. Nevertheless, it is important to consider that under these conditions, the vast majority of T cells present are still in a naïve state, and the percentage of differentiated cells is very low.

For the identification of the homeostatic release of cytokines, also blood was collected from 12-week-old animals and the serum fractions were tested to quantify the levels of released T cell hallmark cytokines. In this case, it was possible to observe a general decrease in the levels of cytokines in the serum (**fig 5.13 E**) but with a moderate increase in the levels of IFNγ in accordance with the increase in the percentage of Th1 cells identified in the spleen (**fig 5.13 A**).

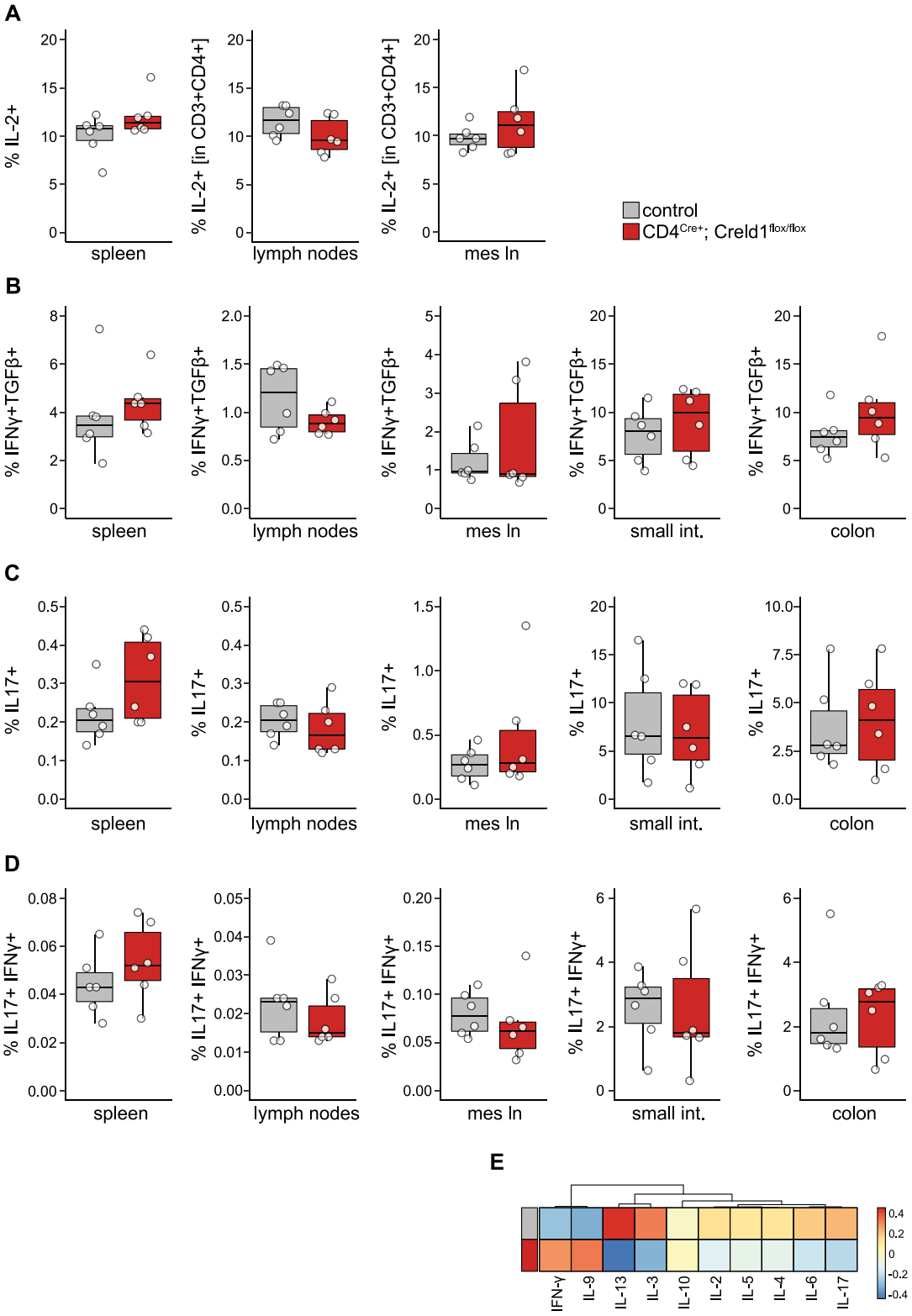

Figure 5.13 T cell differentiate normally in young CD4^{Cre}; Creld1$^{flox/flox}$ mice

*Functional analysis of CD4$^+$ T cell differentiation in 12 weeks old control and CD4^{Cre}; Creld1$^{flox/flox}$ mice. Production of specific cytokines was consequently evaluated by flow cytometry. IL-2-producing cells (**A**), Th1 cells (IFNγ$^+$/TGFβ$^+$ - **B**), Th17 (IL-17$^+$ IFNg-) **C**) and pathogenic Th17 (IL17$^+$/IFNγ$^+$ - **D**) were quantified as percentage in CD4$^+$ cells. Serum analysis from the same animals for T cell related cytokines is shown as heatmap of mean of scaled log2 cytokine levels (**E**)(n=6). Statistical significance was tested by unpaired t-test (* p<0.05, ** p<0.01, *** p<0.001, **** p<0.0001).*

5.3 Characterization of the immune status of one-year-old conditional Creld1 KO mice

The immune system composition and functionality undergoes profound age-related changes. Concerning the lymphoid compartment, the involution of the primary lymphoid organs affects both, the generation of early lymphoid precursors, as well as the output of mature T cells from the thymus. This leads to a reduction in the total number of T cells in the peripheral tissues and an impairment of the effector capacity of the remaining cells; collectively this phenomenon is defined as immunosenescence.

5.3.1 *$CD4^{Cre}$; $Creld1^{flox/flox}$ one-year-old mice show minor macroscopic changes*

At the macroscopic level, *$CD4^{Cre}$; $Creld1^{flox/flox}$* one-year-old mice did not show any behavioural differences compared to controls and the frequency of naturally occurring age-related diseases was not different in the conditional KO model. Body weight showed a slight reduction in *$CD4^{Cre}$; $Creld1^{flox/flox}$* animals (**fig 5.14 A**). Spleen weight also appeared slightly reduced in the conditional KO model (**fig 5.14 B**). Interestingly kidney weight was higher in *$CD4^{Cre}$; $Creld1^{flox/flox}$* animals compared to controls whereas liver weight was unchanged (**fig 5.14 D** and **C** respectively). Concerning the gut of one-year-old animals, in accordance with the results at 12 weeks of age, the length of both the small intestine and the colon was slightly increased (**fig 5.14 E** and **F**).

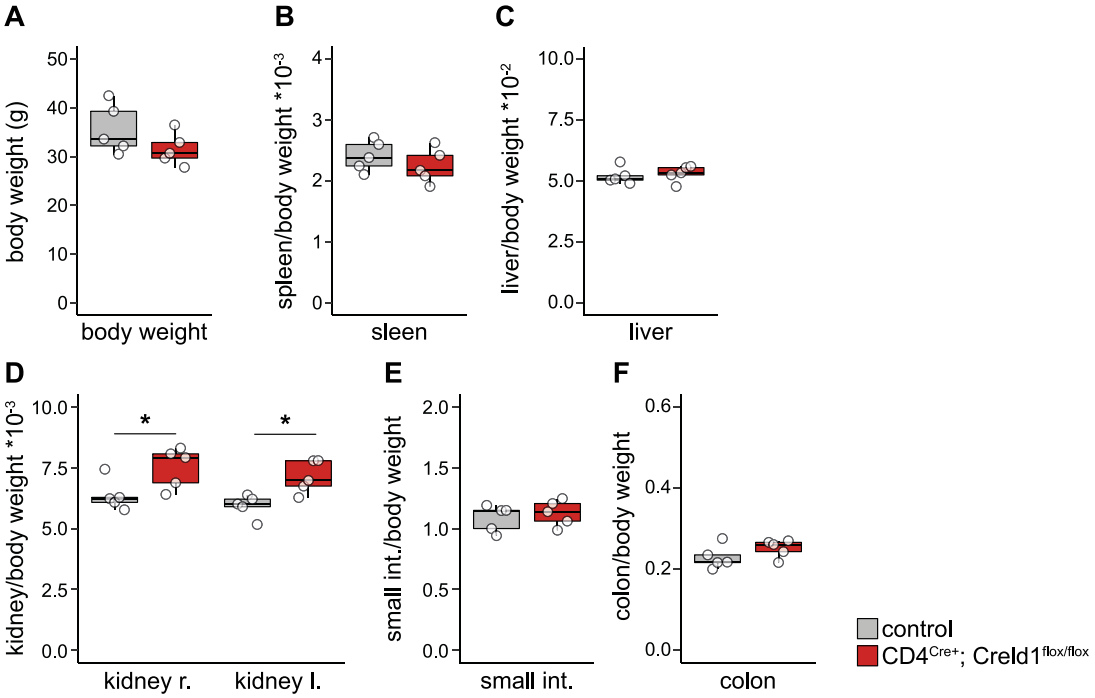

Figure 5.14 One-year-old CD4^{Cre}; Creld1$^{flox/flox}$ mice have no major macroscopic changes

*Analysis of physical parameters of one-year-old control and CD4^{Cre}; Creld1$^{flox/flox}$ animals. Body weight (**A**), normalized weight of spleen (**B**), liver (**C**), right and left kidney (**D**), small intestine (**E**) and colon (**F**) (n=5). Statistical significance was tested by unpaired t-test (* p<0.05, ** p<0.01, *** p<0.001, **** p<0.0001).*

5.3.2 *CD4^{Cre}; Creld1$^{flox/flox}$ one-year-old mice show drastic reductions in T lymphocytes found in secondary lymphoid organs*

Next, secondary lymphoid organs from aged *CD4^{Cre}; Creld1$^{flox/flox}$* animals were analysed for the distribution of the different T cell populations. The identification of the different T cell populations was performed as described above (**fig 5.8**).

Surprisingly, mesenteric lymph nodes from *CD4^{Cre}; Creld1$^{flox/flox}$* animals showed a drastic reduction in cell numbers for all analysed T cell populations (**fig 5.15 A**). Nevertheless, overall the relative cell percentage was unchanged in *CD4^{Cre}; Creld1$^{flox/flox}$* mice except for CD8^{+} and regulatory T cells (**fig 5.15 B**). Furthermore, a tendency towards reduced cell numbers was observed in the spleen (**fig 5.15 C**) with no changes in the relative percentage being observed (**fig 5.15 D**).

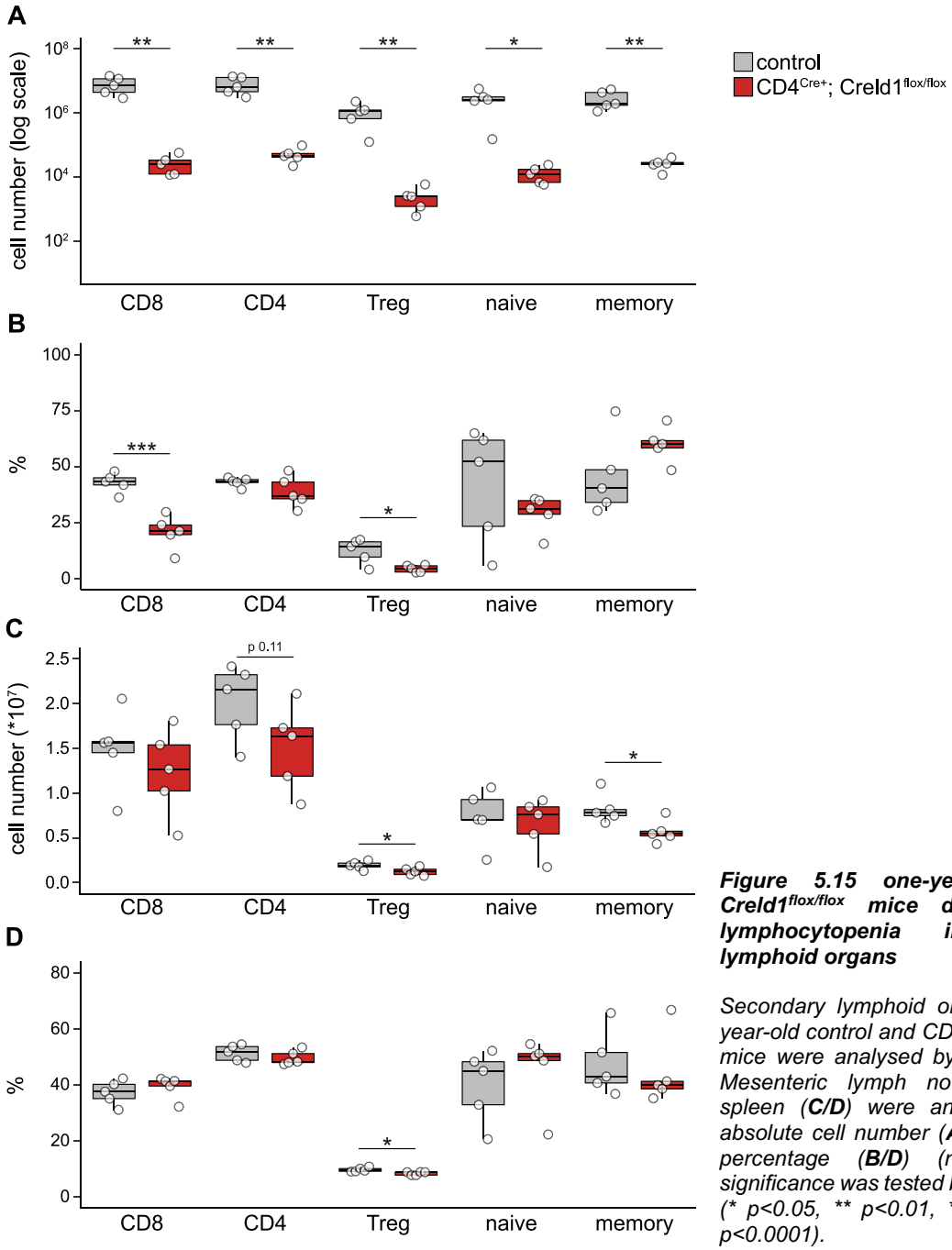

Figure 5.15 one-year-old CD4^{Cre}; Creld1$^{flox/flox}$ mice develop severe lymphocytopenia in secondary lymphoid organs

*Secondary lymphoid organs from one-year-old control and CD4^{Cre}; Creld1$^{flox/flox}$ mice were analysed by flow cytometry. Mesenteric lymph nodes (**A/B**) and spleen (**C/D**) were analysed for both absolute cell number (**A/C**) and relative percentage (**B/D**) (n=5). Statistical significance was tested by unpaired t-test (* p<0.05, ** p<0.01, *** p<0.001, **** p<0.0001).*

5.3.3 *T cells in peripheral tissues exhibit the same phenotype as in secondary lymphoid organs in aged mice*

Peripheral tissues were analysed to examine if the reduction in total cell numbers clearly apparent in secondary lymphoid organs were also present in the periphery. To address this question, the T cells in the small intestine and colon were analysed (**fig 5.16 A/B** and **C/D** respectively). There was a clear reduction in total T cells numbers, especially for $CD4^+$ T cells and T_{regs} (**fig 5.16 B** and **D**). Interestingly, in these tissues the frequency of T_{regs} cells was higher (**fig 5.16 A** and **C**) despite the percentage of $CD4^+$ T cells in all the lymphocyte populations being reduced in conditional KO animals compared to controls.

As further proof of the general reduction of $CD4^+$ T cells in *$CD4^{Cre}$; $Creld1^{flox/flox}$* conditional KO mouse, serum from one-year-old animals was analysed showing a marked reduction in the presence of all T cell cytokines measurable in blood (**fig 5.16 E**).

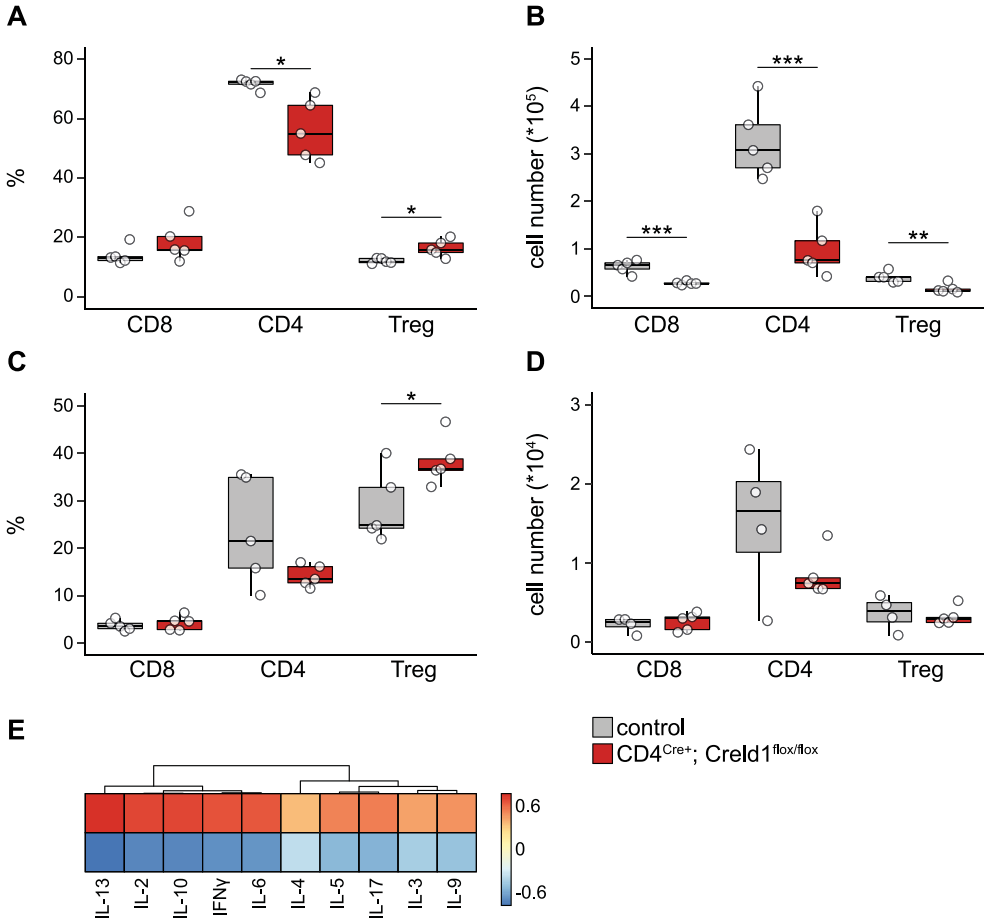

Figure 5.16 one-year-old CD4^{Cre}; Creld1$^{flox/flox}$ mice show decreased numbers of T cells in the peripheral tissues

*Lymphocytes from 12-week-old control and CD4^{Cre}; Creld1$^{flox/flox}$ mice were analysed in peripheral tissues by flow cytometry. Relative percentages (**A/C**) and total cell numbers (**B/C**) were quantified in small intestine (**A/B**) and colon (**C/D**). **E**: Serum analysis from the same animals for T cell-related cytokines was shown as a heatmap of the mean of scaled cytokine levels (n=5). Statistical significance was tested using an unpaired t-test (* p<0.05, ** p<0.01, *** p<0.001, **** p<0.0001).*

Taken together, these findings suggest a vital role for Creld1 in the maintenance of T cells in the periphery despite no major involvement in the later developmental processes.

Due to the complexity of mechanisms involved in the maintenance of the T cell pool *in vivo,* it was difficult at this stage to mechanistically understand why older animals suffer from lymphocytopenia. *In vitro* experiments were performed to gain a better understanding of the molecular pathways involved in the effects observed upon Creld1 depletion in CD4^{+} T cells.

5.3.4 *Mesenteric lymph node T cells show a differentiation bias towards Th1 and Th17*

T cell specification into different T helper types was analysed in secondary lymphoid organs and tissues of one-year-old animals. Purified cell suspensions were stimulated for 4 hours with PMA and Ionomycin in the presence of protein secretion inhibitors. Cells were then stained extra- and intracellularly and analysed by flow cytometry. T helper cell subtypes were defined as described above (*5.2.4*) for Th1, Th17 and pathogenic Th17 (**fig 5.17 A/B/C** respectively). Here, we observed a higher differentiation capacity into Th1, T17 and pathogenic Th17 in the colon and especially in the mesenteric lymph nodes, while the percentage of differentiated T helper cells in the spleen did not change significantly.

Based on these results and the reduced number of T cells in all analysed organs, the phenotype could be explained by either an altered survival fitness of differentiated T helper cells or a cell intrinsic bias in differentiation. The recently demonstrated increased resistance of Th17 cells to apoptotic cell death and their requirement for *Fas* expression to functionally differentiate (Meyer Zu Horste *et al.*, 2018) would support the first hypothesis.

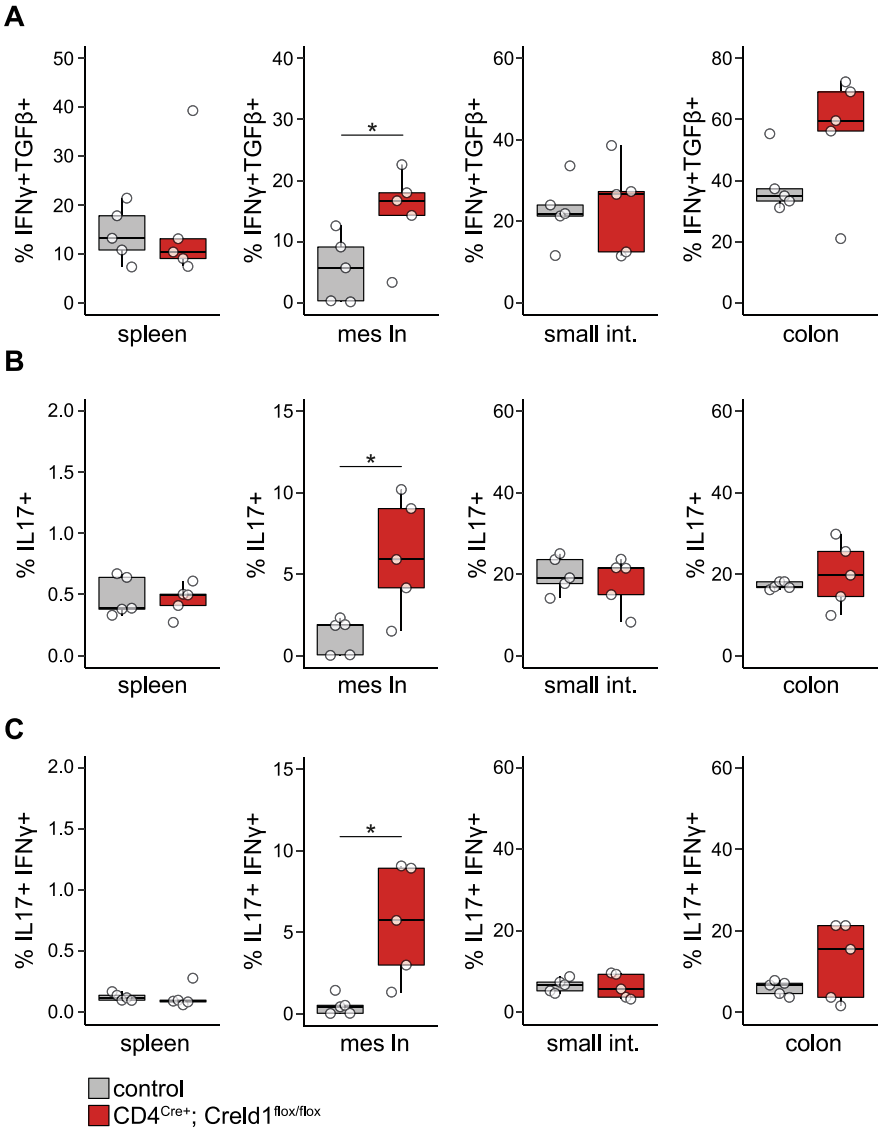

Figure 5.17 Mesenteric lymph nodes T cells show differentiation bias towards Th1 and Th17

Purified cell suspension from one-year-old animals were stimulated for four hours with PMA and Ionomycin in the presence of inhibitors of protein secretion. ***A****: Th1 cells (TNFα^{+} and IFNγ^{+}).* ***B****: Th17 (IL17^{+} IFNγ)$^{-}$.* ***C****: pathogenic Th17 (IL17^{+} IFNγ^{+}) (n=5). Statistical significance was tested using an unpaired t-test (* p<0.05, ** p<0.01, *** p<0.001, **** p<0.0001).*

5.4 Creld1 regulates cell survival and apoptosis in CD4⁺ T cells

5.4.1 *Creld1 KO CD4⁺ T cells are more susceptible to cell death*

The finding that one-year-old mice develop severe lymphocytopenia in peripheral tissues led us to investigate the susceptibility of Creld1 KO CD4⁺ T cells to cell death. For this purpose, splenic CD4⁺ T cells were isolated and incubated in culture medium for up to 3 days without any proliferative or activation stimuli (**fig 5.18 A**).

Surprisingly, Creld1-deficient T cells showed consistently higher levels of cell death after either 24, 48, and 72 hours of *ex vivo* culture (**fig 5.18 B**).

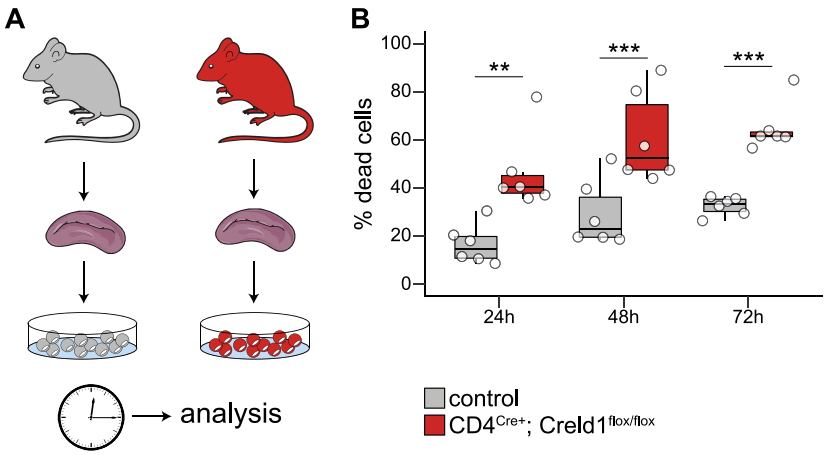

Figure 5.18 Creld1 KO CD4+ T cells are susceptible to cell death

***A**: Schematic representation of the experimental setting used. Viability of spleen-derived CD4⁺ T cells from control and CD4^{Cre}; Creld1$^{flox/flox}$ mice was assessed at 24, 48 and 72 hours in culture without stimulation (**B**) (n=6). Statistical significance was tested using the one-way ANOVA with Bonferroni post-hoc test (* p<0.05, ** p<0.01, *** p<0.001, **** p<0.0001).*

5.4.2 *Creld1-deficient CD4⁺ T cells show enhanced apoptotic cell death*

To perform an in-depth analysis on the increased death rate, we decided to investigate the levels of apoptosis in the cells cultured *in vitro.* In fact, apoptosis is one of the main pathways of cell death for T cells.

First, the induction of apoptosis was assessed in freshly isolated CD4⁺ T cells. In this context extremely low levels of Fas expression at the plasma membrane were detectable and no difference was apparent between control and Creld1-deficient T cells (**fig 5.19 A**). On the

contrary, the percentage of cells negative for Bcl2 was significantly increased in Creld1 deficient cells (**fig 5.19 B**), Bcl2 is an important anti-apoptotic protein. Its cleavage leads to the activation of the Caspase cascade, which induces apoptotic cell death. This result was already suggesting an enhanced susceptibility of Creld1 deficient T cells to apoptotic cell death. To further confirm this hypothesis, cells were incubated for eight hours and then analysed by flow cytometry. Here increased levels of Fas expression at the plasma membrane were measured (**fig 5.19 C**) and in accordance with our previous findings, the percentage of Bcl2-negative cells was significantly increased in Creld1 KO $CD4^+$ T cells (**fig 5.19 D**). Furthermore, we also analysed the level of cleaved Caspase 3 (with active protease activity) and found that this was increased in KO cells (**fig 5.19 E**).

Taken together, these data highlight the importance of Creld1 for the maintenance of T cell survival and could explain why aged CD4-specific Creld1-deficient animals develop premature involution of the immune system in comparison to control mice.

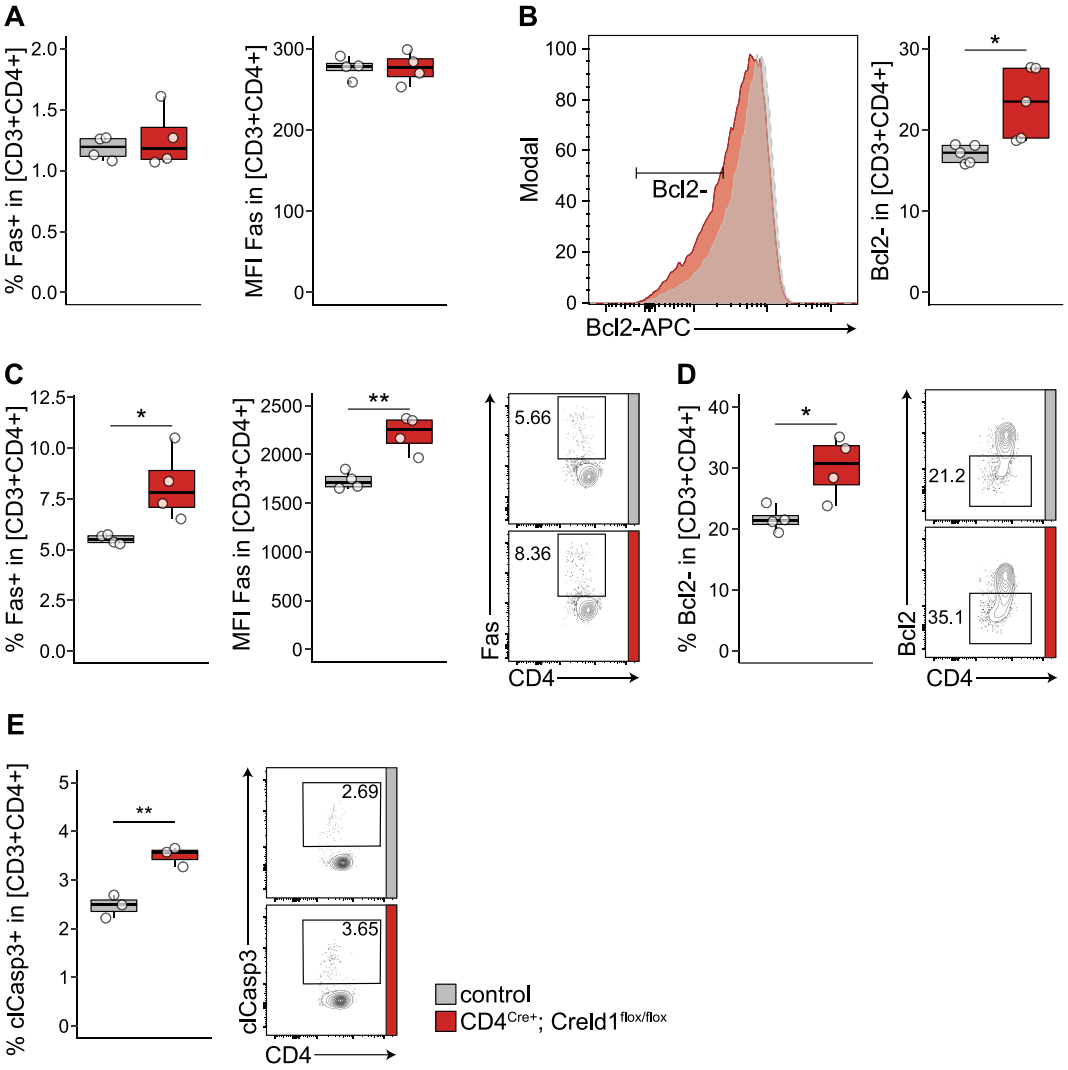

Figure 5.19 Creld1 KO CD4⁺ T cells are susceptible to apoptotic cell death

*Analysis of apoptosis induction in control and CD4^{Cre}; Creld1$^{flox/flox}$ mice derived CD4⁺ T cells. Freshly harvested cells were analysed by flow cytometry for Fas expression (n=4 **A**) and Bcl2 cleavage (n=5 **B**). Cells were also kept 8 hours in vitro culture and analysed for Fas expression and Bcl2 cleavage (**C/D** respectively n=4). In addition, at 8 hours in vitro culture Caspase 3 cleavage was also quantified (n=3 **E**). Statistical significance was tested by unpaired t-test (* p<0.05, ** p<0.01, *** p<0.001, **** p<0.0001).*

5.4.3 *IL-7 and IL-15 treatment does not rescue the apoptotic phenotype observed in Creld1 deficient T cells*

The last decades of research on T cell homeostasis and maintenance found that IL-7 and IL-15 are two important stimuli for the homeostatic survival of T cells *in vivo* together with tonic TCR stimulation. The effect of IL-7 and IL-15 was measured in Creld1 deficient T cells to assess effects on viability and more importantly to understand if these cytokines could rescue the susceptibility to apoptotic cell death. CD4⁺ T cells were harvested from the spleen of

control or *CD4^{Cre}; Creld1$^{flox/flox}$* animals and incubated *ex vivo* for eight hours with or without IL-7 or a combination of IL-7 and IL-15. The percentage of cleaved Caspase-3 was quantified by flow cytometry showing no improvement in viability upon treatment. IL-7 or IL-15 were not sufficient to rescue the effect of Creld1 deficiency in CD4$^+$ T cells. Therefore, further investigation was needed to understand the molecular mechanisms underpinning Creld1-dependent viability of CD4$^+$ T cells (**fig 5.20 A**).

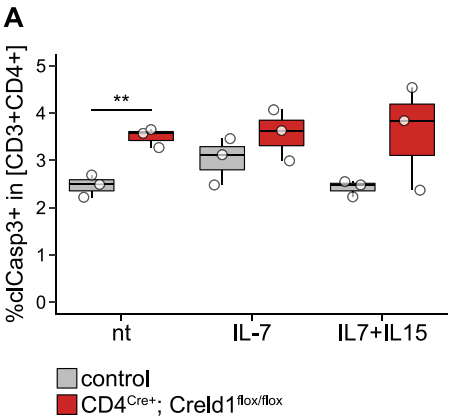

Figure 5.20 IL-7 and IL-15 cannot rescue the apoptotic phenotype of Creld1-deficient cells

*Control and CD4^{Cre}; Creld1$^{flox/flox}$ mice spleen-derived CD4$^+$ T cells were treated with IL-7 or IL-7 and IL-15 in combination. Caspase 3 cleavage was assessed (**A** n=3). Statistical significance was tested by unpaired t-test (* p<0.05, ** p<0.01, *** p<0.001, **** p<0.0001).*

5.4.4 *RNA-seq analysis of Creld1 deficient T cells indicate effects on apoptosis and activation*

With the aim of extending our knowledge on the molecular function of Creld1, naïve CD4$^+$ T cells from control or *CD4^{Cre}; Creld1$^{flox/flox}$* 12-week-old animals were isolated by FACS and directly analysed by RNA-seq or incubated for eight hours *ex vivo*. In this context, cells were also stimulated with α-CD3 and α-CD28 antibodies to mimic physiological T cell activation (**fig 5.21 A**). Also in this case, after incubation total RNA was then extracted and analysed by RNA-seq. After rlog transformation of the raw counts the expression table was used to evaluate single pathways in the different comparisons and consequently significant genes for each comparison were used to generate a co-expression network as shown in the schematic in figure 5.21B. Carefully looking at the difference between genotypes in the three different conditions, it was clear that most of the differences between control and KO naïve CD4$^+$ T cells were found in the 8 hours control samples where we could previously show KO CD4$^+$ T cells were highly apoptotic compared to controls (**fig 5.21 C**). Focusing on freshly isolated and

8h control samples a general downregulation of the T cell homeostasis signature was observed (**fig 5.21 D**) together with an upregulation of both a T cell-specific signature for T cell apoptosis and a more general apoptotic signature (**fig 5.21 E F and G**). These results were in clear accordance with what we previously observed both *in vitro* and *in vivo* showing that Creld1 is critical for the maintenance of T cell viability. Extending the analysis to our stimulated samples, we still observed an upregulation of an apoptotic signature, in this case related to activation-induced cell death (AICD – **fig 5.21 H**). Interestingly, under these conditions a genetic signature related to T cell overactivation was apparent. Indeed, we found increased expression of many of the activation markers associated with this phenotype such as *IL-2RA* (CD25), *CD44* and *CD69* (**fig 5.21 I**).

Analysis of the co-expression network allows the identification of gene modules showing a common expression pattern across the analysed conditions.

Within the three analysed conditions five modules of co-expression were identified. Each module had a different behaviour in the comparison between each condition (**fig 5.21 J and K**). It was apparent that naïve T cells showed transcriptional changes highly correlated to the cells incubated for eight hours without any stimulation. This result is again in accordance with our previous findings since we were able to detect signs of early apoptosis on a transcript level already in freshly isolated cells. Moreover, the difference was much more pronounced in cells cultured *in vitro*. It was apparent that in this situation most of the genes contributing to the co-expression network were downregulated in Creld1 deficient cells. Further analysis of the functional enrichment of these modules (light green and yellow) showed that several molecular pathways were downregulated. An example for this can be observed in the light green module which was related to a mechanism of proliferation (*G2/M transition* and *mitotic prometaphase*) or survival signalling like *WNT signalling*. In the other two modules, dark green and yellow green, down regulated in naïve or eight hours *ex vivo* cells respectively, it was found that other fundamental T cell pathways were upregulated such as the mTOR signalling and the JAK/STAT pathway (**fig 5.21 K**). Here we could clearly observe how Creld1 deficiency in $CD4^+$ T cells affected cellular homeostasis.

Interestingly, the overall transcriptional program appeared reverted in stimulated T cells showing how Creld1 KO $CD4^+$ T cells might be overresponsive to stimulation (**fig 5.21 J** and **K**).

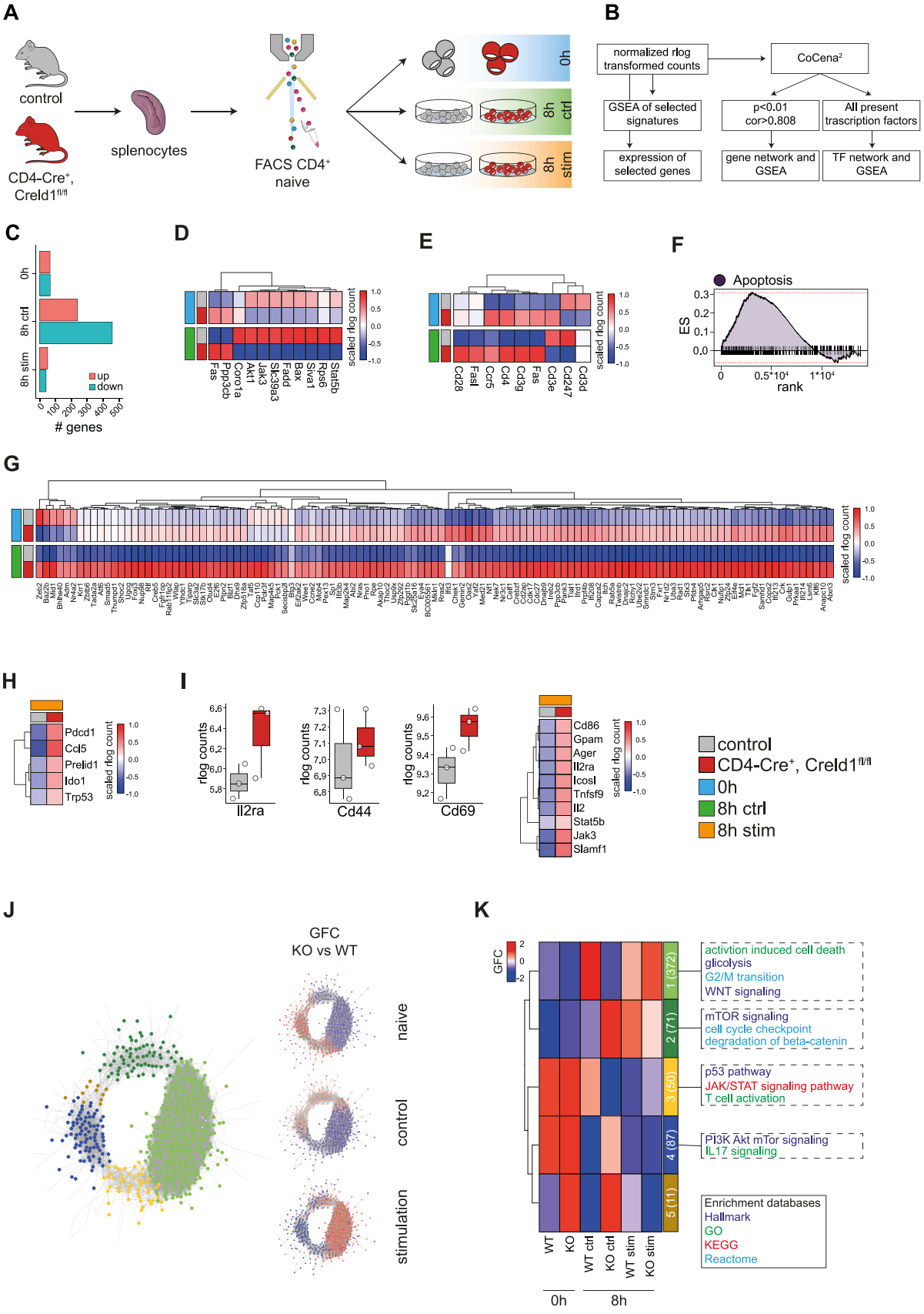

legend in next page

5.4.5 *Transcription factor analysis reveals a possible mechanism underlying decreased viability and overactivation of Cred1 deficient T cells*

To find common transcriptional programs affected under the different conditions analysed, a network of co-expressed transcription factors was generated (**fig 5.22**). As for the whole transcriptome (**fig 5.21**), naïve T cells show similar transcriptomic changes to cells cultured for eight hours *ex vivo* (**fig 5.22 A**). Interestingly, here the turquoise module (**fig 5.22 A and B**), down regulated in both naïve and control cells, showed an enrichment in the Wnt signalling pathway and apoptosis in accordance with the light green module in the gene expression network (**fig 5.21 J** and **K**). The green and red modules, upregulated in stimulated cells, showed how the stimulation of these cells seemed to have a stronger effect at transcriptional level in KO cells compared to controls. In these modules, in fact, transcription factors related to IL-2 signalling and T cell activation were found to be up regulated (**fig 5.22 A** and **B**).

As previously described (section 1.6), Creld1 was recently connected to NFATc1 activation. A more detailed analysis of the transcriptional regulation in Creld1 deficient $CD4^+$ T cells after 8 hours ex vivo culture revealed a general downregulation of NFAT signalling in accordance with what had been previously reported (Mass *et al.*, 2014) (**5.22 C and D**).

Figure 5.21 RNAseq analysis of Creld1 deficient T cells confirms the apoptotic phenotype and uncovers an unbalanced activation

*RNAseq analysis of control and $CD4^{Cre+}$; $Creld1^{flox/flox}$ naïve T cells was performed according to the schematic overview (**A** and **B**). CoCena analysis was performed on the samples using 918 genes as input deriving from the comparison between each condition (**C**). GSEA was performed for several available gene sets, T cell homeostasis and T cell apoptosis are shown in (**D**) and (**E**) respectively. A broad list of genes relating to apoptosis was tested showing a clear apoptotic signature in KO cells (**F** and **G**). Apoptotic signature was then tested also in stimulated cells (**H**). Stimulated cells also show a profile of overactivation compared to controls (**I**). CoCena² network is shown in figure J showing specific modules regulated in the three conditions. Group fold change and functional enrichment is shown (**K**). Heatmaps show mean of scaled expression values.*

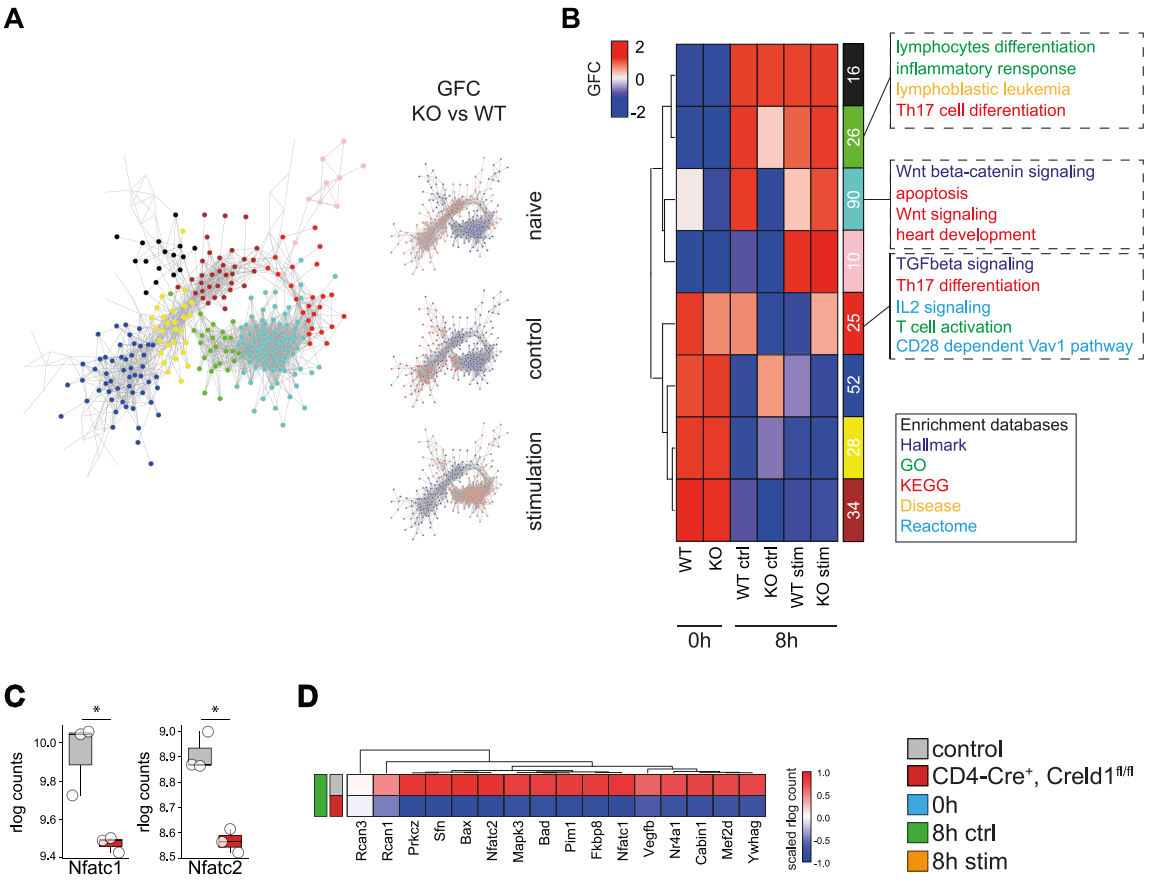

Figure 5.22 Transcription factor analysis reveals a possible mechanism underlying decreased viability and over activation of Cred1 deficient T cells

RNA-seq analysis of transcription factors in naïve CD4+ T cells from control and CD4^{Cre+}; Creld1$^{flox/flox}$ mice was performed. ***A****: CoCena transcription factor network coloured by CoCena modules or group fold change for each comparison.* ***B****: Heatmap representing the group fold change of each CoCena module for each experimental condition. NFAT expression was analysed in the 8 hours control condition (****C****) as well as its target genes (****D****). Heatmaps show mean of scaled expression values.*

5.5 Creld1-deficient T cells overreact to stimulation but still show impaired survival

The previously observed signs of overactivation in the transcriptome analysis of α-CD3/α-CD28 stimulated cells led us to analyse CD4$^+$ T cell activation in more depth.

T cells are physiologically activated by the engagement of the T-cell receptor with MHC II on the APC concomitantly with activation of co-stimulatory molecules such as CD28 by the

respective ligands (CD80/CD86) on the APC. This stimulation is fundamental for the functional activation of CD4⁺ T cells in the protection of the body from pathogens.

To assess whether Creld1 KO CD4⁺ T cells are prone to respond stronger to stimulation, control or Creld1 deficient CD4⁺ T cells were purified from mouse spleens and stimulated with α-CD3/α-CD28 antibodies to mimic the physiological interaction of CD4⁺ T cells and APCs (**fig 5.23 A**).

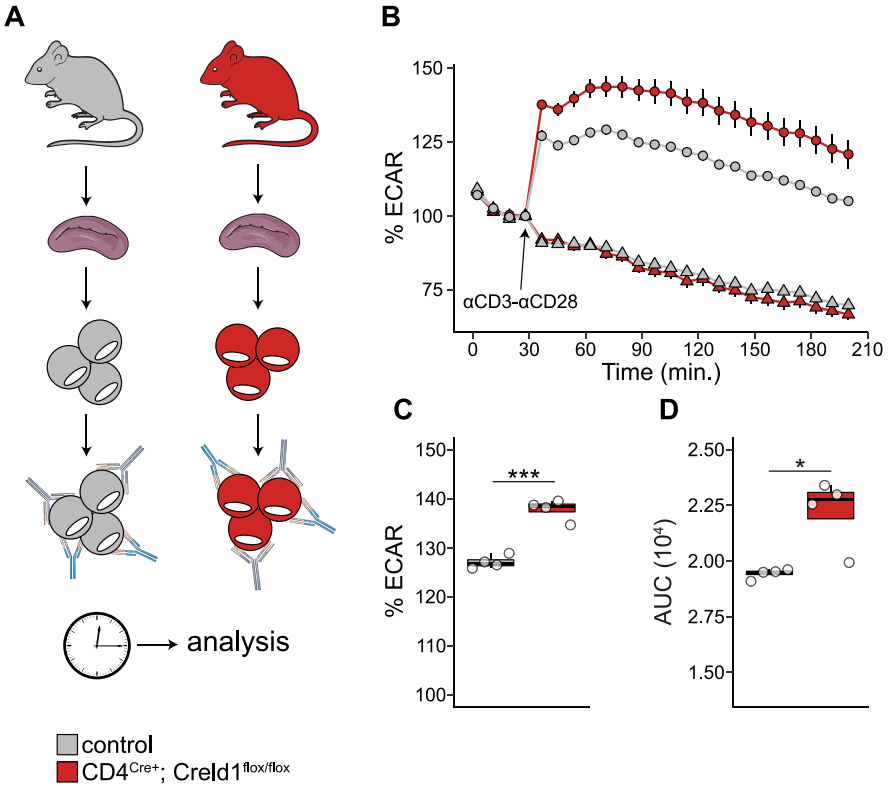

Figure 5.23 Creld1 deficient CD4⁺ T cell show accelerated activation kinetics

***A**: Schematic representation of the experimental setting used to assess the capacity of control and CD4^{Cre}; Creld1$^{flox/flox}$ to react to stimulation. Extracellular acidification rate (ECAR) with and without stimulation with α-CD3 and α-CD28 antibodies was quantified over time (**B**). Quantification of induction peak (**C**) and area under the curve (AUC) **D**) (n=4). Statistical significance was tested by unpaired t-test (* p<0.05, ** p<0.01, *** p<0.001, **** p<0.0001).*

5.5.1 *Creld1-deficient CD4⁺ T cells show accelerated activation kinetics*

Recent studies on metabolic changes that occur in T cells upon stimulation showed that CD4⁺ T cells highly depend on glycolysis as an energy source upon activation (Menk *et al.*, 2018). Measurement of glycolytic activity can be used as robust indication of the activation state of these cells upon TCR engagement.

To assess glycolytic activity in stimulated and unstimulated CD4⁺ T cells, CD4⁺ lymphocytes were purified and extracellular acidification rate (ECAR) was measured as surrogate of glycolytic activity using the Seahorse assay. After 30 minutes of baseline measurements each

well was injected with either α-CD3/α-CD28 antibodies (circle) or vehicle (PBS - triangle), to allow the stabilization of the cells, and changes in ECAR were measured over 2.5 hours (**fig 5.23 B**). It was already clear from the first measurement after injection that metabolic changes in T cells takes place very rapidly. Creld1 deficient cells show consistently higher ECAR levels over all measured time points, both in maximal activation (**fig 5.23 C**) and area under the curve **(fig 5.23 D**), confirming that Creld1 might also play a role in the balance between the quiescent and active state of $CD4^+$ T cells.

5.5.2 *Activated Creld1-deficient cells show higher levels of surface activation markers*

Functional activation of $CD4^+$ T cells leads to the cell surface expression of a pattern of proteins defined as activation markers. These proteins generally have an important role in the response of the T cell to pathogens and can be used as a hallmark of their activation state.

CD25, the IL-2 receptor alpha (*IL-2RA*), is the high affinity receptor for IL-2 leading to an incremented IL-2 signalling in these cells; CD44 is an important adhesion molecule in effector T cells and interestingly a target of Wnt signalling and CD69 is the earliest inducible molecule upon stimulation, mainly involved in T cell proliferation.

Stimulation of naïve $CD4^+$ T cells from control or $CD4^{Cre}$; $Creld1^{flox/flox}$ mice revealed a significantly increased percentage of stimulated Creld1-deficient cells expressing the activation markers CD25 and CD69 and CD44, even if not statistically significant, showed a clear tendency to be upregulated in Creld1 KO $CD4^+$ T cells (**fig 5.24 A**, **C** and **B** respectively).

So far, we have shown the effects of Creld1 deletion in the early events triggered by the stimulation of the T cell receptor. Over time, stimulated $CD4^+$ T cells, will expand and start producing cytokines in order to initiate an appropriate immune response.

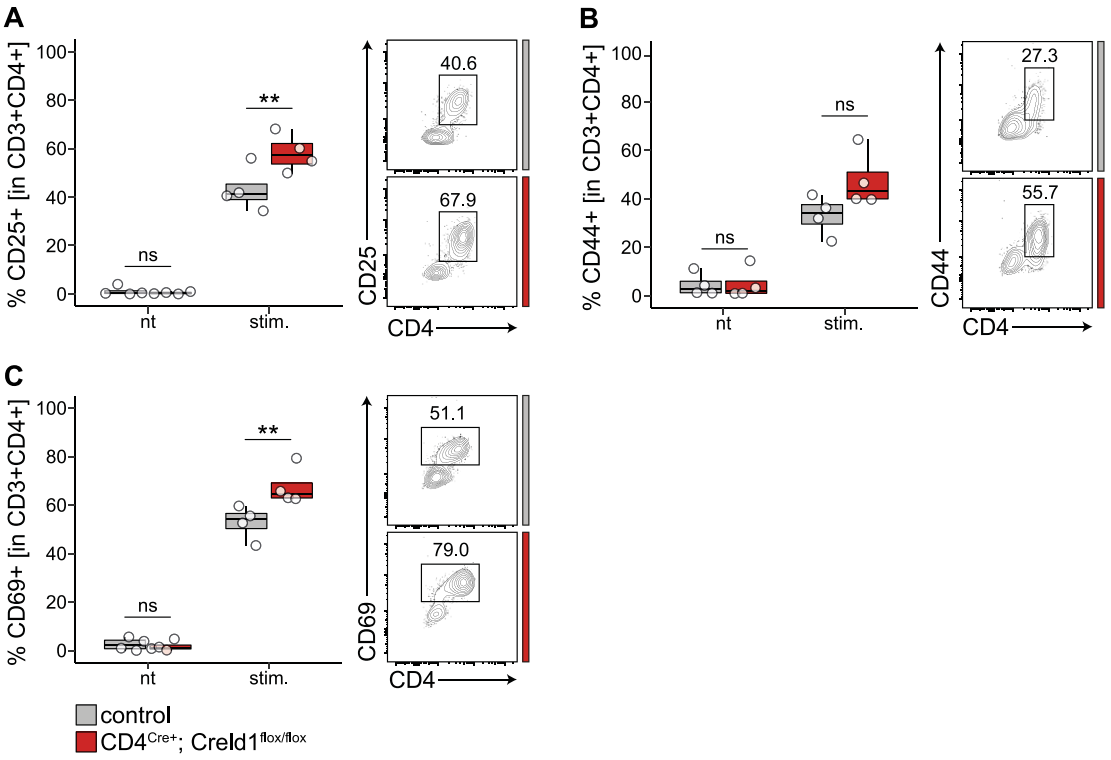

Figure 5.24 Stimulated Creld1 deficient cells show higher levels of activation markers

*Naïve CD4⁺ T cells were stimulated for 24 hours with α-CD3 (1 µg/ml) and α-CD28 (1 µg/ml) antibodies and analysed by flow cytometry for the activation markers CD25 (**A**), CD44 (**B**) and CD69 (**C**). Summary of four independent experiments and exemplary flow cytometry plots are shown (n=4). Statistical significance was tested using the one-way ANOVA with Bonferroni correction for multiple testing (* p<0.05, ** p<0.01, *** p<0.001, **** p<0.0001).*

5.5.3 *Long-term stimulation of Creld1 deficient T cells show lower proliferative capacity coupled with higher apoptotic rates*

To assess the proliferative capacity, proxy of a balanced stimulation of the cells over time, control and Creld1 deficient T cells were labelled with CFSE and stimulated for three days *ex vivo*. CFSE will covalently label the cells and the fluorescence intensity over time will show the number of cellular divisions that each cell underwent.

Initially, Creld1 deficient T cells showed a slightly reduced proliferative capacity (**fig 5.25 A/B**), combined with reduced total number of cells (**fig 5.25 C**). We then assessed the cell death rate in stimulated cells and observed an increased death rate in Creld1 deficient cells (**fig 5.25 D**). Furthermore, the difference in percentage of dead cells after three days of stimulation (circa 20%, **fig 5.25 D**) was almost the same as the difference in total cell numbers shown

before (**fig 5.25 B**). Moreover, under these experimental settings after 8 hours of stimulation Creld1 deficient cells showed clear signs of apoptosis compared to controls with increased levels of Bcl2 cleavage and Fas expression at the surface (**fig 5.25 E/F** respectively).

We therefore postulated that it is not the proliferative capacity to be diminished, but rather the ability of the lymphocytes to survive during the three days of incubation confirming the susceptibility of these cells to apoptosis as described above.

To further confirm our hypothesis Creld1 deficient T cells and controls were incubated over three days with PMA and ionomycin. Again, an increased death rate was observed (**fig 5.25 G**) demonstrating that the susceptibility to apoptotic cell death was not dependent on weaker TCR stimulation.

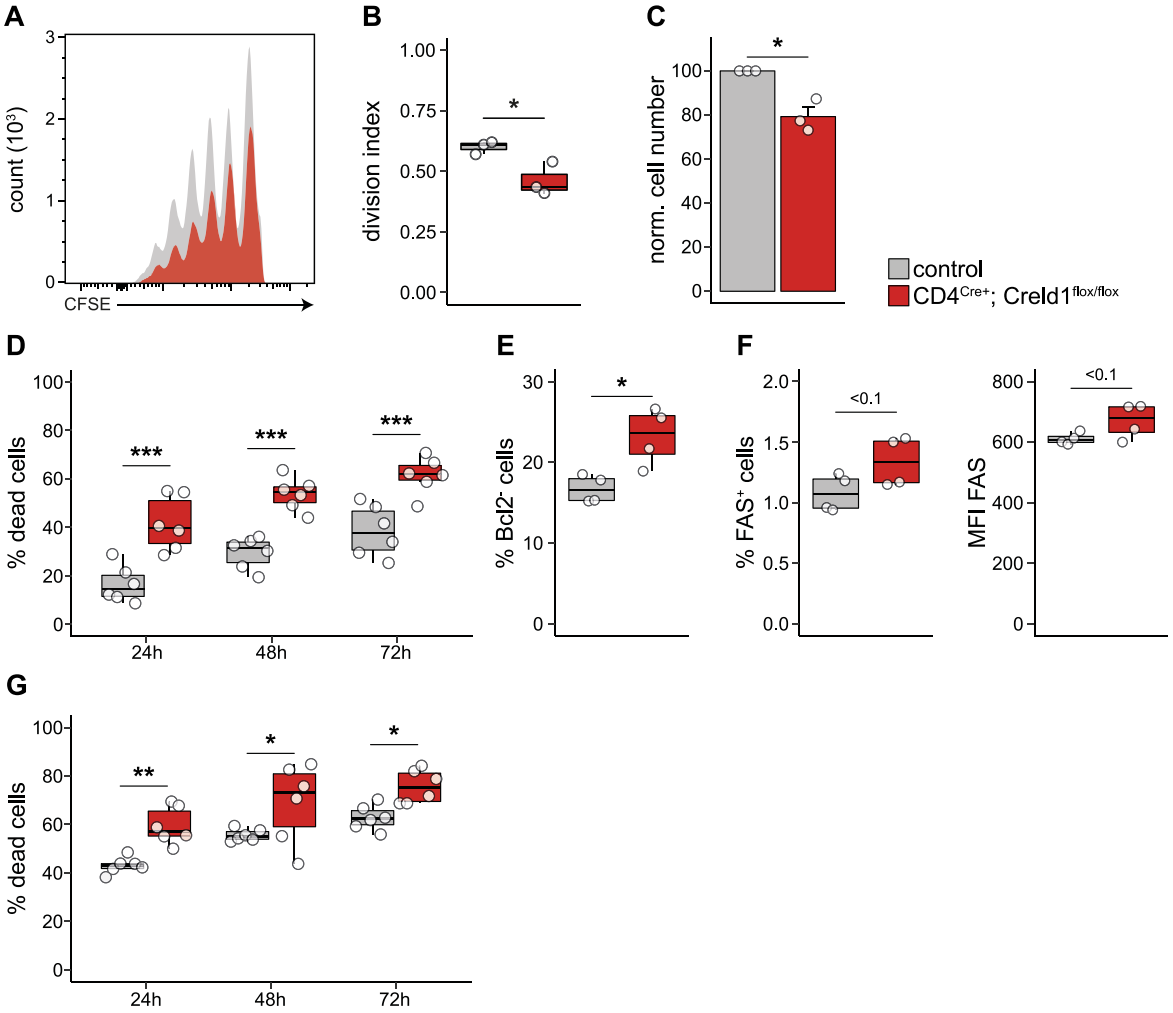

Figure 5.25 Long-term stimulation showed a lower proliferative capacity coupled with higher apoptotic rate

*Conventional CD4⁺ T cells (CD4⁺/CD25⁻) from control and CD4^{Cre}; Creld1$^{flox/flox}$ animals were stained with CFSE and stimulated with α-CD3 and α-CD28 conjugated beads. **A**: Proliferation profile over 3 days. **B**: Division index after 3 days (n=3). Quantification of total cell numbers after 3 days (n=3 **C**) and percentage of dead cells over 3 days with α-CD3 and α-CD28 stimulation (n=6 **D**). Stimulated cells were also checked for the apoptosis markers Bcl2 and Fas (**E** and **F** respectively n=4). **G**: Percentage of dead cells in PMA/ionomycin-stimulated cells (n=6). Statistical significance was tested by unpaired t-test or one-way ANOVA with Bonferroni correction for multiple testing (**D** and **G**) (* p<0.05, ** p<0.01, *** p<0.001, **** p<0.0001).*

5.5.4 *NFAT-luciferase mouse model recapitulates the survival and proliferation phenotype of Creld1 deficient CD4$^+$ T cells*

As Creld1 was recently found to be important in the regulation of NFATc1 activation during heart development (Mass *et al.*, 2014), we obtained a transgenic mouse line carrying a luciferase reporter responsive to NFAT. These mice carry a transgenic genomic locus consisting of 9 consecutive NFAT binding sites upstream of a TATA box and a gene coding for the luciferase reporter gene (**5.26 A**).

To prove that Creld1 is involved in NFAT activation in CD4$^+$ T cells, control or *CD4^{Cre}; Creld1$^{flox/flox}$* were crossed with the *NFAT-luc* reporter mice (**fig 5.26 B**). Spleen derived CD4$^+$ T cells were purified and treated *ex vivo* for up to three days.

Luciferase intensity revealed a marked reduction in NFAT activity in cells incubated *ex vivo* without any further stimulation (**fig 5.26 C**) already one day after purification (**fig 5.26 D left**). On the contrary α-CD3/α-CD28 stimulated cells showed increased NFAT activation after 24 hours however similar to our previous results, a lower activity after three days of stimulation was measured (**fig 5.26 D**).

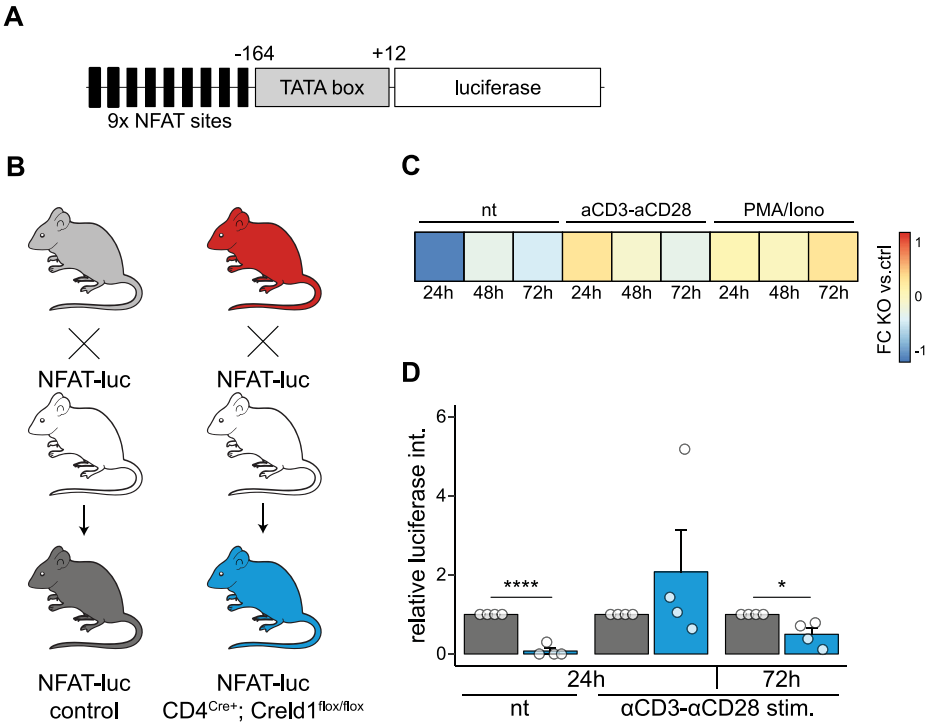

Figure 5.26 NFAT-luc mouse model recapitulates both survival and proliferation phenotype of Creld1 deficient CD4 T cells

***A**: schematic overview of the NFAT-luc locus. CD4^{Cre+}; Creld1$^{flox/flox}$ and control animals were crossed with NFAT-luc reporter mice (**B**). Spleen derived CD4^{+} T cells were treated in vitro for 1 to 3 days and relative luciferase intensity was measured (**C-D**) (n=4). Statistical significance was tested by unpaired t-test (* p<0.05, ** p<0.01, *** p<0.001, **** p<0.0001).*

These results collectively support that unstimulated Creld1 deficient cells are unable to maintain basal NFAT activity resulting in increased cell death. However, stimulated cells initially overreact to the stimulation in the first 24 hours but are not able to survive to the same level as control cells. The dichotomic behaviour of NFAT activity in Creld1 deficient T cells could indicate a differential regulation of the transcription factor by two independent pathways differentially affected by Creld1 depletion.

5.6 Creld1 is a type I transmembrane protein functionally localizing at the plasma membrane

The molecular mechanism behind Creld1 activity remains largely unknown. As previously described, the predicted Creld1 protein structure suggests that the protein is membrane bound

due to the two predicted transmembrane domains and a signal peptide. The rest of the protein includes two EGF-like domains and two cbEGF-like domains commonly present in membrane bound or secreted proteins.

5.6.1 *Creld1 localizes at the plasma membrane*

At first, we decided to investigate the sub-cellular localization of Creld1. Creld1 mRNA was cloned downstream of a monomeric RFP as a fusion protein to easily monitor the localization of the protein within the cells. As previously, reported RFP-Creld1 signal localized at the endoplasmic reticulum (ER) of the cells (**fig 5.27 A top/left**). Due to the presence of a signal peptide and two predicted transmembrane domains this result was not unexpected, but structural analysis of the composition of Creld1 amino acid sequence didn't show a clear presence of an ER retention motif. Furthermore, prediction algorithms classify Creld1 as an extracellular protein, mainly due to the presence of an EGF-like domain mostly found in extracellular-facing proteins (DeepLoc - Almagro Armenteros *et al.*, 2017 - eukaryotic protein subcellular localization predictor).

To investigate a possible localization of Creld1 at the plasma membrane RFP-Creld1 transfected NIH-3T3 cells were stained 24 hours after transfection with an α-Creld1 antibody without permeabilization with the aim of enhancing the signal coming from the plasma membrane. Under these conditions, the majority of the signal from the fusion protein was still localizing at the ER but it was possible to identify specific staining at the plasma membrane which was not present in cells treated only with the secondary antibody (**fig 5.27 A**).

As further proof of the specificity of the Creld1 signal at the plasma membrane, RFP-Creld1 transfected cells were shortly treated with Brefeldin A before extracellular staining. Brefeldin A inhibits the transport of proteins form the ER to the Golgi apparatus, which is the intermediate step before presentation of proteins at the plasma membrane or protein secretion. Inhibition of protein transport to the plasma membrane was sufficient to block the signal of Creld1 at the plasma membrane further supporting the specificity of the plasma membrane signal (**fig 5.27 B**).

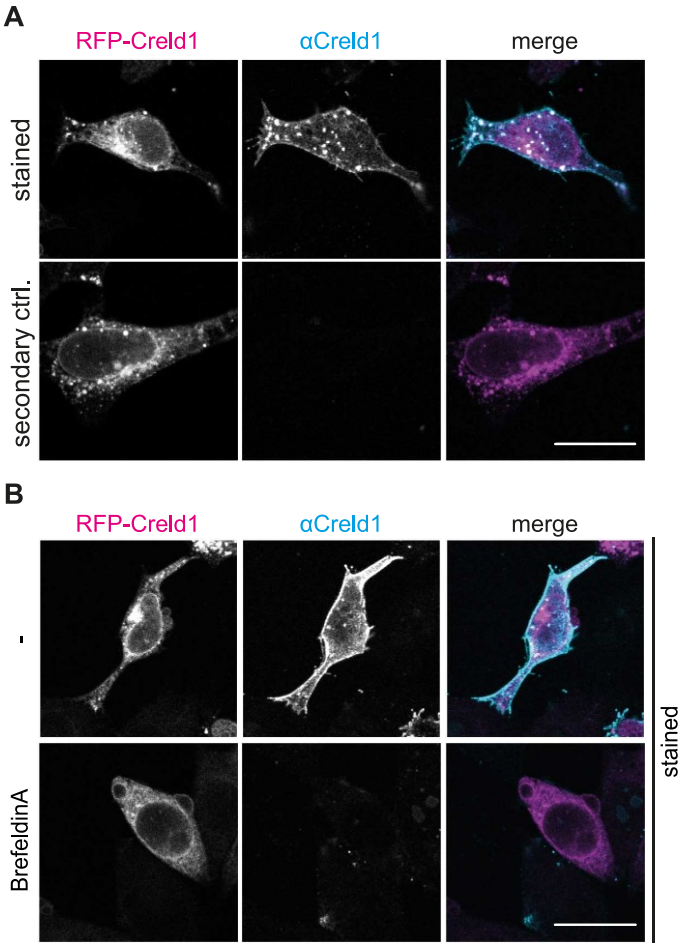

Figure 5.27 Creld1 localises at the plasma membrane in NIH-3T3 cell

*NIH-3T3 cells were transfected with RFP-Creld1 expression vector and stained against Creld1 without permeabilization (**A**), as control cells were stained only with the secondary antibody used without incubation with αCreld1 antibody (**A**). **B**: Brefeldin A-treated cells. Scale bar 25µm.*

5.6.2 *Creld1 is a type I transmembrane protein*

To further characterize the localization of Creld1 we focused on the orientation of Creld1 insertion into the plasma membrane. An interesting and powerful approach to investigate the orientation of a transmembrane protein was developed by Lorenz and colleagues in 2006 (Lorenz *et al.*, 2006). This approach, named fluorescence protease protection (FPP), is based on the consecutive treatment of living cells with permeabilizing agents and proteases while monitoring fluorescence signal from a protein of interest fused with a fluorescent reporter. Briefly, living cell were imaged on a confocal microscope, first digitonin was added to the cell, permeabilizing the cell membrane leading to the diffusion of all cytosolic soluble proteins; trypsin was then added to the medium allowing the enzymatic digestion of all ER-bound protein domains facing the cytosol. In this step if the fluorescent tag is facing the cytosol this will be digested and the fluorescence will fade. Further, Triton-x100 is added to the solution

leading to a strong permeabilization of the ER membrane allowing free diffusion of trypsin to the ER which consequentially leads to digesting ER-lumen proteins.

In our experiment three controls were used to validate the method, cells were co-transfected in binary combination with Creld1 either tagged at the N-terminus or at the C-terminus (**fig 5.28 A**) and a soluble protein (**EYFP**), or two variants of CD3δ either tagged at the C-terminus with CFP or at the N-terminus with YFP (**fig 5.28 B**). As expected, the permeabilization of the plasma membrane by the action of Digitonin leads to the gradual diffusion of the soluble protein EYFP. The addition of trypsin efficiently degraded the CFP tagged at the C-terminus of the CD3δ receptor while the fluorescence coming from the YFP-CD3δ protein resisted trypsin treatment and faded only after further permeabilization with Triton X-100. Surprisingly, the same procedure on the opposite-tagged Creld1 fusion proteins showed a different behaviour in each of them contradicting the prediction of two transmembrane domains that would lead to booth termini facing the ER-lumen (**fig 5.28 B**).

Here, it was clearly visible that the C-terminus of the protein was susceptible to trypsin treatment proving that it faces the cytosol, as previously shown (Mass *et al.*, 2014), while the N-terminus of the protein was resistant to trypsin degradation until complete permeabilization with Triton X-100. This marked difference was also noticeable in the kinetic of the change in fluorescence intensity (representative experiment in figure **5.27 C**). In combination with our findings concerning the localization at the plasma membrane, this experiment defined a structural model of how Creld1 is oriented in the plasma membrane. Collectively, Creld1 is a type I transmembrane protein with most of its domains facing the extracellular space (**fig 5.28 D**).

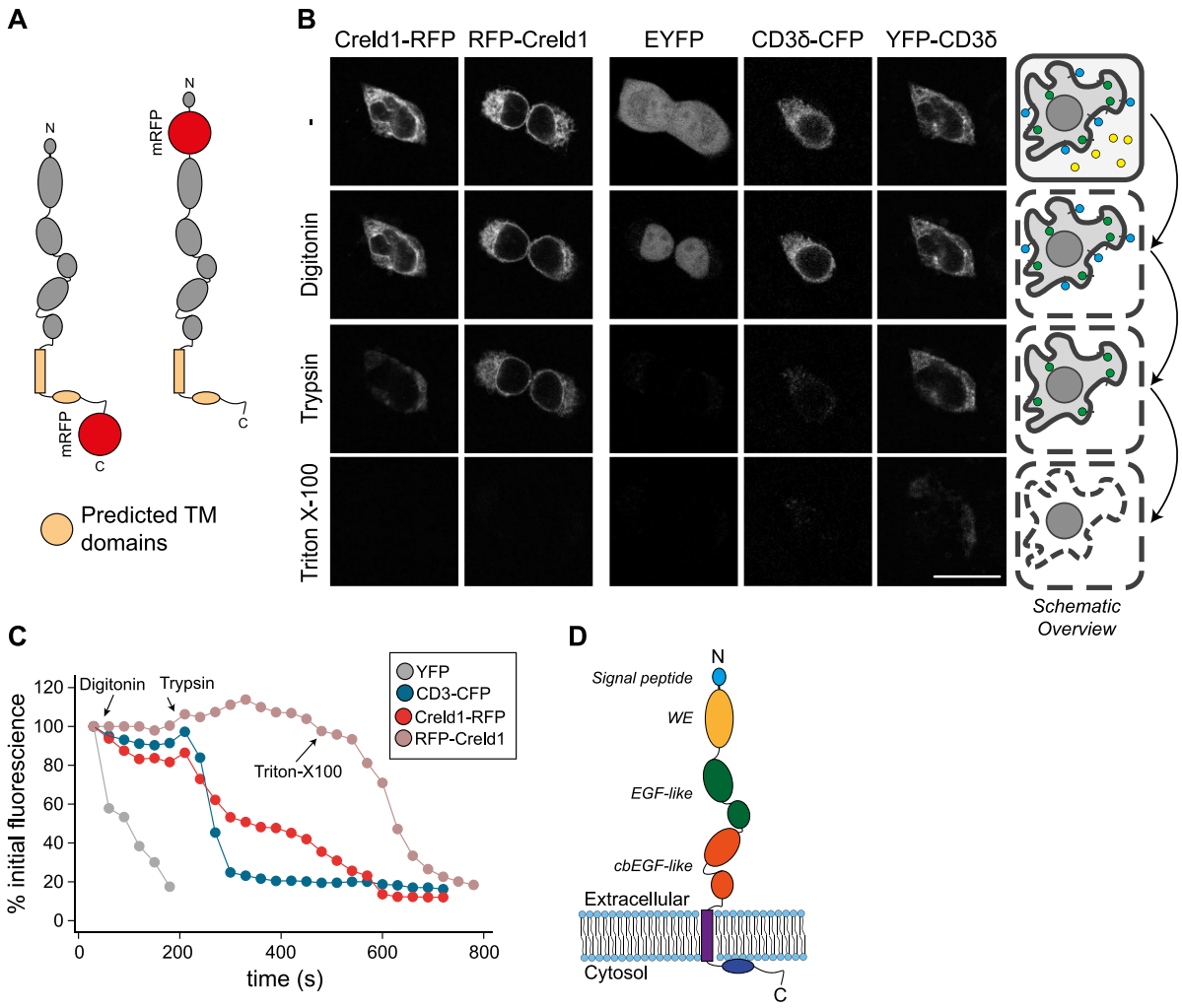

Figure 5.28 Creld1 is a type I transmembrane protein

***A**: Schematic representation of the RFP-tagged Creld1 recombinant proteins. **B**: Fluorescence protease protection assay was performed. As control a soluble protein (EYFP), a tagged transmembrane protein facing the cytosol (CD3δ-CFP) and a transmembrane protein tagged in the ER lumen (YFP-CD3δ), were transfected in combination with tagged Creld1 expression vectors. Scale bar 25µm. **C**: exemplary plot for loss of fluorescence intensity during the consecutive treatments. **D**: experimental model of Creld1 orientation and localization.*

5.6.3 *Creld1 localization at the plasma membrane is necessary for its activity on NFATc1*

As previously mentioned, Creld1 overexpression in mammalian cells is sufficient to trigger the activation of NFATc1 (monitored as nuclear localization of the transcription factor). In this context, we wanted to asses if the localization of Creld1 at the plasma membrane was also important for its functional activity.

Untreated cells (-) showed normal Creld1 localization at the ER and partially at the plasma membrane. In this situation NFATc1 was activated showing complete localization into the nucleus (**fig 5.29 A first row**).

Interestingly, cells that were treated with Brefeldin A, inhibiting the translocation of Creld1 to the plasma membrane, did not show an activation of NFATc1, with NFATc1 remaining localized in the cytosol of the cell (**fig 5.29 A second row**).

To confirm that the observed effect was not due to the treatment with Brefeldin A -independent of Creld1 activity on NFATc1 - cells were treated with Thapsigargin or a combination of Thapsigargin and Brefeldin A. Thapsigargin is an inhibitor of SERCA, the transporter of calcium from the cytosol to the ER. The inhibition of SERCA will lead to the uncontrolled increase in calcium levels in the cytosol and consequentially activation of the Calcineurin/NFAT pathway. Here we observed that the activation of NFATc1 was still efficient in cells treated with Thapsigargin, with or without Brefeldin A, suggesting that the pathway could be functionally activated and confirming that Creld1 is indeed functionally important at the plasma membrane.

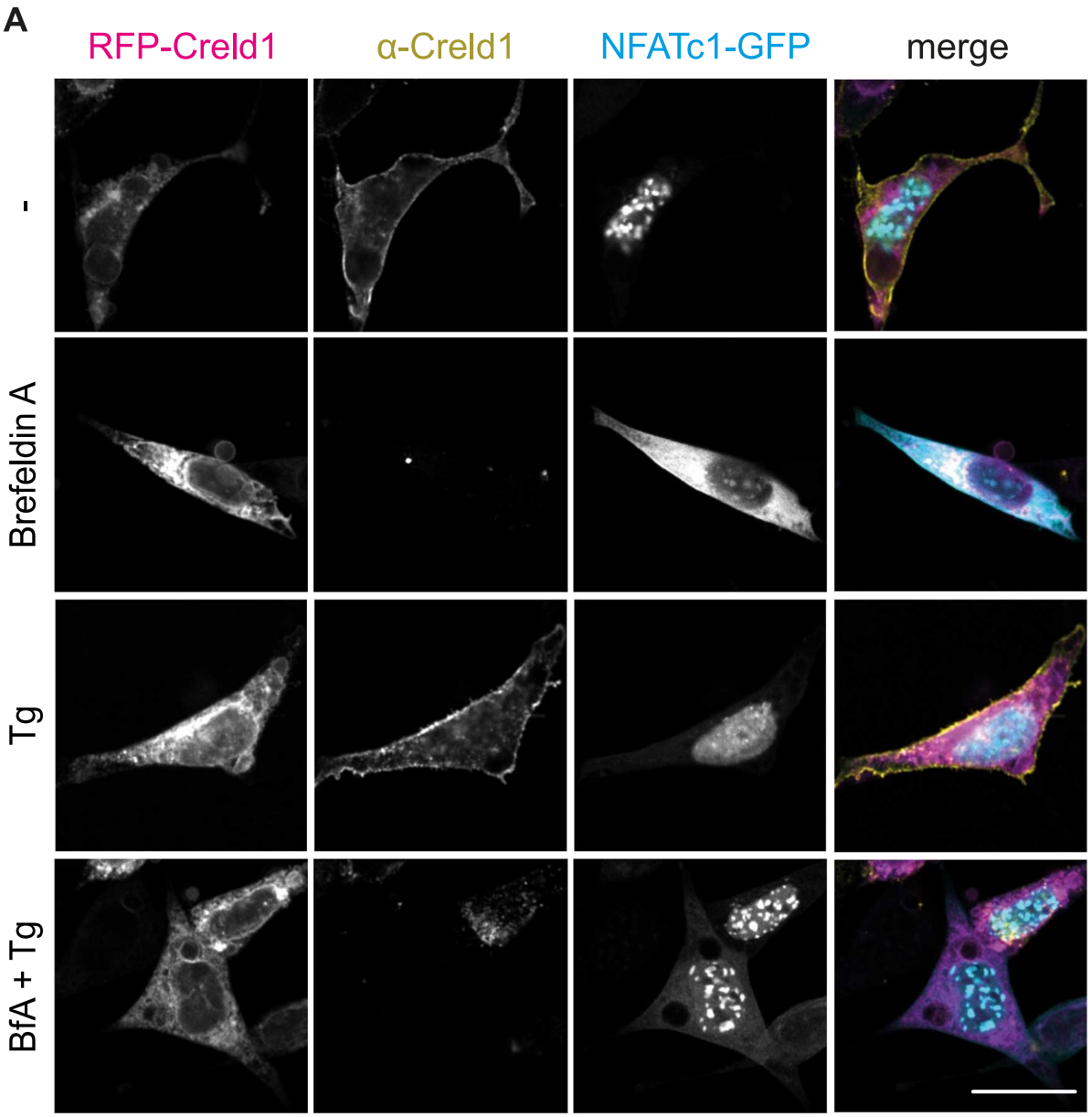

Figure 5.29 Creld1 is required at the plasma membrane to activate NFATc1

*NIH-3T3 cells were transfected with RFP-Creld1 and NFATc1-GFP expression vectors for 24 hours. Cells were then treated with BrefeldinA; Thapsigargin (tg) and the combination of both (**A** – top to bottom). Creld1 expression, membrane localization and NFATc1 localization were monitored by confocal microscopy (**A** – left to right). Scale bar 25µm.*

5.6.4 *Generation of Creld1 deletion mutants*

As described in 1.6, the Creld1 protein consists of several domains some of which are not well characterized. Furthermore, the functional contribution of each of the domains to Creld1 activity remains poorly defined. We decided to investigate the role of the different domains by generating a set of deletion mutants (**fig 5.30 A**). As shown in the schematic overview, mutants

were generated for both the extracellular domains (ΔN) and intracellular domains (ΔC1 and ΔC2). A soluble cytosolic domain only was also generated (solC) to identify the minimal component of Creld1 that could activate NFATc1 *in vitro*.

Each of the generated expression vectors was expressed in NIH-3T3 cells to asses if they correctly localized within the cell. All tested mutants mainly localized at the ER with a detectable Creld1 signal at the plasma membrane after immunostaining against mRFP. The only construct where this signal was lost was the soluble C-terminus mutant for which a diffuse signal in the cytosol and no plasma membrane staining was observed most likely due to the lack of a signal peptide or transmembrane domain driving membrane localization of the protein (**fig 5.30 B**).

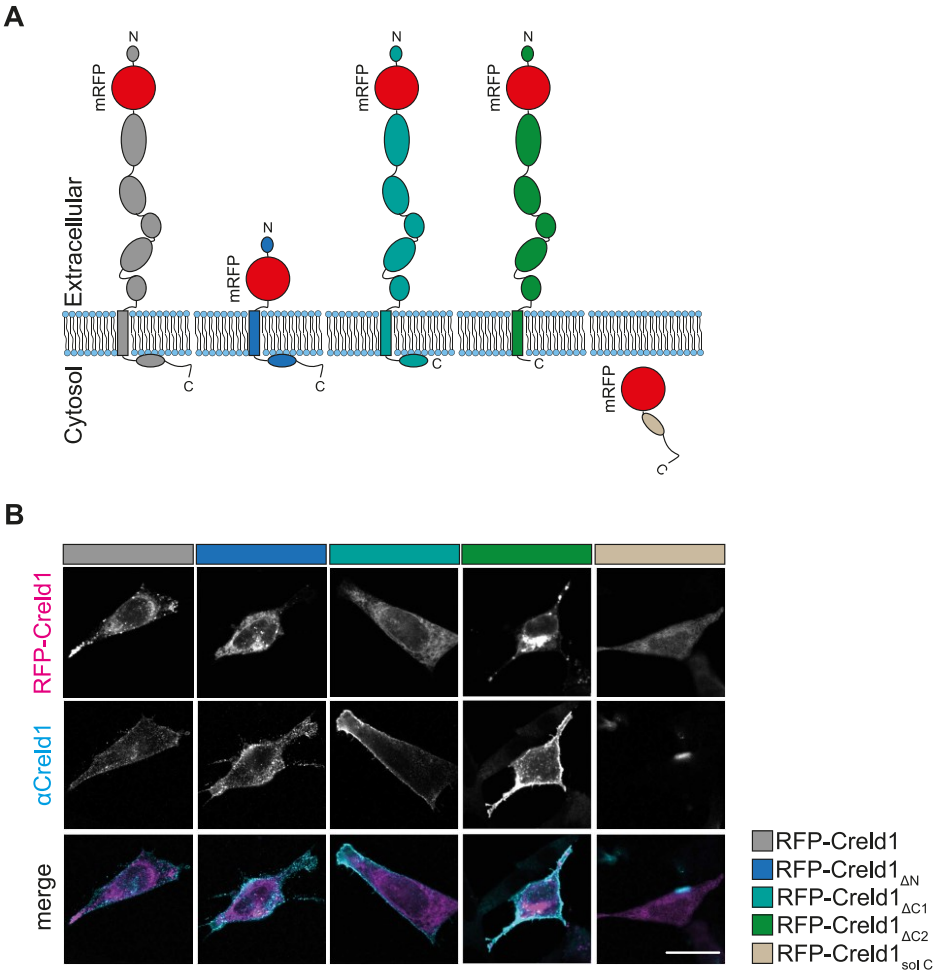

Figure 5.30 Generation and validation of Creld1 deletion mutants

***A**: from left to right, full length Creld1, extracellular domain deletion (ΔN), C terminus deletion (ΔC1), deletion of both C terminus and hydrophobic domain (ΔC2) and the only hydrophobic domain and C terminus (sol C). **B**: staining against Creld1 without permeabilization after 24 hours and analysed by confocal microscopy. From top to bottom: RFP signal of the recombinant protein, αCreld1 staining and merged images. Scale bar 25μm.*

5.6.5 *The C-terminus of Creld 1 is required and sufficient for NFATc1 activation*

To evaluate the importance of the Creld1 structural domains and their ability to activate NFATc1, each of the previously generated vectors were co-transfected with NFATc1 and analysed via confocal microscopy 24 hours post-transfection to visualize the localization of NFATc1 in combination with each of single deletion mutants. The localization of NFATc1 was classified as cytosolic when no signal in the nucleus was detectable, cytosolic/nuclear when the detected signal was mostly nuclear with residual signal in the cytosol or nuclear when almost all signal was detectable in the nucleus (**fig 5.31 A/B**).

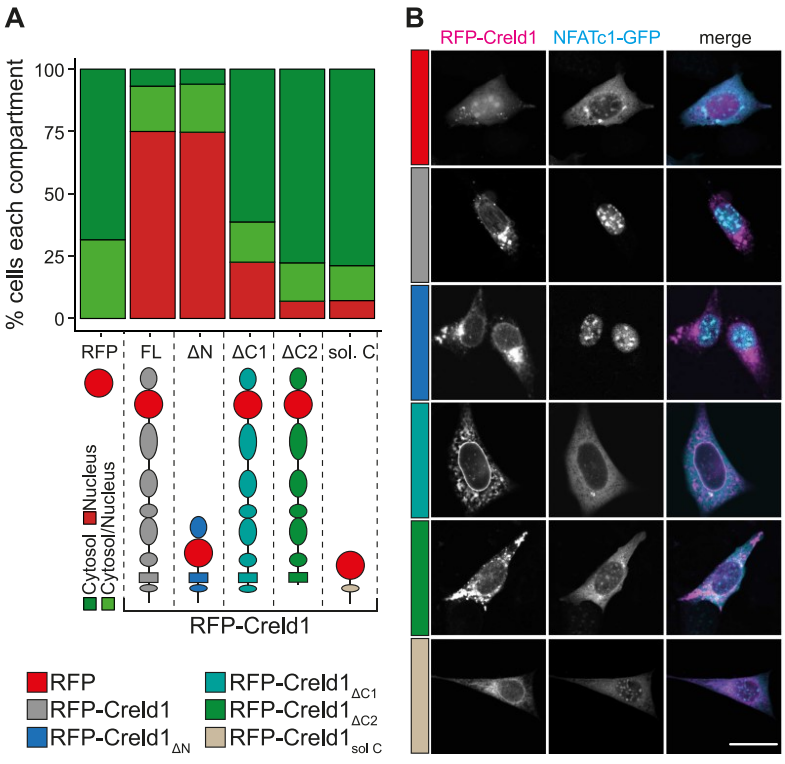

Figure 5.31 Creld1 C-term is required and sufficient for NFATc1 activation

*NFATc1 localization was assessed visually from co-transfected cells. Cells were then grouped by NFATc1 localization (**A**, minimum 50 cell/condition). For each deletion mutant a representative confocal image is shown (**B** – scale bar 25µm).*

Surprisingly, the deletion of the entire extracellular domain did not affect the ability of Creld1 to trigger NFATc1 nuclear translocation. Indeed, the deletion of only the last 14 amino acids (ΔC1) already showed a drastic reduction in the translocation of NFATc1 to the nucleus. This effect was even more pronounced when also the C-terminal hydrophobic domain (previously thought to be a transmembrane domain) was removed.

When only the C-terminal domain of Creld1 was transfected, it was also not able to trigger NFATc1 nuclear translocation. This result was in accordance with the observation that Creld1 must localize at the plasma membrane in order to exert its effect on the activation of the NFAT pathway.

Single deletion mutants for the single extracellular domains were generated (ΔWE, ΔEGF-like, ΔEGF-calcium binding) showing similar NFATc1 translocation compared to WT cells in accordance with the deletion of the entire extracellular portion of the protein (data not shown). This result clearly shows how Creld1 activity on NFATc1 is mediated by the intracellular domains with no requirement of the extracellular fraction in overexpression conditions

5.6.6 *Creld1-dependent NFATc1 activation induces cell proliferation*

NFATc1 is well known to be involved in the regulation of cell proliferation (Menk *et al.*, 2018). Due to the strong effect that Creld1 overexpression has on NFATc1 activation, we hypothesised that Creld1 overexpression could lead to increased cell proliferation via the activation of the NFAT pathway.

In order to prove this, NIH-3T3 cells were labelled with CFSE and consequently transfected with either RFP-Creld1, RFP-Creld1$_{\Delta N}$ or RFP-Creld1$_{\Delta C2}$. Cells were then analysed by flow cytometry after one or three days to evaluate CFSE florescence and consequently proliferation over time.

First the cells were gated by morphology and doublets were removed as described previously. Living, RFP-expressing cells were selected and CFSE fluorescence intensity was evaluated (**fig 5.32 A**). The presence of an RFP tag allowed the identification of those cells efficiently transfected. At one day after transfection, the CFSE intensity for all RFP-tagged Creld1 variants was comparable (**fig 5.30 B**), however at three days post transfection, it was clear that cells transfected with RFP-Creld1 and RFP-Creld1$_{\Delta N}$ expression vectors were able to proliferate significantly more than cells transfected with RFP-Creld1$_{\Delta C}$ (**fig 5.32 C and D**).

With this experiment we could prove that the differences in the ability of Creld1 to translocate to the nucleus related to the activation state of NFATc1 leading to changes in cellular proliferation.

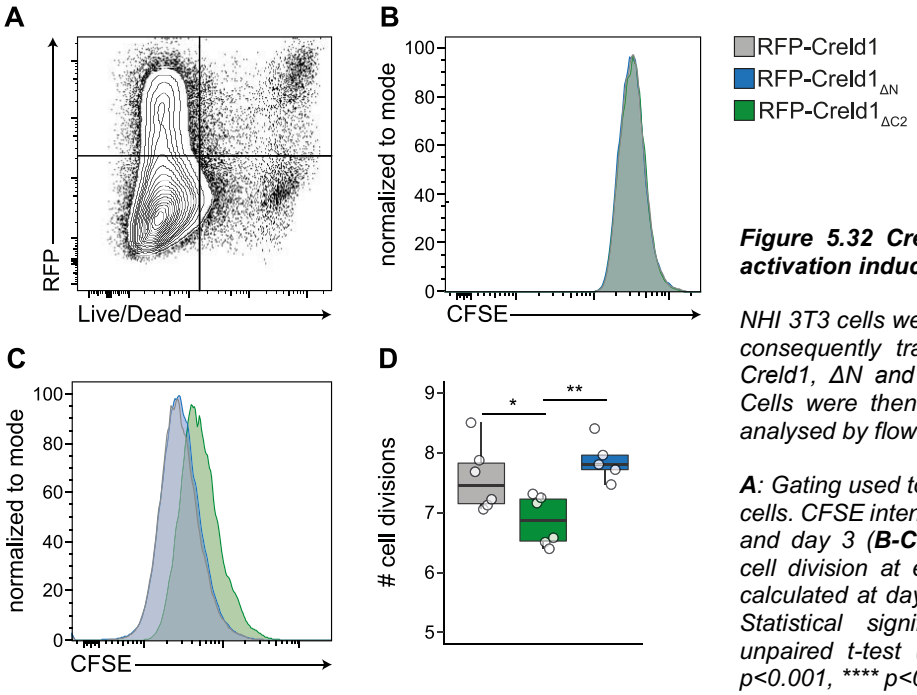

Figure 5.32 Creld1 dependent NFATc1 activation induces cell proliferation

NHI 3T3 cells were stained with CFSE and consequently transfected with full length Creld1, ΔN and ΔC2 expression vectors. Cells were then cultured for 3 days and analysed by flow cytometry at day 1 and 3.

***A**: Gating used to identify transfected living cells. CFSE intensity was analysed at day 1 and day 3 (**B-C** respectively). Number of cell division at each time point was also calculated at day 3 (**D** respectively) (n=6). Statistical significance was tested by unpaired t-test (* p<0.05, ** p<0.01, *** p<0.001, **** p<0.0001).*

5.7 Identification of intracellular Creld1 interaction partners

Knowing that the cytosol facing C-terminus of Creld1 is required for its function in the NFAT pathway and the evidence that the protein needs to localize at the plasma membrane to be activated led to the conclusion that Creld1 must interact with other proteins to exert these functions on NFATc1 activation. NFATc1 activation is generally downstream of Calcineurin activation by release of calcium in the cytosol. We hypothesised that Creld1 must be upstream of this molecular process. We wanted to verify which molecular component could bridge Creld1 activity and Calcineurin activation and therefore we decided to use a co-immunoprecipitation assay to identify binding partners of Creld1.

A standard approach to identify protein-protein interactions is the co-immunoprecipitation of a target protein in native condition leading to the purification of a cluster of interacting proteins together with the target protein (bait protein). Even if well-established, this technique is prone to a lot of unspecific binding of proteins to the protein of interest. To reduce this type of

technical bias we transfected NIH-3T3 fibroblasts with RFP-Creld1 full length, RFP-Creld1 ΔN and RFP-Creld1 ΔC2 (**fig 5.33 A**) and immunoprecipitated 24 hours after transfection using an RFP-specific pull-down that was consequently analysed by MS/MS (service provided by the CECAD at the University of Cologne) to identify proteins interacting with each Creld1 construct (**fig 5.33 B**).

The comparison of the captured proteins between all different conditions allowed the identification of proteins that specifically bound to the intracellular domain of Creld1. In fact, we expected that all proteins that appeared to interact with all three Creld1 variants would have to be classified as being unspecific binding to the antibody complex or associate with the transmembrane region. Proteins found to interact with the full length Creld1, the complete deletion of the extracellular domain (ΔN), but not the deletion mutant for the intracellular domain (ΔC2) were more likely to represent novel binding partners at the intracellular domain of Creld1 providing insight into the molecular mechanism explaining Creld1 activity (see **schematic figure 7.1** for details).

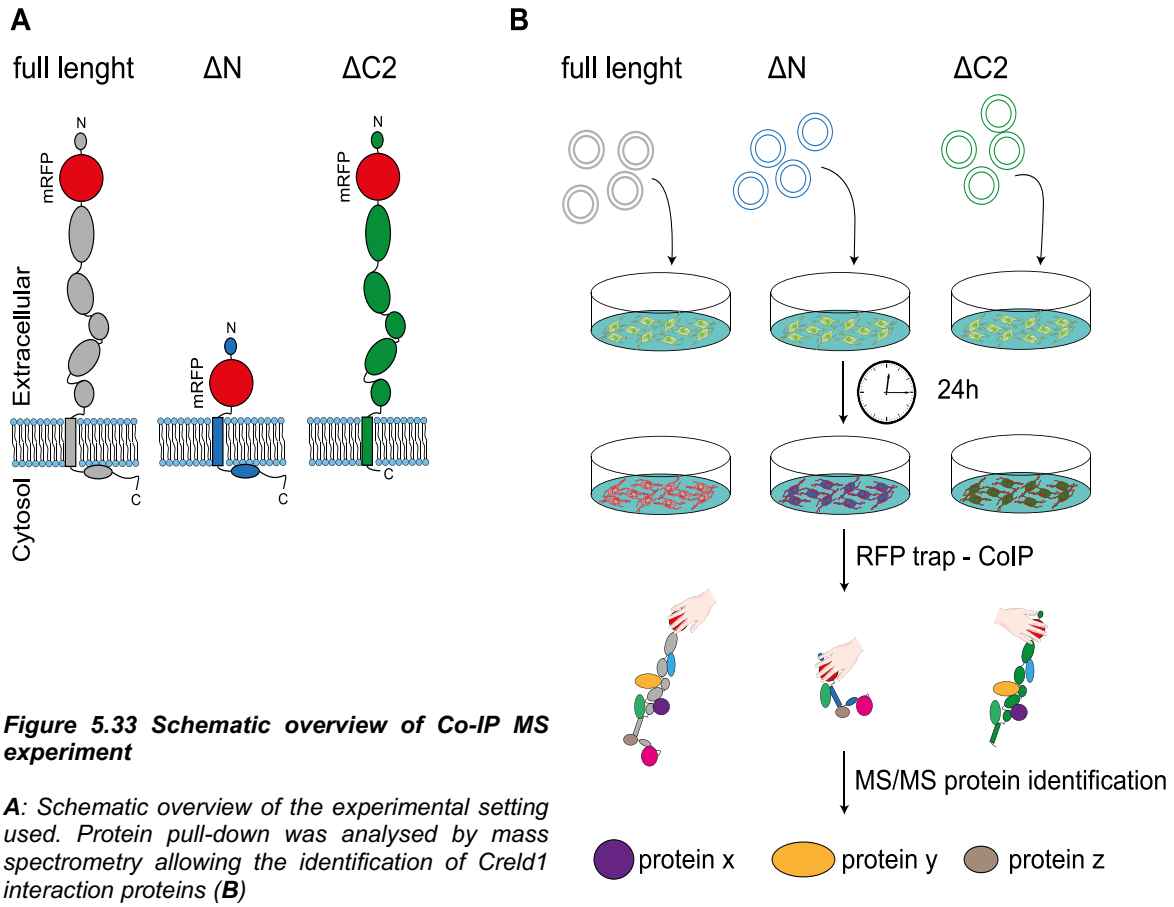

Figure 5.33 Schematic overview of Co-IP MS experiment

***A**: Schematic overview of the experimental setting used. Protein pull-down was analysed by mass spectrometry allowing the identification of Creld1 interaction proteins (**B**)*

5.7.1 *Proteins specifically binding the intracellular domain of Creld1*

Raw data from the MS/MS experiments were first aligned against the murine proteome and quantified using the MaxQuant software. Missing values resulting from the identification of the proteins across all samples were imputed (**fig 5.34 A**). The values identified were then used to generate hierarchical clustering of all the proteins identified for each sample. By this approach, we identified specific clusters shared between the full length and the ΔN variant that were not represented in the data derived from the ΔC2 variant. The principal component analysis of all identified proteins clearly showed how the full length protein and the ΔC2 were separated in the PC1 (Principal Component 1) where most of the variance was identified, whereas full length and ΔN were mainly separated the within PC2 suggesting that the ΔN has a set of binding partners more similar to the full length protein (**fig 5.34 C**).

To identify proteins specifically binding to the C-terminal domain of Creld1, the list of proteins was filtered based on the concept that protein binding to the C-terminal domain of Creld1 will

be present in the full length and ΔN pull down but reduced in the pull down of the ΔC2 since the C-terminal domain was deleted in this construct. The specific thresholds of filtering are shown in figure 5.31 A.

With these cut offs, we found only 9 proteins as bona fide interactors of Creld1 (**fig 5.34 D**). Surprisingly, there was no common function that could be deduced from these 9 proteins directly. We therefore applied an unbiased approach to have more insight into the molecular mechanisms governing the activation of the NFAT signalling pathway.

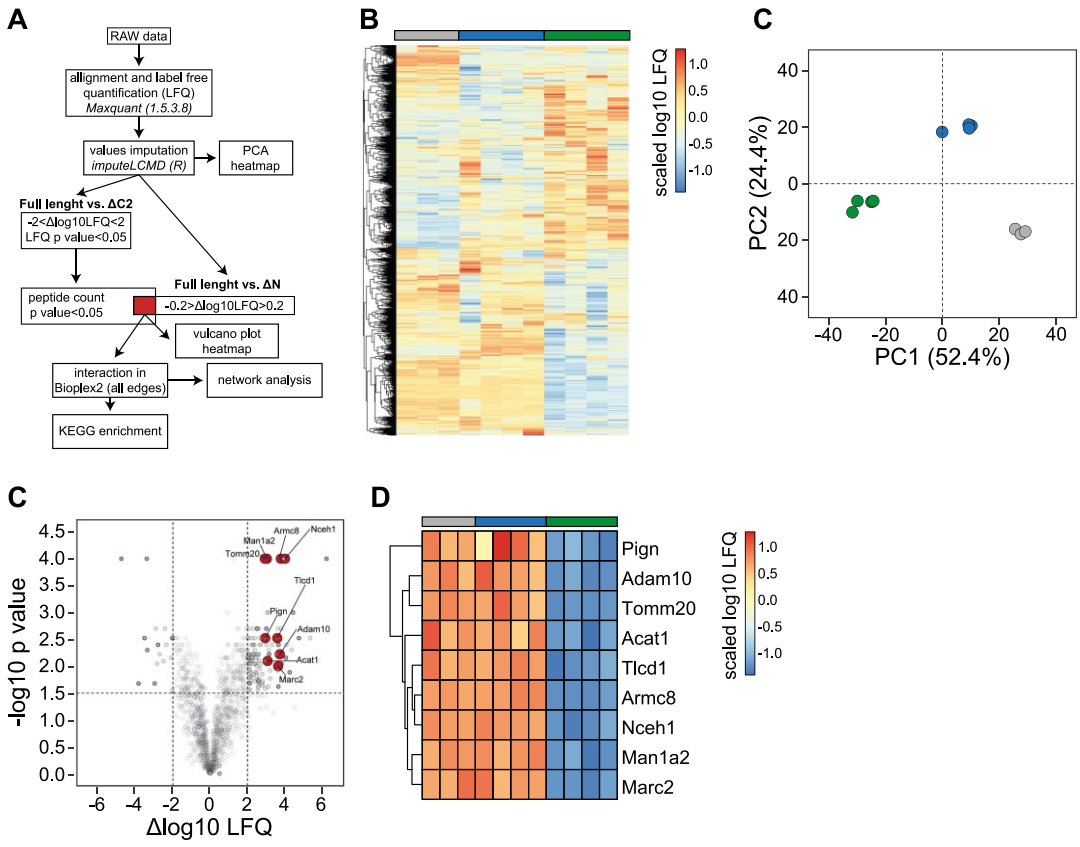

Figure 5.34 Nine proteins specifically bind Creld1 intracellular domain

***A**: schematic overview of the analysis performed to identify the bona fide interactors of Creld1. Hierarchical clustering and PCA of all proteins present identified in the experiment before any filtering (**A** and **B** respectively) are shown. **C**: volcano plot showing the Δlog10 LFQ for the comparison between full length and ΔC2. In red, the proteins that pass the filter process explained in A. **D**: hierarchical clustering of the filtered Creld1 interactors.*

5.7.2 *Cross-reference with the BioPlex2.0 dataset shows enrichment for the WNT signalling pathway*

To identify pathways involved in Creld1 activity in an unbiased fashion we mapped the proteins, we had identified, into a network of protein-protein interactions that had been previously determined within the Bioplex2 database (Huttlin *et al.*, 2015, 2017). This approach resulted in a wider network of protein-protein interactions that was subsequently used to identify enriched pathways. In comparison to several other available datasets, the Bioplex2 database is completely based on experimental data derived from proteome-wide Co-IP mass spectrometry experiments.

The dataset was filtered based on all proteins that were identified in our screen. Only 6 of the input proteins were present in the Bioplex2 network. At this point, starting with our experimentally identified proteins, all first edges of these proteins were selected within the Bioplex2 network and for all these edges the nodes connected to them were kept; thereby identifying interactions between the proteins connected to the Creld1 interactors.

This approach identified a highly interconnected network (**fig 5.35 A**) that showed a significant enrichment of several biological pathways (KEGG) (**fig 5.35 B**). The enrichment for the WNT signalling pathway corroborated our transcriptome data as it was one of the strongest downregulated pathways. Interestingly, this enrichment was centring around the interaction of Creld1 with Armc8, a protein that is so far not well understood. However, it shows high similarity with β-Catenin and interacts with other components of the WNT signalling like NFATc1 as part of the non-canonical WNT pathway. Furthermore, Armc8 was recently described as modulator of the Wnt signalling pathway in vitro (Zhao *et al.*, 2016; Liang *et al.*, 2017).

A further step in the identification of the molecular function of Creld1 was the inclusion of its known interaction partners described in the Bioplex2 dataset. Interestingly here we could identify Frizzled10 as an interesting binding partner for CRELD1. Frizzled family of proteins

are the well-known receptors for WNT (**fig 5.35 C**). Implementing those interactors still showed a high functional enrichment for Wnt signalling pathway (**fig 5.35 D**).

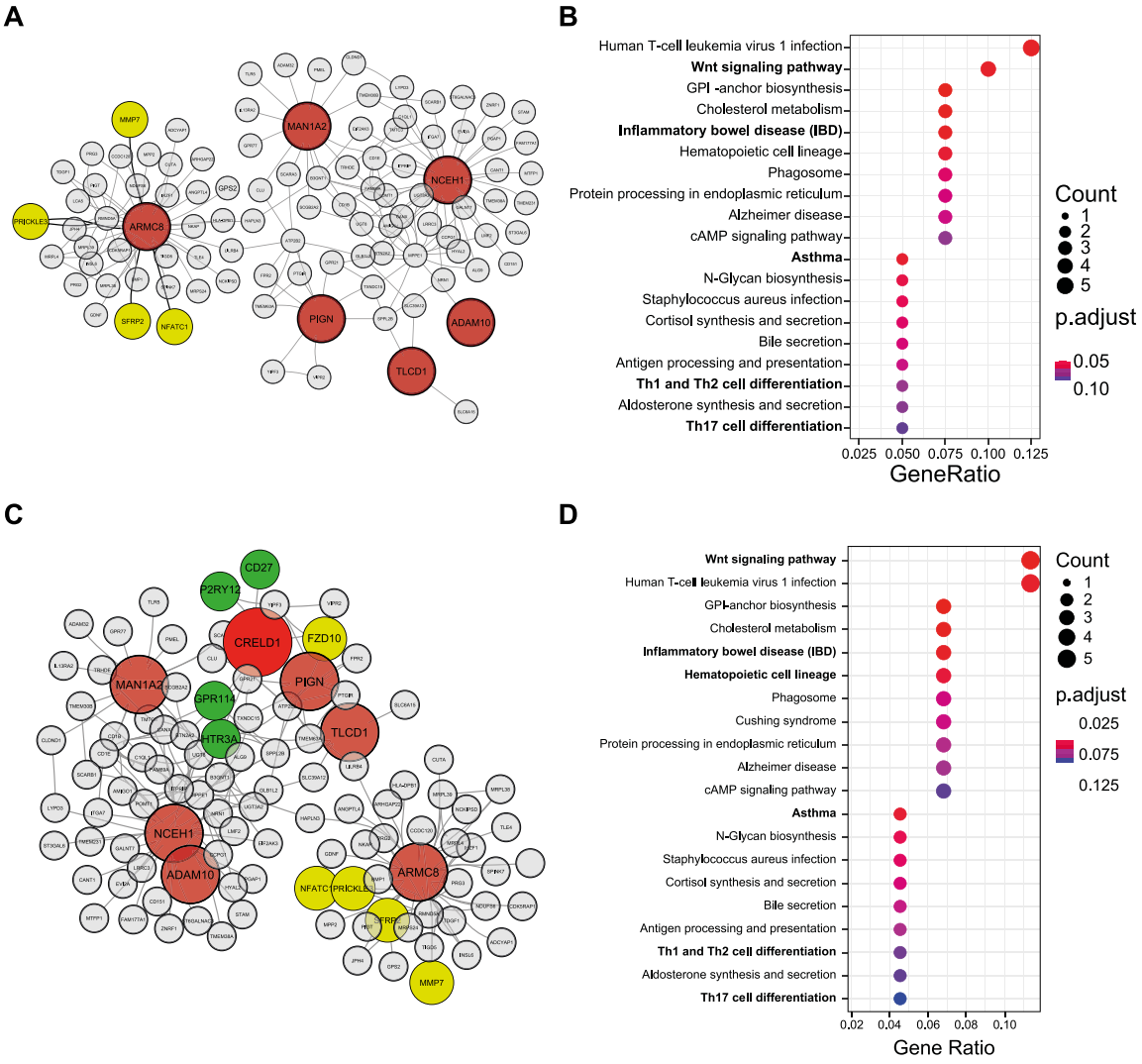

Figure 5.35 WNT signalling is enriched in the network of Creld1 interactors

*Network analysis (**A**) and KEGG enrichment analysis (**B**) of Creld1 interaction partners and their interactors in the Bioplex2 dataset. Same analysis including in the network also the known interactors of CRELD1 in the Bioplex2 dataset; network analysis (**C**) and KEGG enrichment (**D**) are shown.*

5.8 Creld1 regulates the Wnt signalling pathway

The Wnt signalling pathway is a highly evolutionary conserved pathway involved in many fundamental cellular functions. The identification of a direct regulation of the Wnt signalling pathway by Creld1 lead us to investigate this pathway more in-depth. We could now use

Creld1 deficient CD4⁺ T cells and overexpression of Creld1 in murine fibroblast as toolbox to study how Creld1 regulates Wnt signalling.

5.8.1 *Creld1 KO CD4⁺ T cells show decreased activation of Wnt signalling*

As described above, Creld1 KO CD4⁺ T cells display accelerated cell death both *in vivo* and *ex vivo*. Furthermore, considering the transcriptional regulation in KO CD4⁺ T cells, we observed drastic changes compared to control with specific enrichment of Wnt-signalling pathway genes downregulated in KO CD4⁺ T cells.

We further showed that several β-Catenin target genes were downregulated in KO cells suggesting a reduced activity of this signalling pathway (**fig 5.36 A**). Looking at a transcriptome-based network generated only from all present transcription factors, we observed a strong enrichment in Wnt β-Catenin signalling in the turquoise module of the transcription factor network (**fig 5.36 B/C**).

All together, these findings let us to hypothesize that Creld1 regulates the initiation of the Wnt pathway.

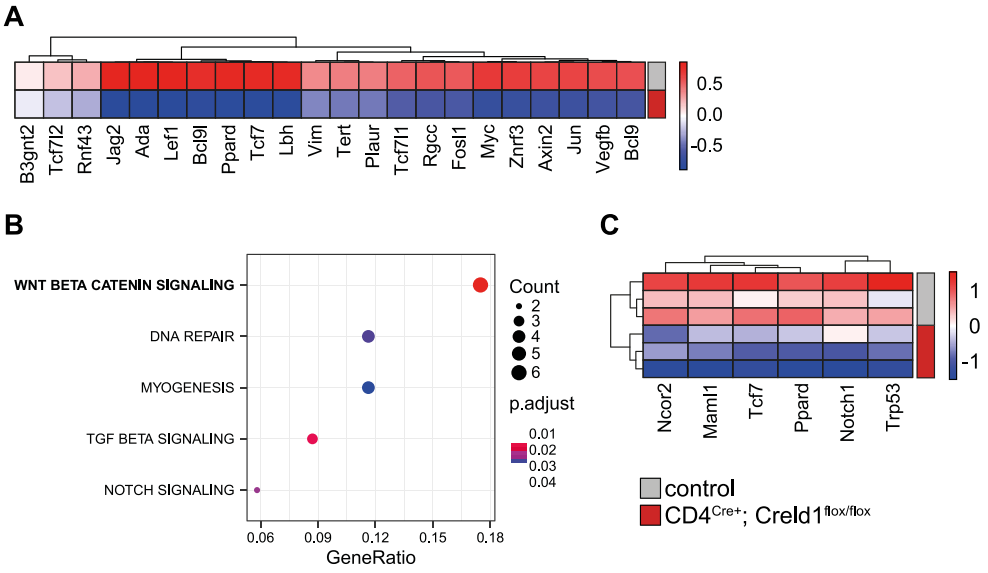

Figure 5.36 Creld1 KO CD4⁺ T cells show decreased activation of Wnt signalling

***A**: scaled mean expression of selected Wnt target genes in control or CD4Cre⁺; Creld1$^{flox/flox}$ CD4⁺ T. **B**: Functional enrichment in turquoise module of the transcription factor network, the scaled expression of transcription factors contributing to the Wnt signalling enrichment are shown in **C**.*

5.8.2 *Creld1 overexpression induces β-Catenin stabilization*

One of the hallmark events in the activation of the Wnt signalling pathway is the inactivation of the β-Catenin destruction complex. Binding of Wnt to the Frizzled receptor induces the activation of the CK1 kinase leading to the recruitment of Axin to the cytoplasmic tail of the LRP co-receptor inhibiting the ubiquitination of β-Catenin.

NIH-3T3 cells were transfected with full length RFP-Creld1 or RFP-Creld1$_{\Delta C2}$ expression vectors; one day after transfection cells were lysed and the expression level of both RFP and β-Catenin were quantified via Western blot. Due to the variability in the transfection efficiency in different experiments, the fold change of β-Catenin compared to control were correlated to the transfection efficiency calculated as RFP intensity normalized on actin. It was clear that full length Creld1 overexpression stabilized β-Catenin (**fig 5.37 A**). Conversely, the overexpression of the non-functional variant (ΔC2), showed a decreased stabilization of β-Catenin indicating that there is a dominant negative effect.

To assess the functional activation of β-Catenin as a transcription factor in the nucleus, a luciferase reporter system was used. This reporter system consisted of the coding sequence of the firefly luciferase downstream seven consecutive TCF/LEF binding sites. This vector will lead to the expression of the firefly luciferase induced by the activation of the β-Catenin-TCF/LEF nuclear complex (TOP - β-Catenin). As control for the experiment a mutated version of the luciferase reporter unable to bind the nuclear complex was used (FOP - β-Catenin).

Furthermore, to control for the transfection efficiency, a control vector expressing the Renilla luciferase was used. The luciferase intensity measured was normalized over the intensity of Renilla luciferase and displayed as ratio between TOP and FOP to exclude non-specific amplification of the signal.

We observed that transfection of RFP-Creld1 in combination with the luciferase reporter system led to the nuclear activation of β-Catenin, while overexpression of the ΔC2 Creld1 did not show a significant change in β-Catenin activation (**fig 5.37 C**)

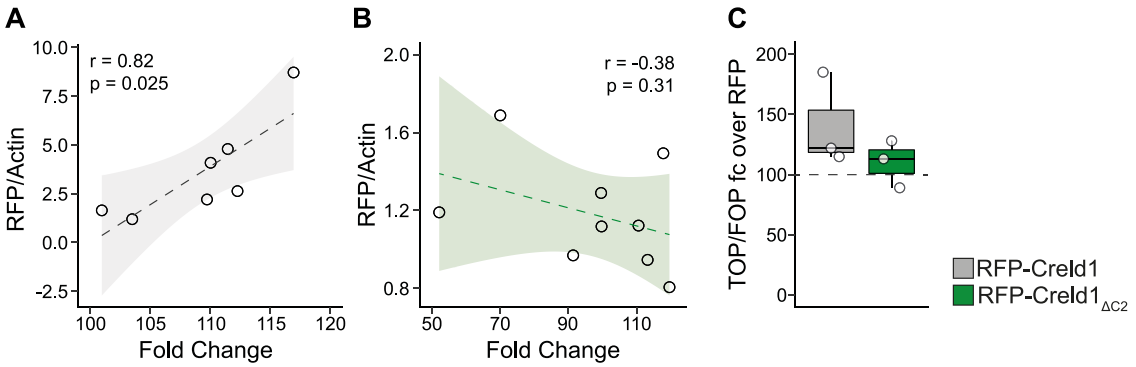

Figure 5.37 Creld1 overexpression induces β-Catenin stabilization

*NIH-3T3 cells were transfected with full length RFP-Creld1 (**A** n=7) or ΔC2 expression vectors (**B** n=8). β-catenin fold change over RFP control was quantified and correlated with the RFP expression as control of transfection efficiency. **C**: β-catenin luciferase expression shown as fold change over RFP control for full length RFP-Creld1 or ΔC2 transfected HIH-3T3 cells (n=3).*

5.8.3 *Creld1 deficiency induces imbalanced T cell differentiation*

It has been recently shown, how perturbances in the Wnt signalling pathway in mature T cells affect the differentiation program upon activation (van Loosdregt and Coffer, 2018). To test whether Creld1 deficient T cells display a similar phenotype, naïve $CD4^+$ T cells were sorted from *$CD4^{Cre}$; $Creld1^{flox/flox}$* or control mice. The purified cells were then simulated with α-CD3 and α-CD28 antibodies in presence of specific cytokines and cytokine-blocking antibodies to drive the differentiation of the cells to a specific Th subset. As a control (Th0), cells were stimulated for the same time with α-CD3/α-CD28 antibodies in medium supplemented with IFNγ and IL-4 blocking antibodies to inhibit spontaneous differentiation into Th1 and Th2 subsets.

To evaluate the stage of differentiation after five days, the cells were treated with PMA and ionomycin. The cells were then extracellularly stained with α-CD3 and α-CD4 antibody and intracellularly for the hallmark cytokines or transcription factors of each T helper cell subset. The cell suspension was then analysed by flow cytometry and $CD4^+$ T cells were selected by the co-expression of both, CD3 and CD4. In this population, Th1 cells were defined by the expression of IFNγ, Th17 for the expression of IL-17, Th2 as IL-4 producing cells and Th9 as IL-9 producing cells. iTregs cells were not stimulated with PMA and ionomycin due to the high

toxicity this stimulation has on this T cell subset. These cells were stained for FoxP3, the hallmark transcription factor for Tregs.

We observed that Creld1 deficient $CD4^+$ T cells showed an increased bias to differentiate into Th1 and Th17 subsets (**fig 5.38 A** and **B** respectively) with the Th2 subset being less represented (**fig 5.38 C**). Concerning Th9 and iTreg differentiation no significant differences were found (**fig 5.38 D** and **E** respectively).

Importantly, our results are in accordance with recent findings on the effect of Wnt signalling on $CD4^+$ T cell differentiation, indeed, perturbation of this pathway promote differentiation to Th1 and Th17 and inhibit Th2 development (reviewed in van Loosdregt and Coffer, 2018) similarly to Creld1 depletion in $CD4^+$ T cells.

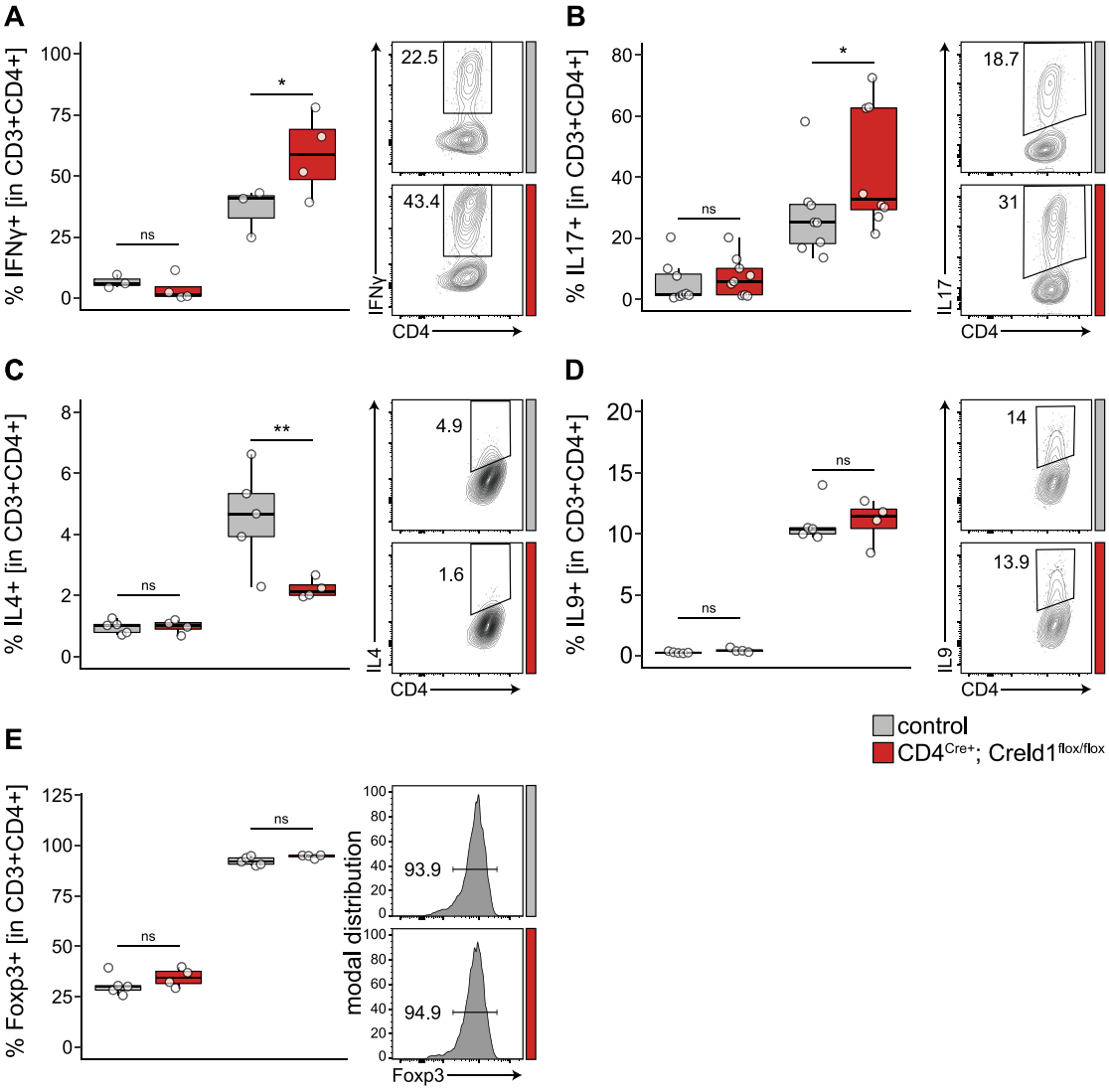

Figure 5.38 Creld1 deficiency induces unbalanced T cell differentiation

*In vitro differentiation of naïve CD4⁺ T cells into Th1, Th17, Th2, Th9 and iTregs (**A to E**). After 5 days of stimulation cells were analysed by flow cytometry and defined by the expression of hallmark cytokines or transcription factors (Th1= IFNγ **A** n=4, Th17=IL-17 **B** n=8, Th2=IL-4 **C** n=5, Th9=IL-9 **D** n=5, iTregs=FoxP3 **E** n=5). Statistical significance was tested one-way ANOVA with Bonferroni correction for multiple testing (* p<0.05, ** p<0.01, *** p<0.001, **** p<0.0001).*

5.8.4 *Pharmacological activation of the Wnt signalling pathway rescues the Creld1 deficient phenotype in CD4⁺ T cells*

The molecular mechanisms behind the physiological activation of the Wnt signalling pathways are well understood. Due to the involvement of this molecular pathway in several pathological conditions, several attempts to pharmacologically modulate this pathway have been developed. A valuable approach to pharmacologically activate the Wnt signalling pathway is the inhibition of the serine/threonine kinase GSK3. The inhibition of this protein will lead to the activation of the CK1 leading to the inactivation of the β-Catenin destruction complex.

We decided to use this pharmacological approach with Creld1 deficient CD4⁺ T cells. As shown before Creld1 depletion in T cells leads to a decreased viability of the cells *in vivo* and *in vitro* leading to increased levels of apoptosis. We also showed that this deficiency in survival was not dependent on IL-7 or IL-15 stimulation. Creld1 KO CD4⁺ cells treated for eight hours *ex vivo* with the GSK-3 inhibitor BI-5521 (Boehringer Ingelheim), were completely rescued concerning increased apoptotic rate of these cells (**fig 5.39 A**). In contrast, the treatment of the cells with Wnt3a showed only a moderate improvement of the apoptotic rate in CD4⁺ T cell (**fig 5.39 A**). Together, these results illustrate how Creld1 is regulating the pathway downstream of Wnt binding to its receptor but upstream to GKS3 inhibition.

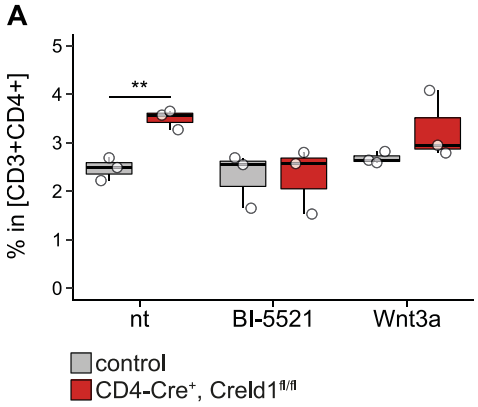

Figure 5.39 GSK3 inhibition rescues Creld1 deficiency in CD4⁺ T cells

*CD4⁺ T cells from control or CD4^{Cre+}; Creld1$^{flox/flox}$ were cultured for 8 hours and treated with BI-5521 (GSK3 inhibitor) or Wnt3a and analysed by flow cytometry. **A**: apoptosis rate by detection of cleaved caspase 3 (n=3). Statistical significance was tested by unpaired t-test (* p<0.05, ** p<0.01, *** p<0.001, **** p<0.0001).*

5.9 Insight into a conserved function of the human CRELD1 gene

The recent advent of population-wide large studies including omics-based data from immune cells in a large number of individuals opens up completely new avenues towards the use of human variation to study the role of individual genes.

Creld1 is a highly conserved protein sharing 96% amino acid similarity with human CRELD1 with a 100% match in the cytosolic C terminus shown to be important for Creld1 activity. Due to this high conservation of the protein in humans, we became interested in whether CRELD1 function might have any relevance also in the human immune system.

5.9.1 *CRELD1 is expressed in human CD4$^+$ T cells*

To investigate *CRELD1* expression in human naïve CD4$^+$ T cells, we analysed a transcriptome dataset of sorted CD4$^+$ T cells from the CEDAR and ImmVar studies (De Jager *et al.*, 2015; Momozawa *et al.*, 2018) - analysis summarized in **supplementary schematic 7.2** and **7.3**. We could observe that *CRELD1* was expressed in all samples in the dataset and showed normal distribution. For further analysis on this dataset we decided to stratify the samples in the CEDAR dataset based on *CRELD1* expression. We defined samples with *CRELD1* expression lower than the 5th percentile of the distribution as CRELD1^{low}, and samples with *CRELD1* expression higher than the 95th percentile of the distribution as CRELD1^{high} (**fig 5.40 B**).

These two populations were used as a surrogate for the comparison between WT and Creld1 deficient CD4$^+$ T cells to further investigate whether CRELD1 function is conserved among mouse and human (**fig 5.40 A**).

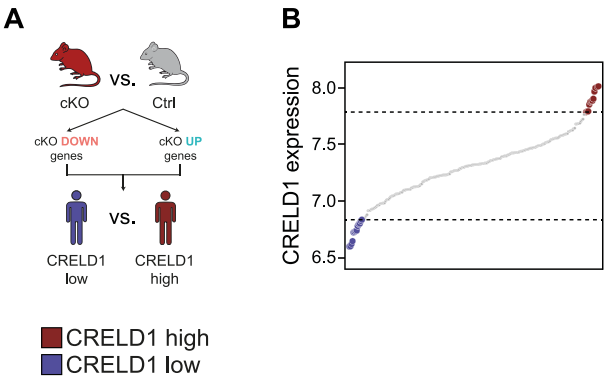

Figure 5.40 CRELD1 expression shows normal distribution in human CD4⁺ T cells

***A**: schematic overview of the analysis performed on the CEDAR dataset. As first step of the analysis the single donors were stratified by CRELD1 expression in CD4⁺ T cells across all donors and grouped as CRELD1 high (>95th percentile) or CRELD1 low (<5th percentile) (**B**).*

5.9.2 *The Creld1-dependent transcriptional signature is conserved in human naïve CD4⁺ T cells*

From the transcriptomic analysis or the *CD4^{Cre}; Creld1$^{flox/flox}$* mouse model we identified specific gene modules differentially regulated in Creld1 deficient T cells and control cells. Next, this information was used to identify if this set of genes is also regulated by CRELD1 in humans. We generated two "Creld1" signatures; the Creld1 DOWN signature derived from the murine T cells includes the genes of module 1 and 3 of the CoCena[2] analysis (**fig 5.21**). These genes are down regulated in Creld1 deficient T cells both in the naïve state and after eight hours of *ex vivo culture*. The other signature generated, named Creld1 UP, include genes upregulated in both naïve and *ex vivo* cultured Creld1 deficient CD4⁺ T cells included in the clusters 2 of the CoCena[2] analysis.

We used the comparison between the gene expression in the CRELD1^{low} and CRELD1^{high} to rank the gene list by differential expression. In this comparison genes up regulated in CRELD1^{low} compared to CRELD1^{high} will rank first in the list and vice versa for genes down regulated in the comparison.

The ranked gene list and the two generated Creld1-dependent signatures were used to perform gene set enrichment analysis (GSEA). The result of the enrichment showed how both, the Creld1 UP signature and the Creld1 DOWN signature, are significantly regulated in the comparison between CRELD1^{low} and CRELD1^{high} (**fig 5.41 A**). We observed that genes downregulated in Creld1 KO CD4⁺ T cells give a negative enrichment meaning that these

genes are mostly down regulated in CRELD1^{low} compared to CRELD1^{high} (**fig 5.41 A and B**). The opposite was shown for the Creld1 up signature (**fig 5.41 A** and **B**). Collectively, changes in human *CRELD1* expression levels between individuals correlate with a broad transcriptional change highly similar to the change previously found in murine KO CD4^{+} T cells.

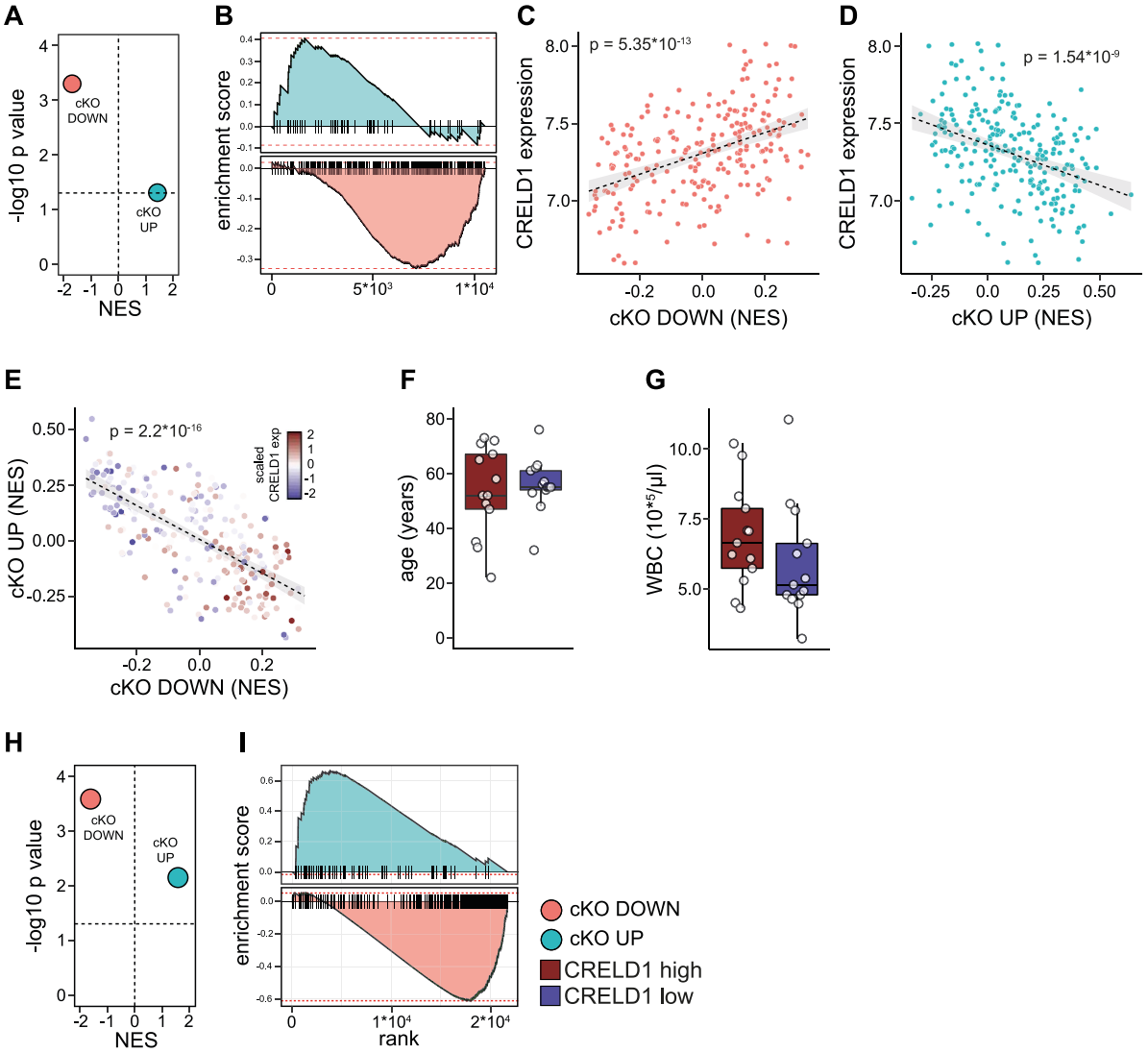

Figure 5.41 Creld1-dependent transcriptome signature is conserved in human naïve CD4⁺ T cells

Signature derived from the CoCena[2] analysis of control or CD4^{Cre+}; Creld1$^{flox/flox}$ CD4^{+} T cells was used to identify if human sample show a similar CRELD1 dependent transcriptional regulation. ***A****: NES (normalized enrichment score) is shown together with the statistical summary of the enrichment.* ***B****: Mapping of the single signature genes in the ranked gene list (CRELD1 low-CRELD1 high). Correlation between signature enrichment and Creld1 expression for both Creld1 down (**C**) and Creld1 up (**D**) signatures.* ***E****: Correlation between the two signature. Difference in donor´s metadata including age (**F**) and WBC count (**G**). Results were confirmed on an independent dataset (ImmVar **H + I**) Correlation was tested by Pearson test (exact p value shown).*

To have an even broader view on the entire cohort of the CEDAR study, each donor sample was tested for the enrichment of both Creld1 down and up signatures (gsva - **fig 5.41 C** and

D respectively). Clearly, the regulation is still apparent and dependent on the expression levels of *CRELD1*. Furthermore, the enrichment of both signatures, as determined for each individual separately, shows a highly negative correlation between each other (**fig 5.41 E**).

Due to the strong phenotype observed in aged cKO mice, where we observed a drastic reduction of T cells in the periphery, we tested for age differences between the CRELD1^{high} and CRELD1^{low} groups. However, this was not the case (**fig 5.41 F**). However, we observed a reduction in the total number of white blood cells – which is in accordance with the phenotype in the conditional KO mice (**fig 5.41 G**). To validate these findings, we performed the exact same analysis in a second large study with 499 individuals (ImmVar), showing the same results (**fig 5.41 H and I**).

5.9.3 *Functional characterization of CRELD1^{low} and CRELD1^{high} groups*

Due to the strong correlation between the transcriptional signature of Creld1 and the differences shown in human CD4$^+$ T cells stratified by *CRELD1* expression, we applied the same approach to identify specific pathways differentially regulated in the two defined groups. CRELD1-stratified data were tested for the enrichment of relevant gene sets to the known molecular function of murine Creld1 (**fig 5.42 A**). All gene sets containing the key word “Wnt” or “Catenin” were tested due to the direct connection between Creld1 and the activation of the Wnt signalling pathway in mice. We observed that the hallmark genes of the WNT signalling pathway are also down regulated in human donors with low *CRELD1* levels showing a possible conservation of the molecular function of Creld1 between mouse and human (**fig 5.42 A** and **E**). Looking more closely into the expression of single genes, we identified a clear downregulation of the main β-Catenin components and target genes (*TCF7* and *LEF1*) and key NFAT target genes (e.g. *RCAN3*) (**fig 5.42 A/B** and **C** respectively)

With the same approach, we analysed the major phenotypes of the KO murine CD4$^+$ T cells in the comparison between donors expressing low and high *CRELD1* in their T cells. As shown in the mouse cKO CD4 T cells, genes involved in apoptosis were positively enriched in

CRELD1^{low} donors (**fig 5.42 A** and **F**), which we also validated in the ImmVar dataset (**fig 5.42 G**).

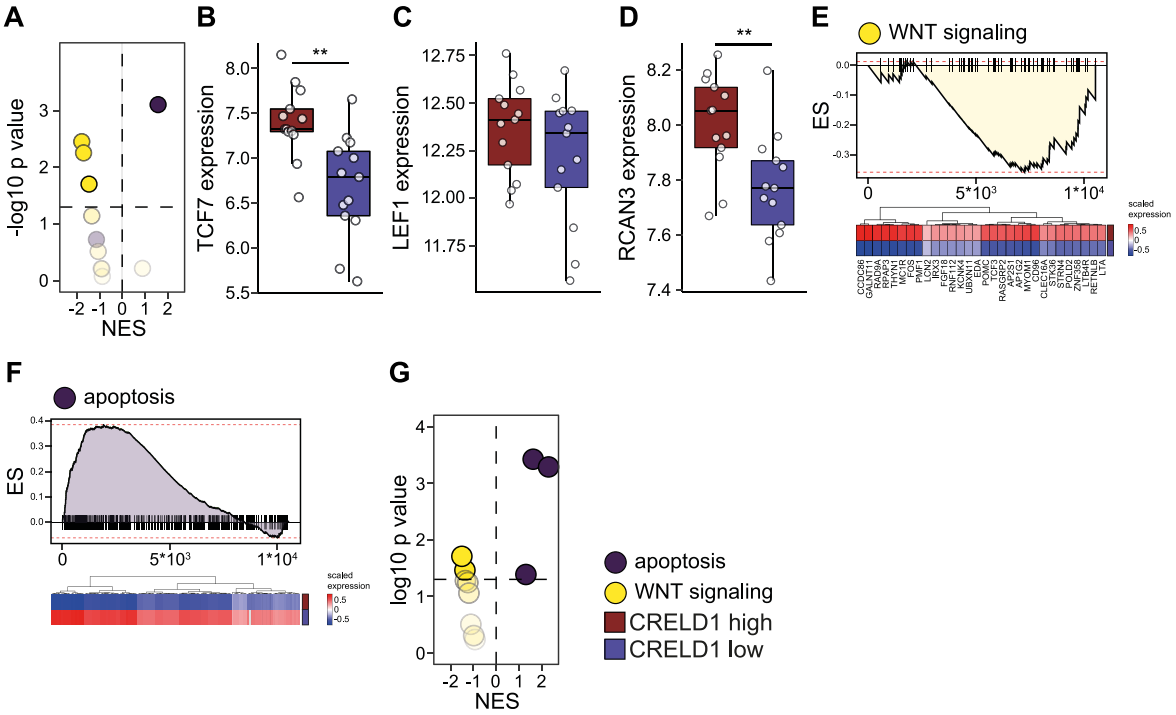

Figure 5.42 Functional characterization of CRELD1^{low} and CRELD1^{high} groups

*Selected immunological gene signatures were tested in the comparison between CD4^{+} T cell sample classified as CRELD1^{high} and CRELD1^{low}. **A**: Normalized enrichment score (NES) and p value of the enrichment of the single signature grouped by molecular pathway or molecular mechanism. The expression of key target genes of WNT (**B** and **C**) and NFAT signalling (**D**) are shown. GSEA for WNT signalling (**E**) and the highest enriched apoptotic signature (**F**) are shown mapped on the ranked gene list. The same analysis was performed on an independent dataset showing similar results (ImmVar **G**). Heatmaps display mean of scaled expression values of the leading edge of GSEA. Statistical significance was tested by unpaired t-test (* p<0.05, ** p<0.01, *** p<0.001, **** p<0.0001).*

5.9.4 *CRELD1 function is conserved among different immune cell types*

The wide importance of the Wnt signalling pathway in most mammalian cells lead us to extend out interest on CRELD1 function to other cell types. Moreover, Creld1 expression was seen in almost all cell types at similar levels (ImmGen/FANTOM), supporting the hypothesis that its function is conserved in most if not all cell types.

Due to the lethality of the full KO mouse for Creld1, the investigation of its function would require the generation of several cKO models for each of the tissues or cell types of interest.

Although such process would give very detailed molecular information, it also would require a lot of time and resources.

Given our detailed analysis of the molecular mechanisms underlying Creld1 activity in T lymphocytes we can use the information acquired previously in both mouse and human to evaluate the role of CRELD1 in other cell types.

The CEDAR dataset includes also transcriptional information from sorted $CD14^+$ monocytes, B cells, $CD8^+$ T cells and tissue biopsies. These samples were processed as described for T cells by separation into two groups; donors with high levels of *CRELD1* ($CRELD1^{high}$) and donors with low *CRELD1* levels ($CRELD1^{low}$).

In all analysed cell types, the two Creld1 signatures show similar behaviour with *CRELD1* expression being similarly correlated to a conserved transcriptional program (**fig 5.43 A** and **B**). Again, we observed regulation of WNT signalling and a marked apoptotic signature illustrating once more that *CRELD1* expression is tightly related to cell viability and WNT signalling activity (**fig 5.43 A** and **B**). The effect of CRELD1 dependent transcriptional regulation was even apparent on total PBMCs (**fig 5.43 C** and **D, supplementary schematic 7.4**). Having shown that the effect can be even seen in a heterogeneous cell population such as PBMC, allowed us to analyse a large number of other PBMC datasets.

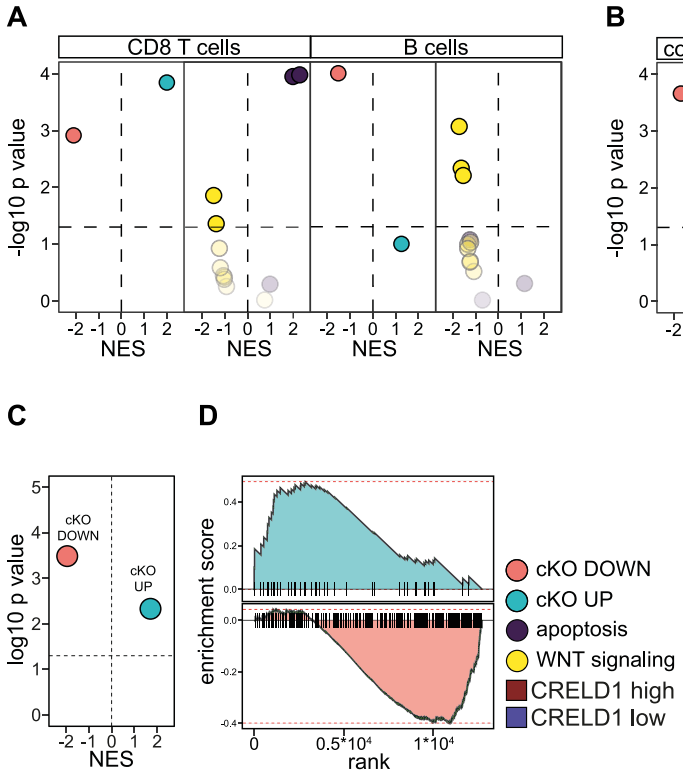

Figure 5.43 CRELD1 function is conserved among different immune cell types

*Lymphoid cells (**A**) and monocytes (**B**) show similar CRELD1-dependent transcriptional regulation to CD4⁺ T cells. **C** and **D** show Creld1 signature enrichment in total PBMC samples stratified in two groups base on CRELD1 expression.*

5.10 CRELD1 is regulated in senescence of the immune system in health and disease

Recent studies have been trying to connect changes at transcriptional or genome level to changes in immune system composition or immune response upon infection (De Jager *et al.*, 2015; Li *et al.*, 2016; Ter Horst *et al.*, 2016; Momozawa *et al.*, 2018; Schmiedel *et al.*, 2018; Alpert *et al.*, 2019). In this thesis, the 500FG dataset, part of the Human Functional Genome Project (HFGP), was used to investigate the effect of CRELD1 on maintenance and activation of the human immune system. This dataset contains transcriptomic information from 95 individuals paired with data on the absolute composition of the blood cells and cytokines secreted in response to several stimuli (see **supplementary schematic 7.5**). Due to the almost consistent expression level of *CRELD1* across different immune cell types (data not

shown), CRELD1 function can be investigated also in total PBMCs without bias of the relative abundance of different cell types in the sample.

5.10.1 *CRELD1 expression level strongly correlate with cellular senescence and "AGE" of the immune system*

In a recent publication Alpert and colleagues (Alpert *et al.*, 2019) describe the process of senescence and aging of the immune system. As introduced previously, the aging of the immune system involves drastic changes in both cellular composition of PBMCs and transcriptional changes. In this publication, several individuals were monitored longitudinally showing that differences within the immune system (cellularity, phenotype, function) appeared to be highly consistent and independent of the age of the donors. On the contrary, the changes within the immune system were mapped onto a pseudo-time, both at the cellular and transcriptional level, which led to the development of a signature related to the age of the immune system (IMM-AGE), rather than the chronological age of the individual. The immune-age (IMM-AGE) signatures where used in the comparison between CRELD1^{high} and CRELD1^{low} individuals (**fig. 5.44 A** and **B**) showing that variation in *CRELD1* expression are representative for the senescence status of the individual's immune system (**fig. 5.44 C/D** and **E**). In fact, individuals with low *CRELD1* expression show clear signs of senescence of the immune system in accordance with the phenotype observed in CD4^{+} T cells. Furthermore, several cell types appeared to be changed in the two binned groups (CRELD1^{high}, CRELD1^{low}) (**fig 5.44 F**), these changes were then correlated with the typical changes in blood composition found by Alpert et al. showing how the phenotypical changes also confirm the previous results of the transcriptomic analysis. In fact, phenotypically, the changes we observed in the comparison between the two groups resembles the typical changes of the "aged" immune system (**fig 5.44 E**). Looking in more detail at the single cell populations (**fig 5.44 G to N**), a drastically decreased number of naïve CD4^{+} T cells was found in individuals with low *CRELD1* expression confirming once more the function of this protein is conserved across mouse and human.

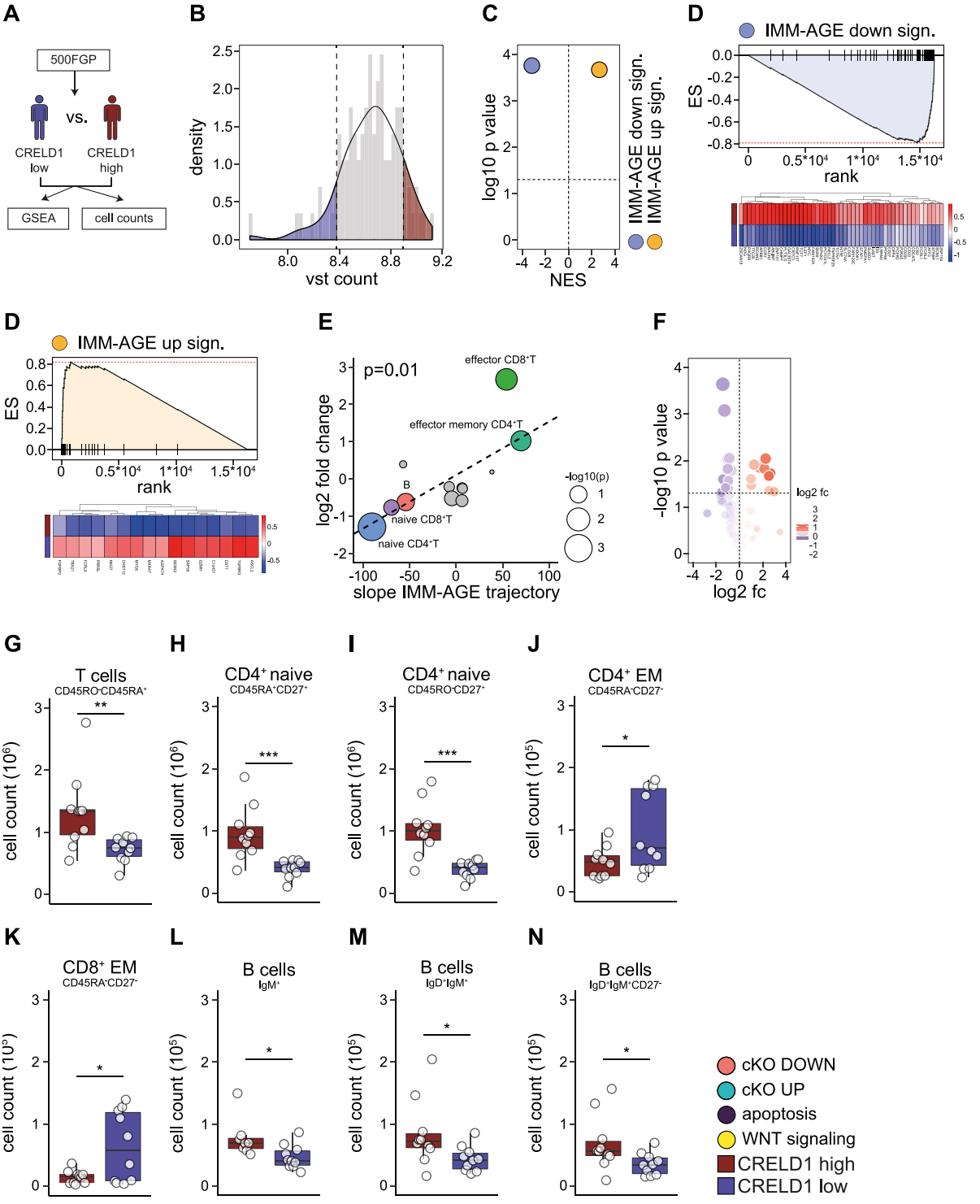

Figure 5.44 CRELD1 expression levels describe cellular senescence and "AGE" of the immune system

***A**: Schematic overview of the analysis performed on the 500FG data. Donors were stratified by CRELD1 expression (**B**) and in the comparison between CRELD1^{low} and CRELD1^{high} the enrichment for the IMM-AGE signatures was tested (**C**, **D** and **E**). Difference in cellular populations in the two groups were compared to hallmark changes in immune system senescence (**E**). Total changes in each population are summarised in **F** and displayed singularly for selected populations (**G** to **N**). Heatmaps display mean of scaled expression values of the leading edge of GSEA. Statistical significance was tested by unpaired t-test (* p<0.05, ** p<0.01, *** p<0.001, **** p<0.0001).*

5.10.2 ***CRELD1 expression is a proxy of WNT signalling activation***

As shown previously for the gene signature analysis in isolated immune cell datasets, also in mixed PBMC *CRELD1* gene expression is shown to be correlated with both canonical and non-canonical Wnt signalling activation showing a marked reduction of key downstream genes (**fig 5.45 A/B** and **C**).

To further characterise the effect of *CRELD1* variation in expression in immune cell activation, a full set of stimulation and cytokines released were analysed in the two groups showing significant changes in response to stimulation (**fig 5.45 D** and **E**). Looking carefully at combinations of cytokine stimulations we observed a reduced T cell-related cytokine response after seven days of stimulation, which is in line with our findings in the CD4-Cre mouse model. The readout of early responses to stimulation appeared to be increased in donors with low *CRELD1* expression. Again, these findings might be due to early overactivation as we had seen this for Creld1 KO T cells in the murine system. In fact, concurrent cellular overactivation and exhaustion has been recently described in the aging immune system (inflame-age and immune-senescence Fulop *et al.*, 2017).

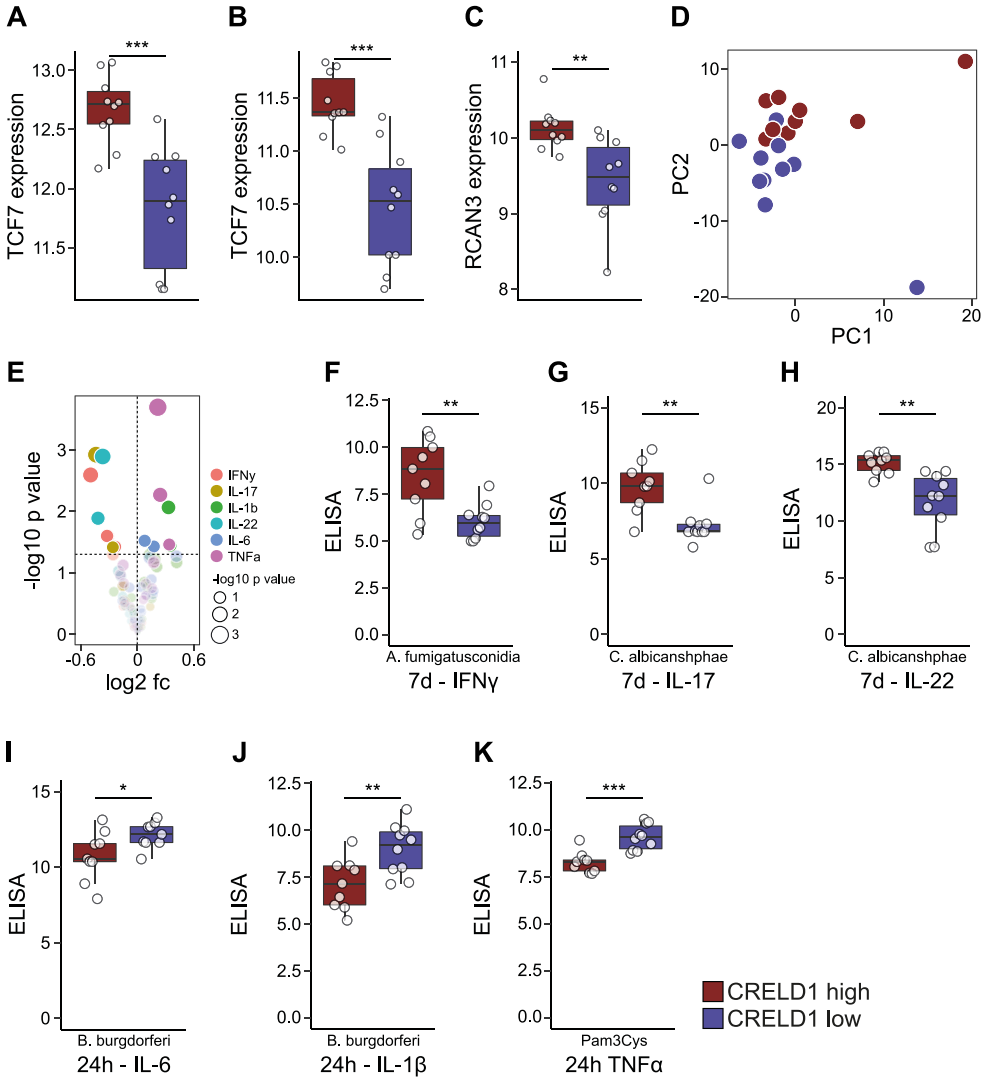

Figure 5.45 CRELD1 expression is a surrogate of active WNT signalling and impact immune system activation

*Expression of downstream genes of WNT signalling of both canonical (TCF7 **A** and LEF1 **B**) and non-canonical (RCAN3 **C**). **D**: Principal component analysis of all features of the 500FG dataset in the two groups of CRELD1 expression. Difference in cytokine response is summarized in **E**. **F** to **K**: single plot for selected cellular response in the two groups. Statistical significance was tested by unpaired t-test (* p<0.05, ** p<0.01, *** p<0.001, **** p<0.0001).*

5.10.3 *CRELD1* is regulated in several diseases correlated with immunosenescence and WNT signalling activation

It is well described that cellular senescence plays an important role in several diseases. We decided to investigate a broad collection of microarray transcriptome datasets for changes in *CRELD1* expression in a wide range of diseases. Several diseases showed differential expression of *CRELD1* compared to healthy controls (**fig 46**). Surprisingly, in all analysed diseases, the changes in *CRELD1* expression were always correlated with changes in Creld1 down signature in accordance with the changes in *CRELD1* expression itself and, more importantly, changes in WNT signalling activation and senescence of the immune system.

Taken together those results show how CRELD1 plays a pivotal role in the maintenance of immune system homeostasis where deviation in the expression of this gene is clearly modulated in several diseases.

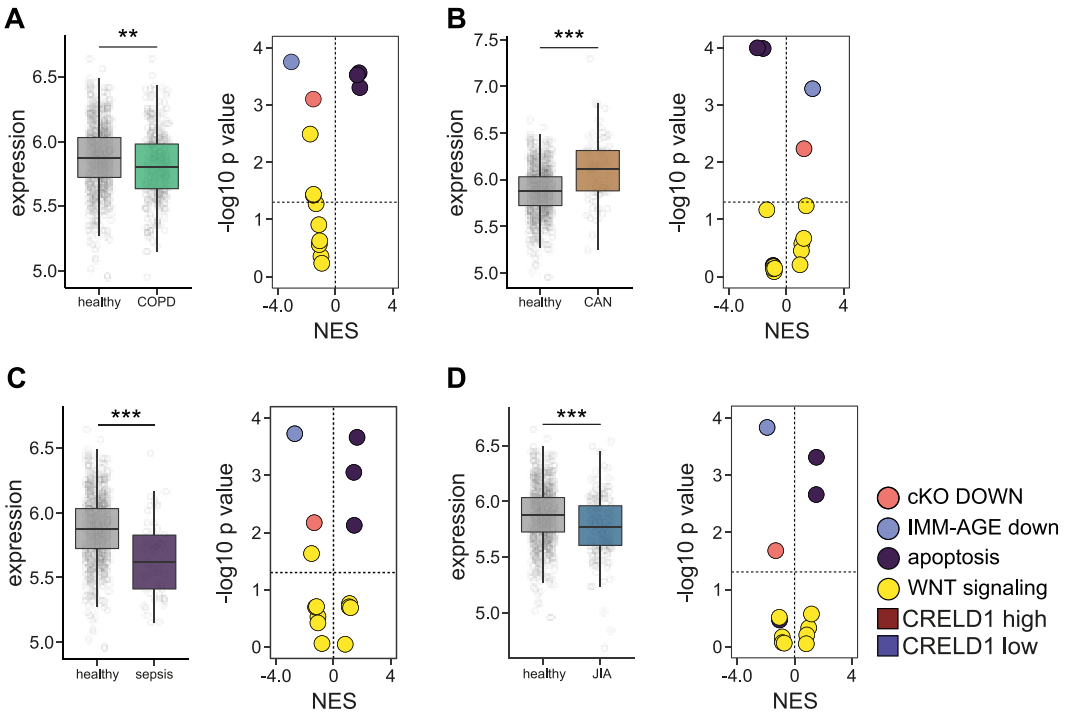

Figure 5.46 CRELD1 is regulated in several disease in correlation to immune-senescence and WNT signalling activation

*CRELD1 expression was compared between healthy donors and several immune-related diseases. Analysis was performed on COPD (**A**), chronic allograph nephropathy CAN (**B**), sepsis (**C**) and juvenile idiopathic arthritis (**D**). Statistical significance was tested by unpaired t-test (* p<0.05, ** p<0.01, *** p<0.001, **** p<0.0001).*

6 Discussion

In my PhD thesis, I investigated the functional mechanisms of Creld1 activity on mammalian cells. Creld1 was recently shown to be fundamental during embryonic heart development with a germline KO model resulting in embryonic lethality (Mass *et al.*, 2014). Under these conditions, Creld1 was shown to regulate NFATc1 activation leading to impaired proliferation of endocardial cells. A more detailed molecular description of Creld1 function as well as the possible function of the protein in other cell types was still absent. Here I unravelled how Creld1 is a type I transmembrane protein functionally dependent on its cytosolic domain to control both canonical and non-canonical Wnt signalling *in vitro* and *in vivo*. Furthermore, I showed how Creld1 depletion in $CD4^+$ T cells dramatically affects cell viability, activation kinetics and functional differentiation. The function of Creld1 was then extended to human CRELD1 also in other cell types with both immunological and non-immunological functions showing that the expression of this protein is functionally related to senescence of the immune system.

6.1 Creld1 is a type I transmembrane protein regulating canonical and non-canonical Wnt signalling

6.1.1 *Creld1 localization*

Initially, Creld1 was described as a U-shaped protein with two transmembrane domains, with both N- and C-termini facing the ER lumen or the extracellular space (Rupp *et al.*, 2002). This assumption was based on an *in silico* structural prediction due to the presence of a signal peptide and two regions with high hydrophobicity (**fig 6.1 A**). In contrast, Mass and colleagues showed that the Creld1 C-terminus is facing the cytoplasm and the protein is localizing exclusively at the ER when expressed in NIH-3T3 cells. In this model, both Creld1 termini are facing the cytosol relying on the prediction of two consecutive transmembrane domains (**fig**

6.1 B). Realizing the discrepancy between the two models and to uncover the correct localization, Creld1 was tagged both at the C terminus and N terminus, and the localization of both fluorescent tags was assessed by protease protection assay. Thereby, I showed that the two termini of the protein have a different orientation; the C-terminus is facing the cytosol as described previously but the N-terminus is facing the ER-lumen or the extracellular space (chapter 5.6). This experimental result allowed the description of a third, fully experimentally-derived model in which Creld1 spans only once the cellular membrane (**fig 6.1C**).

As shown previously, Creld1 localizes primarily in the endoplasmic reticulum when the protein is overexpressed in mammalian NIH-3T3 cells. This result was not in accordance with *in silico* prediction of Creld1 localization where Creld1 is predicted as an extracellular membrane protein (by DeepLoc-1.0 algorithm - Almagro Armenteros *et al.*, 2017, data not shown). Furthermore, Creld1 contains two EGF and two EGF-like domains primarily found in membrane-bound or soluble extracellular proteins (van Loosdregt and Coffer, 2018). Here, I showed that a certain percentage of Creld1 molecules localizes at the plasma membrane (see **fig 5.27**) in accordance with *in silico* prediction. The reason why the protein is not accumulating at the plasma membrane is not yet fully understood but one could speculate that the amount of protein at the plasma membrane is tightly regulated by protein cleavage or internalization as it has been shown for other cell surface proteins such as CTLA-4 (Rowshanravan, Halliday and Sansom, 2018) or the MMPs (Uekita *et al.*, 2001; Truong *et al.*, 2016). Furthermore, supporting this hypothesis, inhibition of protein synthesis with cycloheximide leads to a rapid

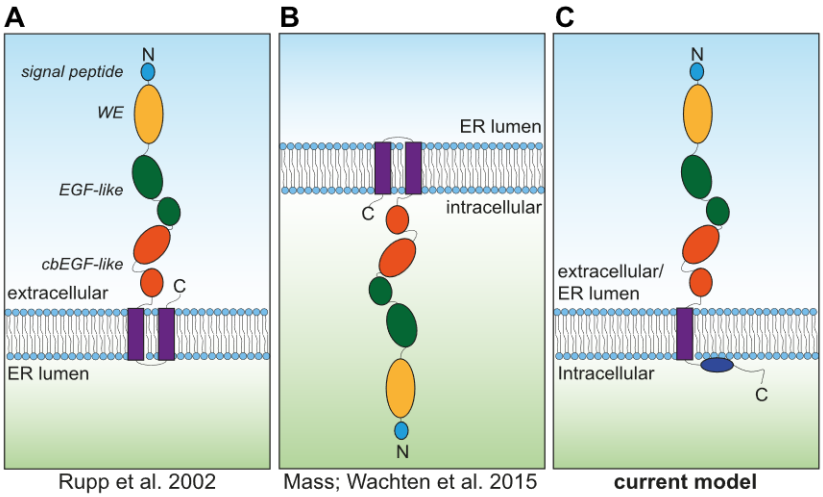

Figure 6.1 Creld1 molecular structure model: from in silico prediction to fully experimental

***A**: First description of Creld1 structure from Rupp and colleagues in 2002 based on in silico prediction. **B** Mass et al. showed in 2015 how the C-term of the protein localizes in the intracellular space, and, in overexpression, the protein localises primarily to the ER. In this thesis we showed how Creld1 functionally localises at the plasma membrane and show opposed orientation of N and C term (**C**).*

decrease of Creld1 levels at the ER (data not shown). This new model of Creld1 localization completely changed our perspective of how to look at the molecular mechanism of Creld1 activity focusing on different roles on signalling by the extracellular and intracellular domains.

6.1.2 *Creld1 C-terminus regulates NFAT activation and β-Catenin stabilization*

Creld1 overexpression was shown to be sufficient to activate NFATc1 in a murine fibroblast cell line (Mass *et al.*, 2014). This simple readout was used to clarify the importance of the different protein domains in the activation of the downstream pathway. Surprisingly, I found that most of Creld1 predicted domains are not required for Creld1 mediated activity on NFATc1 except for the two short intracellular domains consisting of a hydrophobic region, previously thought to be a transmembrane domain and a short amino acid sequence with no predicted secondary structure. The deletion of this region abolishes NFATc1 activation in NIH-3T3 cells showing that the intracellular domains of Creld1 are sufficient and required for its molecular activity in an overexpression setting (**fig 5.31**). Interestingly these domains were found to have a high conservation in all vertebrates further supporting their importance. Moreover, the fact that the NFAT pathway could only be activated when Creld1 was able to localize to the plasma membrane led to the conclusion that Creld1 must cooperate with other membrane-associated proteins to activate a specific molecular pathway. Co-IP experiments at this point were crucial to identify a link between Creld1 and the Wnt signalling pathway (**fig 5.34** and **5.35**); this interaction was then validated *in vitro* showing how Creld1 overexpression but not Creld1 ΔC2 can stabilize β-Catenin at the protein level and β-Catenin-dependent transcriptional activity. Interestingly, prediction of the tertiary structure of Creld1 showed high homology with the low-density lipoprotein receptor (data not shown) and several low-density lipoprotein receptor related proteins (LRP), key components of the Wnt signalling pathway acting as a co-receptor to Frizzled, which has been shown to be fundamental in the activation of the downstream pathway (MacDonald and He, 2012). Furthermore, Creld1 contains a conserved binding domain (K-G-R) for the Wnt-pathway-associated kinase CK1 (Kawakami, Suzuki and Ohtsuki,

2008). This domain locates in the C-terminus of the protein shown to be required for Creld1 function.

Taken together these results suggest that Creld1 regulates both canonical and non-canonical Ca2+/NFAT Wnt signalling pathways suggesting a model in which Creld1 resides at the plasma membrane where it regulates the activation of the Wnt signalling pathway similar to LRP5/6 (**fig 6.2**). The possibility of Creld1 to also bind Wnt was not experimentally assessed but Creld2 (a soluble member of the Creld family of proteins with high homology to Creld1 extracellular domains Maslen *et al.*, 2006)) was shown to interact with two distinct WNT isoforms (Bioplex2 – WNT4 and WNT7A).

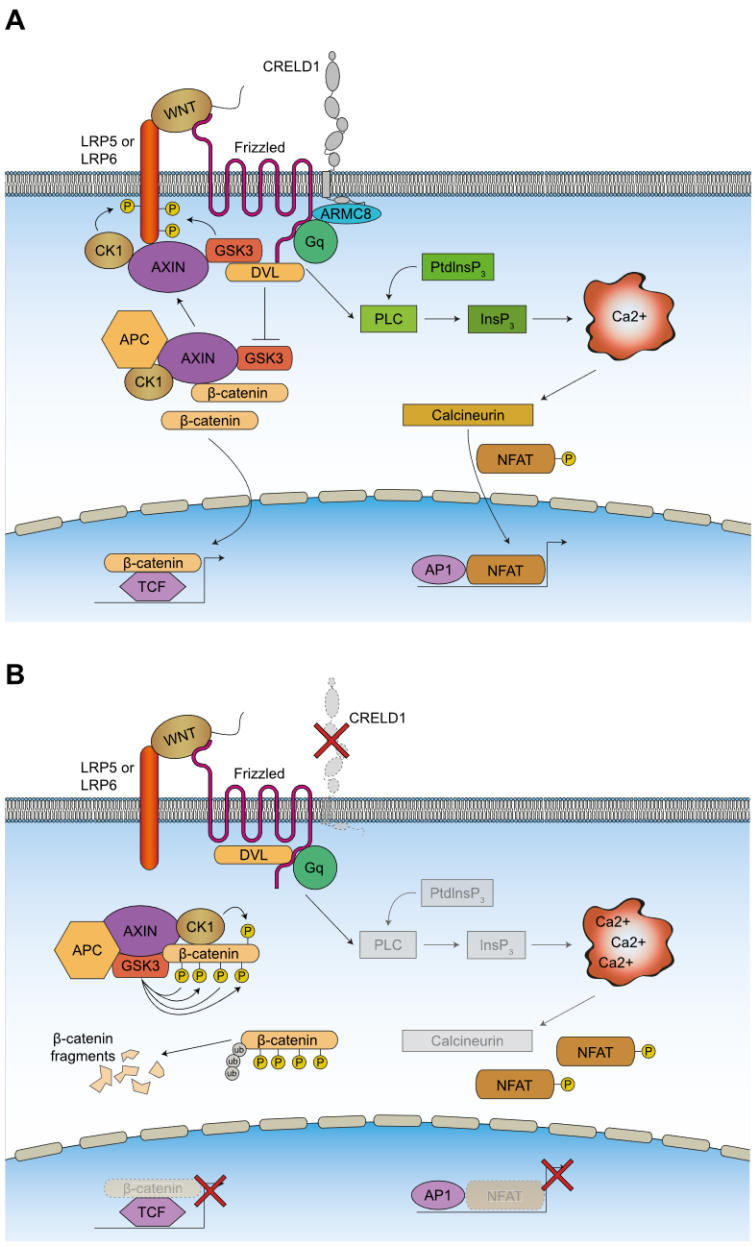

Figure 6.2 A novel model of Creld1-dependent regulation of canonical and non-canonical Wnt signalling

*In this thesis, I could show how Creld1 plays a crucial role in the regulation of both canonical and non-canonical Wnt signalling pathway. Creld1 localise at the plasma membrane and bids to ARMC8, a protein functionally related to Wnt signalling. I could show how Creld1 overexpression activates canonical Wnt signalling with an increased stabilization of β-catenin and non-canonical Wnt signalling with activation of NFAT as depicted in **A**. In absence of Creld1 both canonical and non-canonical Wnt signalling were shown not to be activated in KO CD4⁺ T cells confirming the role of Creld1 as modulator of Wnt signalling (**B**).*

6.2 Creld1 regulates Wnt signalling in CD4$^+$ T cells *in vivo*

Despite the fact that mice with conditional KO (cKO) of Creld1 in T lymphocytes do not show any major phenotype in development and organization of the immune system both, in the thymus and in the periphery (chapter 5.2), viability of these cells was drastically affected by Creld1 depletion when CD4$^+$ T cells were cultured *ex vivo*. I showed that KO CD4$^+$ T cells have an increased apoptotic rate compared to control cells (chapter 5.4). Furthermore, an *in vivo* loss of T cells was observed in old cKO animals (12-13 months old) where the total number of T lymphocytes in both secondary lymphoid organs and tissues were found to be drastically reduced (chapter 5.3). As expected from the analysis of the Creld1 molecular mechanism of action in murine fibroblasts, a general inactivation of the Wnt-Catenin signalling pathway was measured which was further supported by a pharmacological rescue of the apoptotic phenotype by inhibiting the kinase GSK3 (**fig 5.39**), a key negative regulator of Wnt signalling. A limited number of studies regarding the importance of Wnt signalling in the maintenance of T cell homeostasis have been conducted in the last few years, for example overexpression of a stabilized variant of β-Catenin in Tregs was shown to have a dramatic effect on cell death over time (Ding *et al.*, 2008). On the other hand, Wnt signalling, specifically β-Catenin stabilization was shown to have a negative effect on the activation kinetics of CD4$^+$ T cells. Overexpression of stabilized β-Catenin induced anergy in conventional CD4$^+$ T cells (CD4$^+$CD25$^-$) resulting in decreased proliferative capacity and cytokine secretion *in vitro* (Ding *et al.*, 2008; Driessens *et al.*, 2011). This mechanism was first described as a β-Catenin-dependent induction of Cbl-b and Itch, two important factors for T cell tolerance and anergy (Ding *et al.*, 2008). Interestingly, this result was not confirmed by a more recent publication where it was shown that β-Catenin stabilization could directly affect PLC-γ activation by reducing the phosphorylation of LAT at tyrosine 136 leading reduced to calcium flux upon TCR stimulation (Driessens *et al.*, 2011). Accordingly, in Creld1 deficient CD4$^+$ T cells we observed the opposite phenotype compared to β-Catenin overexpressing T cells (summarised in **fig**

6.3). An increased activation kinetics was detected in both the expression of activation markers at the surface and the metabolic switch to glycolysis upon TCR stimulation (chapter 5.5) coupled with an unbalanced calcium flux (data not shown). After longer stimulation times, the apoptotic phenotype remained prevalent, showing overall decreased cell numbers after 3 days of stimulation.

As introduced before, T cell differentiation is an important effector function of $CD4^+$ T cells, allowing a tailored protection against different classes of pathogens. This process was also linked in multiple recent publications to Wnt signalling. TCF-1, one of the main transcription factors downstream Frizzled stimulation, inhibits differentiation of both Th1 and Th17 subsets (Yu *et al.*, 2011). For Th17 cells, this effect was shown to be a direct regulation of the IL-17 locus (Ma *et al.*, 2011; Yu *et al.*, 2011). It was also shown how TCF-1 promotes Th2 differentiation regulating GATA-3 expression (Notani *et al.*, 2010; Yu *et al.*, 2011). In accordance with the literature available on Wnt, Creld1 deficient T cells showed reduced differentiation into Th2 cells *in vitro* and increased differentiation into Th1 and Th17 cells both *in vitro* and *in vivo*. Furthermore, it was shown that the proliferative capacity is an important factor in Th2 cell differentiation (Gett and Hodgkin, 1998). Moreover, it was also suggested that Fas, normally a pro-apoptotic molecule, is important for differentiation to the Th17 subset (Meyer Zu Horste *et al.*, 2018) and we demonstrate an increased Fas expression on protein levels in Creld1 KO $CD4^+$ T cells. Collectively, our own data on the role of Creld1 in defining Th cell differentiation goes along with known functionality of Wnt signalling in Th cell differentiation further supporting that Creld1 is acting via Wnt signalling in T cells.

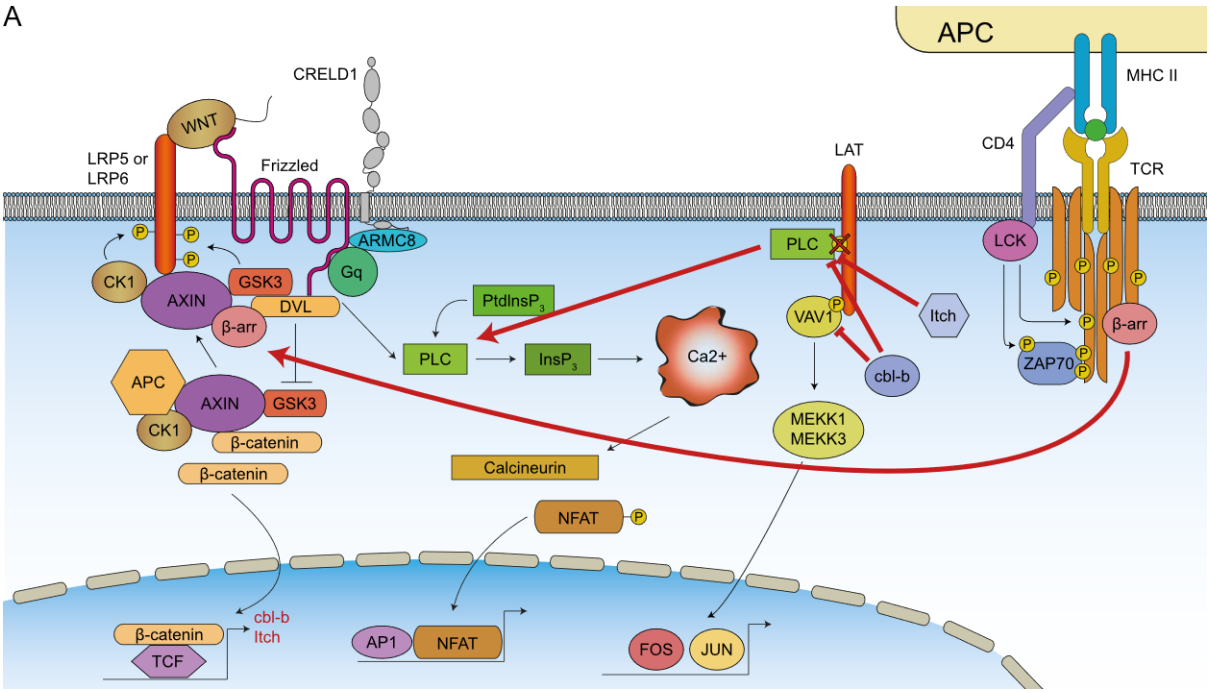

Figure 6.3 Wnt and TCR signalling oppose each other in T cells activation

*Several publications in recent years showed how Wnt signalling can balance TCR-mediated T cell activation. Several molecular components are required for both pathways and can act as a rate-limiting step in the concomitant activation of both pathways such as PLC and β-arrestin. On the other hand it was shown how β-Catenin could regulate both the phosphorylation of LAT, inhibiting TCR mediated activation of PLC and could positively regulate the expression of both Cbl-b and Itch, two ubiquitin ligases acting as inhibitory molecules in the TCR signalling at multiple levels (**A**).*

6.2.1 *Creld1 deficiency induces premature senescence and aging of the lymphoid compartment in vivo*

While we could not detect any obvious differences in the immune system of young Creld1 deficient animals, old animals (between 12 and 13-month-old), showed a drastic reduction of lymphocytes in both secondary lymphoid organs and peripheral tissues (chapter 5.3).

The gradual decline in the total number and proliferative capacity of the adaptive immune system, especially the lymphoid compartment is a well-known process in humans but the molecular mechanisms underlying this decline are poorly understood (Dewan *et al.*, 2012; Fülöp *et al.*, 2017; Ventura *et al.*, 2017; Pawelec, 2018). This process has been primarily attributed to the involution of the thymus in aging (Aw, Silva and Palmer, 2007). However, more recently, immunosenescence was not only found to be due to lower thymic output of healthy naïve T cells but was also shown to be due to reduced peripheral expansion and

memory formation (Aw, Silva and Palmer, 2007; Nguyen, Mendelsohn and Larrick, 2017) highlighting also cell-intrinsic effects in the aging immune system. In fact, even if the total number of "new" $CD4^+$ or $CD8^+$ T cells maturing in the thymus is drastically decreased with age, the clonality of the TCR repertoire is kept in the recent thymic emigrants (Czesnikiewicz-Guzik *et al.*, 2008). In the periphery, on the contrary, the clonality was shown to be reduced which is in line with a modified fitness in peripheral expansion (Czesnikiewicz-Guzik *et al.*, 2008; Wertheimer *et al.*, 2014; Nguyen, Mendelsohn and Larrick, 2017). The degeneration of the lymphoid compartment with aging was shown to have a dramatic effect on human health, as it is highlighted in a highly reduced efficiency of vaccination in the elderly (Ongrádi *et al.*, 2009). Furthermore, considering the importance of the adaptive immune system in the protection against tumour progression, one can easily speculate on how the deterioration of the immune system would increase the risk of immune evasion of cancer together with a concomitant inefficiency of cancer immunotherapy (Pawelec *et al.*, 2009; Hurez *et al.*, 2012; Schreiber *et al.*, 2012; Pawelec, 2017).

We clearly demonstrated that Creld1 deficiency in T lymphocytes accelerates the process of senescence in mice. In fact, 6-month-old mice already started to show reduced cellularity in the spleen (data not shown) with a worsening phenotype by 12 months. In both, control and Creld1 conditional KO animals, we observed a strong involution of the thymus in both, size and cellularity, compared to young mice, while no differences were apparent between genotypes (data not shown). We conclude from these findings that Creld1 is important for the homeostatic maintenance of T cells in the periphery, a model, which is further supported by *in vitro* studies and mechanistically connected to an impairment in the Wnt signalling pathway.

As of today, the treatment of lymphocytopenia is still a challenge. In recent years, treatment with CYT107 (rhIL-7) was shown to be successful in several clinical trials (Francois *et al.*, 2018). This treatment strategy primarily aims to block apoptosis in the cells inducing increased viability and proliferation of T cell in the periphery.

However, our study suggests that other pathways, such as Wnt signalling, might also be important in this process. Senescence of the immune system was also recently shown to have

a strong environmental and genetic component (Su, Aw and Palmer, 2013; Alpert *et al.*, 2019). Therefore, the investigation of novel therapeutic strategies and the development of precision medicine approaches require integration of new knowledge as provided in this thesis to be in the position to develop novel first- and second-line treatments for age-related lymphocytopenia.

Furthermore, it is important to point out that the process of cellular senescence is not restricted to immune cells but is known to be a common process that cells experience. This mechanism is tightly connected to aging itself (Narita and Lowe, 2005; Baker *et al.*, 2011). In this context the involvement of WNT signalling was explored in much more detail in the last decade. For example, it was shown how senescence can be induced solely by inhibition of WNT signalling (Ye *et al.*, 2007; Elzi *et al.*, 2012).

6.3 CRELD1-dependent transcriptional regulation is conserved in human and can be used as proxy of WNT signalling activation and cellular senescence

6.3.1 *Transcriptional analysis of human CD4$^+$ T cells recapitulates CRELD1 function across species*

The exponential growth of available transcriptomic and genomic data from healthy donors in the last years allows for the meta-analysis of big cohorts with data including a wide spectrum of parameters such as ethnicity, age and other characteristics (e.g. smoking habits, alcohol consumption) (De Jager *et al.*, 2015; Li *et al.*, 2016; Ter Horst *et al.*, 2016; Momozawa *et al.*, 2018). Furthermore, I postulate that modern research highly relies on data-driven approaches to understand complex diseases. Together with the requirement to make such omics data publicly available, transcriptional information from hundreds of studies investigating a broad

variety of diseases (currently over 3 million samples are available on GEO) can be 'repurposed' for new research questions.

In this study the transcriptional information of several hundreds of healthy donors was used to validate the conservation of CRELD1 function in humans (chapter 5.9). The natural variation in CRELD1 expression was used to identify two groups of donors, some of which have high and some with low *CRELD1* expression. At the moment, the source of variation for *CRELD1* expression in humans is not fully known; it was shown that some SNPs (Single Nucleotide Polymorphism) seem to have an influence on the expression of the gene (eQTL – GTEx database), however, our initial analysis in this direction was not conclusive for example due to low allele frequencies (data not shown). Furthermore, it was recently shown that there is a moderate but significant difference in *CRELD1* expression in males compared to females (Fülöp *et al.*, 2017). One could also imagine that other parameters might have an influence on the expression of the gene such as environment, age and inflammatory status.

We clearly demonstrated that the transcriptional program correlated with *CRELD1* expression is highly conserved between mouse and human. Conservation was shown by comparing the transcriptional information derived from human $CD4^+$ T cells of the two groups, $CRELD1^{high}$ and $CRELD1^{low}$ respectively, assuming that this difference would resemble the difference between Creld1 KO and control $CD4^+$ T cells. GSEA clearly revealed that almost the same genes to be either down- or upregulated in both comparisons. Based on the similarity of the transcriptional programs we tend to speculate that the function of the Creld1 protein is also conserved between humans and mice. Furthermore, from the comparison between individuals with either $CRELD1^{high}$ and $CRELD1^{low}$ $CD4^+$ T cells, it was rather evident that all the main pathways found in KO murine T cells (Wnt signalling, apoptosis signatures) were also enriched in humans (chapter 5.9). Collectively, these data strongly suggest that CRELD1 could be used as a surrogate for WNT signalling in human $CD4^+$ T cells and potentially be recognized as a senescence hallmark in the lymphoid compartment.

6.3.2 *CRELD1 expression is a hallmark of cellular senescence and immune aging in PBMC*

Extending the analysis to other cell types, I observed that CRELD1-dependent transcriptional regulation is also conserved in those cell types. Furthermore, regulation of WNT signalling appeared to be correlated to *CRELD1* expression once again providing evidence that CRELD1 might be used as surrogate for active WNT signalling (chapter 5.10).

Analysis of other lymphoid or myeloid immune cells showed similar results compared to $CD4^+$ T cells. *CRELD1* gene expression and protein levels are found to be almost constant in immune cells, supporting a potentially conserved role in different cell types (NCBI/ImmProt/FANTOM5). The effect of CRELD1 was then analysed in whole PBMCs showing also here that CRELD1 might be used as a hallmark for active WNT signalling.

Functionally, the segregation of individuals based on *CRELD1* expression ($CRELD1^{high}$ and $CRELD1^{low}$) highlight drastic changes in composition and immune responses of PBMCs highly correlated with a phenotype of aging and senescence of the immune system. Donors with low CRELD1 expression displayed a transcriptional signature of senescence of the immune system coupled with typical changes in cell population such as a marked reduction of naïve $CD4^+$ T cells, a phenotype also evident in our conditional KO mouse model (**fig 5.44**) (Nikolich-Žugich, 2014, 2018; Carr *et al.*, 2016; Alpert *et al.*, 2019). Furthermore, in terms of immune responses, we also observed typical signs of “aging”, with reduced T cell mediated responses and increased innate responses with higher secretion of IL-6 (phenomenon known as inflammaging, Xia *et al.*, 2016; Fulop *et al.*, 2017; Jose *et al.*, 2017). Once again, CRELD1 appears to be an important modulator of WNT signalling in the maintenance of homeostasis in immune cells regulating the balance between cell survival and activation.

The broad availability of transcriptional information also from diseased donors allowed us to analyse the regulation of CRELD1 in different diseases. In diseases such as COPD where it is known that the WNT signalling pathway is down-regulated (Kneidinger *et al.*, 2011; Baarsma *et al.*, 2017; Qu *et al.*, 2019) CRELD1 expression was changed accordingly to the regulation

of WNT signalling itself (**fig 5.46**). Other diseases were shown to have an increased CRELD1 expression compared to healthy controls for example in chronic allograft nephropathy (CAN) associated with an increased WNT signature. Similarly to COPD, it was reported that WNT signalling has a pathological role in the development of CAN controlling the epithelial-mesenchymal transition (Tang *et al.*, 2019).

6.4 Reported mutations in the CRELD1 gene

Several studies indicate CRELD1 as a risk factor for atrioventricular septal defect (AVSD) (Robinson *et al.*, 2003; Genet, 2005; Evans, 2007; Posch *et al.*, 2008; Guo *et al.*, 2010; Ghosh *et al.*, 2012; Zhian, Belmont and Maslen, 2012; Alca, 2015; Li *et al.*, 2019). As introduced before, *Creld1* gene deletion in mice results in lethality due to developmental impairment of the heart (K. Redig *et al.*, 2014; Mass *et al.*, 2014) confirming once again a similar function for both mouse and human protein.

AVSD has a prevalence of 5% of all congenital heart diseases and is successfully treated by surgery in childhood with no reported long-term effects.

Multiple mutations have been reported in the last decade showing clear predisposition to AVSD for CRELD1. I cloned several reported Creld1 mutants and tested them for the capacity of inducing NFATc1 translocation to the nucleus in our overexpression system. Interestingly none of the reported mutations affected NFATc1 translocation with the only exception of the mutant E414K where a modest reduction was found (data not shown). This specific mutation localizes in the C-terminus of Creld1, a region shown here to be required for the activity of CRELD1 on NFATc1.

CRELD1 predisposition to AVSD is often correlated with Down syndrome (DS). This results allows to speculate on how a severe loss-of-function mutation of CRELD1 might not be viable in human where only a moderate effect was found for pathological mutants, also highlighting the multifactorial nature of AVSD. Some other genes were suggested to be involved in this predisposition also in correlation with DS such as GATA4, NKX2.5 and BMP4. Surprisingly all

these genes have also been connected to WNT signalling; GATA4 was found to be directly regulated downstream of WNT signalling activation (Martin, Afouda and Hoppler, 2010), NKX2.5 is an early transcription factor involved in cardiac development found to be upstream of R-Spondin3 expression, a potent WNT agonist (Cambier *et al.*, 2014) furthermore shown to be itself promoted by activation of WNT signalling (Liu *et al.*, 2009). Finally, BMP4 was found to be a context-dependent modulator of the WNT signalling pathway (Voorneveld *et al.*, 2015). Taken together, these results indicate that cardiac development and AVSD pathogenesis are highly dependent on the modulation of WNT signalling during early stages of development and it appears that each of the mutations identified is associated with a low penetrance for the disease suggesting a highly multifactorial pathology.

6.5 General considerations on Creld1 as a signalling molecule

Growing interest has emerged over the last decade on CRELD1 function. This protein was first correlated with AVSD regulating NFATc1 activation (K. Redig *et al.*, 2014; Mass *et al.*, 2014). Nevertheless, CRELD1 is expressed at similar levels in all tissues (NCBI – Illumina bodyMap2 transcriptome 2.0, FANTOM5) where its function remains widely unknown. I demonstrated, for the first time that Creld1 regulates both the canonical and non-canonical Wnt signalling pathway both *in vitro* and *in vivo* revealing also conservation of function in humans.

The current model used to dissect the pathways involved the overexpression of recombinant proteins in a cell culture system. In this setting, we observed that the Creld1 C-terminus anchored to the plasma membrane and that this is required to activate NFATc1 activity. In this experimental setting, the extracellular domains do not seem to be important for this function since several pathological mutations located in this region of the protein had no influence on our readouts. However, one might speculate that overexpression of the protein could lead to the activation of the pathway independently from a physiological stimulation. This effect has been demonstrated for several receptor-like proteins such as LRP6 (Tung *et al.*, 2012).

Possibly, the Creld1 extracellular domains have a regulatory function interacting with other soluble or membrane-bound proteins allowing a context-dependent activation of the Wnt signalling pathway. This question would be best studied by a domain-specific KI (knock-in) approach in the endogenous locus. Furthermore, investigations on the physiological regulation of Creld1 activity could open new opportunities for the development of pharmacological strategies to modulate its activity and consequently Wnt signalling.

Wnt signalling is currently a major focus in pharmacological discovery due to the relevance of this molecular pathway throughout life from embryonic development to aging. When using "Wnt" as a keyword, more than 80 clinical studies are currently found on clinicaltrials.gov, mostly investigating a possible beneficial effect of inhibiting Wnt signalling as a cancer therapy (ClinicalTrial.gov). Despite the interest in this molecular mechanism, not many pharmacological options are available (Tran and Zheng, 2017). Currently explored drugs mostly target intracellular components of the pathway making delivery and targeting challenging *in vivo*. Clinically innovative targets for the modulation of Wnt signalling are needed and Creld1 could be an interesting candidate due to its expression at the cell surface (Nusse and Clevers, 2017).

Clearly, a more detailed analysis of the mechanism of action of Creld1 can be of great medical and pharmaceutical interest. Future research should focus on understanding important aspects such as the possible role of the extracellular domain in the modulation of its activity. Another aspect still not completely addressed is the regulation of Creld1 expression at the plasma membrane; based on the results of this work, internalization or cleavage of the protein can result in the inhibition of the pathway. This mechanism should be investigated in relation to different cellular states/stimulations.

Furthermore, due to a different genomic organization in mouse compared to human where CRELD1 pre-mRNA can be differentially spliced leading to two isoforms of the protein CRELD1A and CRELD1B, it would be of higher relevance to focus on the human system in future research.

6.6 Relevance of this research

Collectively, I could show how Creld1 function is not restricted to heart development in embryogenesis but is also tightly involved in the regulation of fundamental cellular mechanisms such as cell survival, proliferation, differentiation and senescence in $CD4^+$ T cells. Creld1 function was also molecularly linked to the Wnt signalling pathway both *in vitro* and *in vivo* first in mouse and then confirmed in human using the genetic and environmental variability as quasi-knock out model to investigate gene function.

I propose Creld1 as a novel Wnt signalling modulator, possibly also of pharmacological interest due to the current lack of good candidates for pharmacological modulation of Wnt signalling, opening up further research in the context of Creld1 modulation and in the more detailed analysis of the Creld family of proteins.

Furthermore, I highlight how variation in gene expression - independent of the source of variation - can be used as a valuable tool for the investigation of gene function in humans, highlighting for CRELD1 a genetic signature entirely recapitulating the phenotype of gene deletion in murine $CD4^+$ T cells.

7 Supplementary schematics

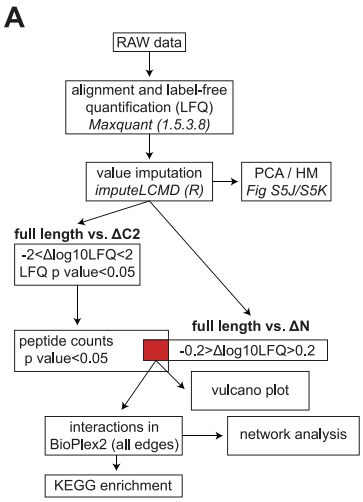

Schematic 7.1 Pre-processing and analysis of Co-IP mass spectrometry data

***A**: Schematic overview of the analysis performed on the mass spectrometry data. Shortly row data were first aligned with Maxquant and missing values imputed. Significant enriched protein were selected as shown and integrated with the Bioplex2 dataset.*

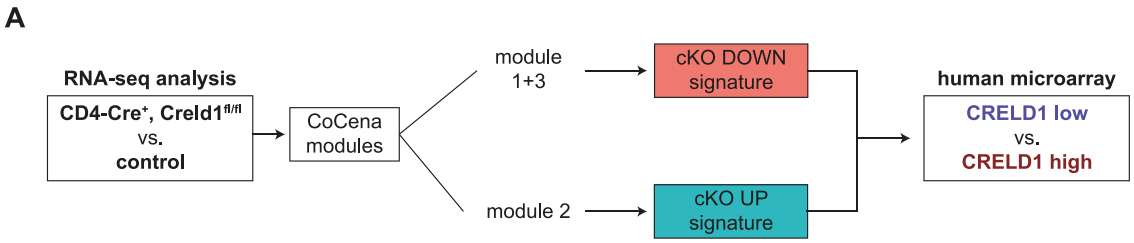

Schematic 7.2 Definition of cKO DOWN and cKO UP signatures

A: Genes differentially expressed in the CoCena network were used to generate the two signatures cKO DOWN and cKO UP.

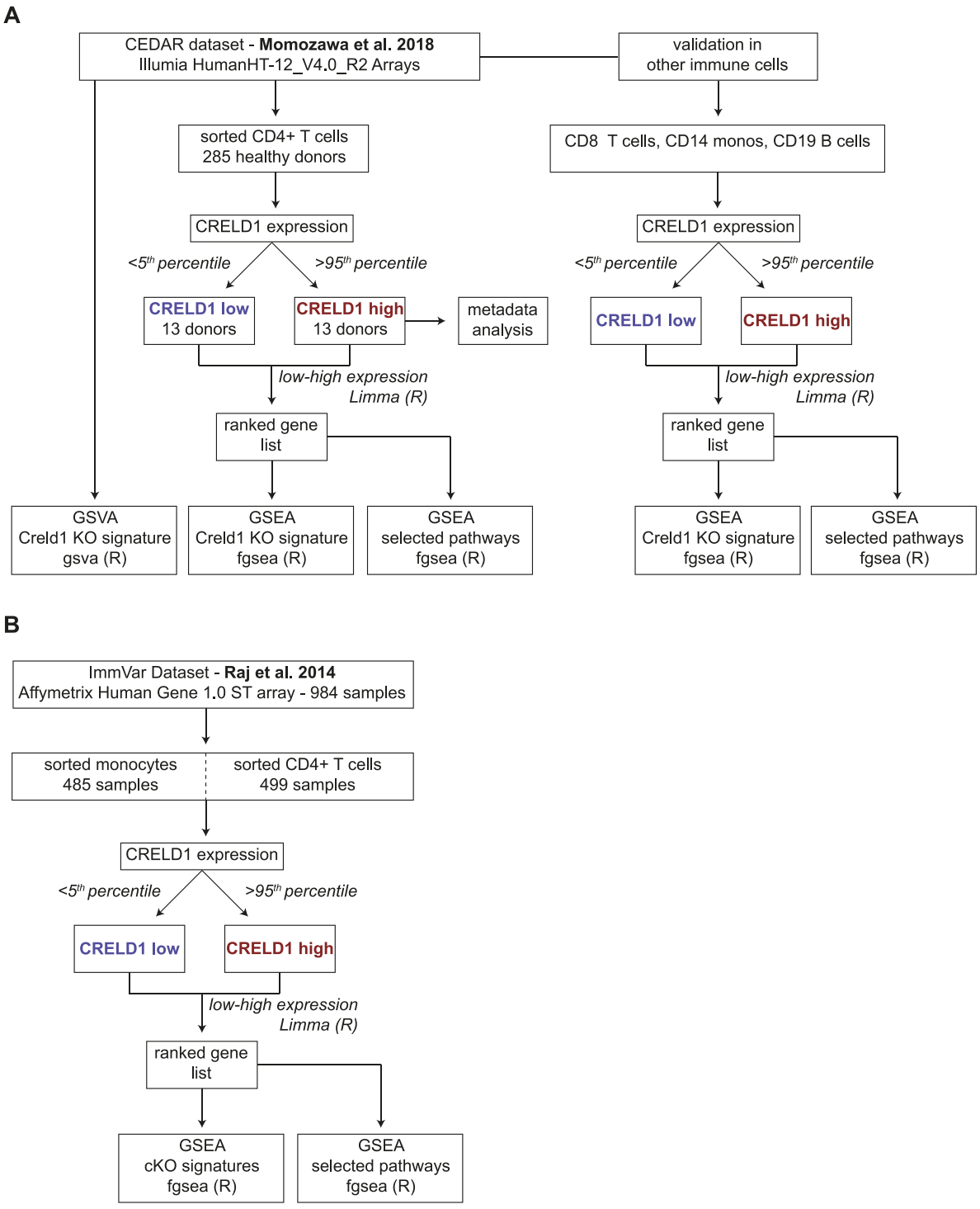

Schematic 7.3 Schematic of the analysis performed on CEDAR and ImmVar datasets

CEDAR (**A**) and ImmVar (**B**) dataset were pre-processed as shown and used for the analysis of the effect of CRELD1 expression in different cell type.

A

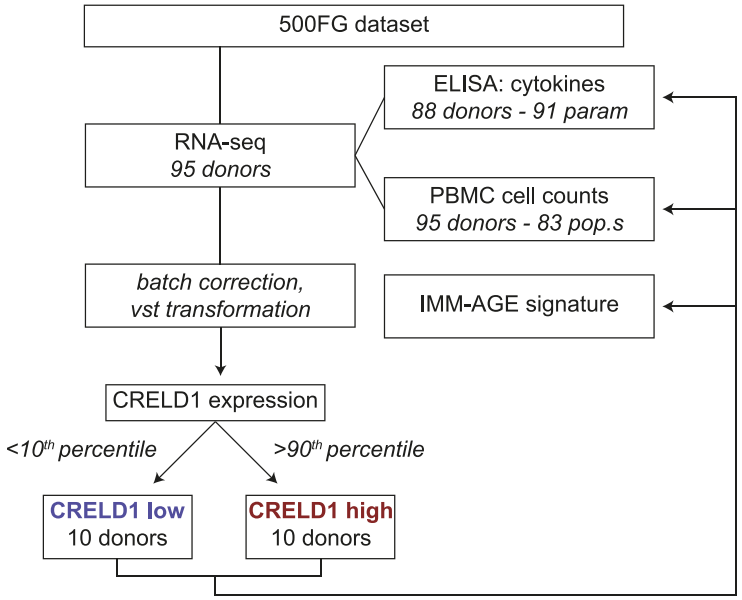

Schematic 7.5 Schematic overview of the analysis performed on the collection of PBMC

A: Transcriptional and functional data from the 500FG dataset were used to asses the effect of CRELD1 expression withing the cohort.

A

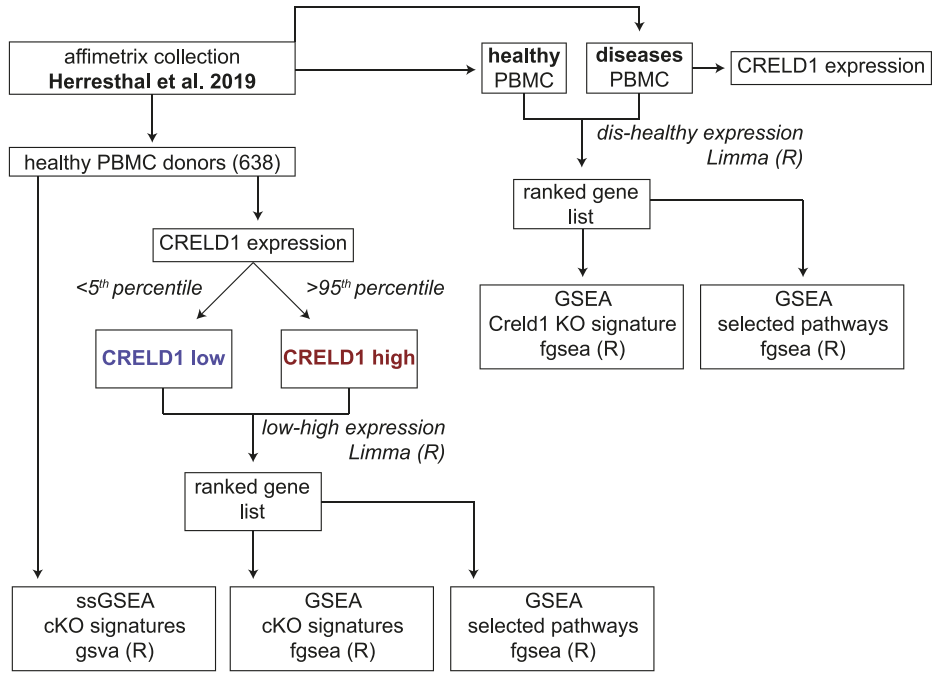

Schematic 7.4 Schematic overview of the analysis performed on the 500FG dataset

A: Collection of microarray expression data from Herresthal et al. 2019 were corrected by batch and analysed as described. For the comparison to diseases all healthy sample from different studies were compared to disease samples.

8 Acknowledgments

First and most importantly, I would like to thank Prof. Joachim Schultze for giving me the opportunity to conduct my PhD in his laboratory and for letting me experience a high-level scientific environment. Most importantly, he was always willing to engage in interesting scientific discussions promoting innovative ideas and approaches to science. Thanks to Prof. Michael Hoch for recruiting me to the LIMES institute and for the initial supervision. I would also like to thank here Pr. Doz. Marc Beyer for been the second examiner in the committee of my final examination and for interesting scientific discussions throughout my PhD.

A special thank goes to Dr. Anna Aschenbrenner for the constant supervision on the project and an endless number of scientific discussions. In modern science where scientific progress is not achieved by single scientist shouting “eureca”, a constant confrontation on the next experiment to be performed or in the interpretation of the previous one is fundamental for the progression of scientific discovery. We came up with many successful ideas and we probably have many more stored for the next years.

Further, I would like to thank all present and past members of the Hoch group that I had the pleasure to work with. Especially Paul who have been my “buddy” everyday here in the LIMES, I´m really grateful for the technical and conceptual help, but also for all the highly educative YouTube videos we watched together. Thanks also to Melanie, Mariangela and Reinhard for the all the time spent discussing and “having fun” in the last years.

Also thanks to all members of the Schultze group, especially Jonas, Thomas and Steffi for the analysis of the transcriptome data.

Thanks to all collaborator that directly or indirectly contributed to this project, especially Prof. Mihai Netea and Prof. Leo Joosten for the access to the 500FG data.

Thanks also to the big family of the LIMES institute and DZNE, especially to all the people contributing to this project, Maren, Lisa for the great help in this journey, Lilly for the critical revision of my thesis, Lorenz, all the bioinformatics office and all scientist and not scientist friends supporting me during the last years.

Last but not least thanks to all my family, especially my mother Marlen, motivating me every day and providing me with goodies from the home land.

Thanks to all friend from the motherland, still loving me even after my germanization.

9 References

Alca, M. A. (2015) ‘Germline Mutations in NKX2 - 5 , GATA4 , and CRELD1 are Rare in a Mexican Sample of Down Syndrome Patients with Endocardial Cushion and Septal Heart Defects’, pp. 802–808. doi: 10.1007/s00246-014-1091-3.

Almagro Armenteros, J. J. *et al.* (2017) ‘DeepLoc: prediction of protein subcellular localization using deep learning.’, *Bioinformatics (Oxford, England)*, 33(24), p. 4049. doi: 10.1093/bioinformatics/btx548.

Alpert, A. *et al.* (2019) ‘A clinically meaningful metric of immune age derived from high-dimensional longitudinal monitoring.’, *Nature medicine*, 25(3), pp. 487–495. doi: 10.1038/s41591-019-0381-y.

Arts, R. J. W., Joosten, L. A. B. and Netea, M. G. (2016) ‘Immunometabolic circuits in trained immunity.’, *Seminars in immunology*, 28(5), pp. 425–430. doi: 10.1016/j.smim.2016.09.002.

Asim, A. *et al.* (2018) ‘CRELD1 gene variants and atrioventricular septal defects in Down syndrome.’, *Gene*. Elsevier, 641(October 2017), pp. 180–185. doi: 10.1016/j.gene.2017.10.044.

Aw, D., Silva, A. B. and Palmer, D. B. (2007) ‘Immunosenescence: emerging challenges for an ageing population.’, *Immunology*, 120(4), pp. 435–46. doi: 10.1111/j.1365-2567.2007.02555.x.

Baarsma, H. A. *et al.* (2017) ‘Noncanonical WNT-5A signaling impairs endogenous lung repair in COPD.’, *The Journal of experimental medicine*, 214(1), pp. 143–163. doi: 10.1084/jem.20160675.

Baker, D. J. *et al.* (2011) ‘Clearance of p16Ink4a-positive senescent cells delays ageing-associated disorders.’, *Nature*, 479(7372), pp. 232–6. doi: 10.1038/nature10600.

Baldwin, K. K. *et al.* (1999) ‘A T cell receptor-specific blockade of positive selection.’, *The Journal of experimental medicine*, 189(1), pp. 13–24. doi: 10.1084/jem.189.1.13.

Bassler, K. *et al.* (2019) ‘The Myeloid Cell Compartment-Cell by Cell.’, *Annual review of immunology*, 37, pp. 269–293. doi: 10.1146/annurev-immunol-042718-041728.

Borggrefe, T. *et al.* (2016) ‘The Notch intracellular domain integrates signals from Wnt, Hedgehog, TGFβ/BMP and hypoxia pathways.’, *Biochimica et biophysica acta*, 1863(2), pp. 303–13. doi: 10.1016/j.bbamcr.2015.11.020.

Bourgeois, C. *et al.* (2008) ‘Ablation of thymic export causes accelerated decay of naive CD4 T cells in the periphery because of activation by environmental antigen.’, *Proceedings of the National Academy of Sciences of the United States of America*, 105(25), pp. 8691–6. doi: 10.1073/pnas.0803732105.

Brewer, J. R., Mazot, P. and Soriano, P. (2016) ‘Genetic insights into the mechanisms of Fgf signaling.’, *Genes & development*, 30(7), pp. 751–71. doi: 10.1101/gad.277137.115.

Buchmann, K. (2014) ‘Evolution of Innate Immunity: Clues from Invertebrates via Fish to Mammals.’, *Frontiers in immunology*, 5, p. 459. doi: 10.3389/fimmu.2014.00459.

Cambier, L. *et al.* (2014) ‘Nkx2-5 regulates cardiac growth through modulation of Wnt signaling by R-spondin3.’, *Development (Cambridge, England)*, 141(15), pp. 2959–71. doi: 10.1242/dev.103416.

Carr, E. J. *et al.* (2016) ‘The cellular composition of the human immune system is shaped by age and cohabitation.’, *Nature immunology*, 17(4), pp. 461–468. doi: 10.1038/ni.3371.

Clevers, H. (2006) 'Wnt/beta-catenin signaling in development and disease.', *Cell*, 127(3), pp. 469–80. doi: 10.1016/j.cell.2006.10.018.

Clevers, H. and Nusse, R. (2012) 'Wnt/β-catenin signaling and disease.', *Cell*, 149(6), pp. 1192–205. doi: 10.1016/j.cell.2012.05.012.

Crabtree, G. R. and Olson, E. N. (2002) 'NFAT signaling: Choreographing the social lives of cells', *Cell*, 109, pp. 67–79. doi: 10.1016/S0092-8674(02)00699-2.

Crist, S. A., Sprague, D. L. and Ratliff, T. L. (2008) 'Nuclear factor of activated T cells (NFAT) mediates CD154 expression in megakaryocytes.', *Blood*, 111(7), pp. 3553–61. doi: 10.1182/blood-2007-05-088161.

Czesnikiewicz-Guzik, M. *et al.* (2008) 'T cell subset-specific susceptibility to aging.', *Clinical immunology (Orlando, Fla.)*, 127(1), pp. 107–18. doi: 10.1016/j.clim.2007.12.002.

D'Alessandro, M. *et al.* (2018) 'CRELD1 is an evolutionarily-conserved maturational enhancer of ionotropic acetylcholine receptors.', *eLife*, 7. doi: 10.7554/eLife.39649.

Dashkevich, A. *et al.* (2016) 'VEGF Pathways in the Lymphatics of Healthy and Diseased Heart.', *Microcirculation (New York, N.Y. : 1994)*, 23(1), pp. 5–14. doi: 10.1111/micc.12220.

De, A. (2011) 'Wnt/Ca2+ signaling pathway: a brief overview.', *Acta biochimica et biophysica Sinica*, 43(10), pp. 745–56. doi: 10.1093/abbs/gmr079.

Dewan, S. K. *et al.* (2012) 'Senescent remodeling of the immune system and its contribution to the predisposition of the elderly to infections.', *Chinese medical journal*, 125(18), pp. 3325–31. Available at: http://www.ncbi.nlm.nih.gov/pubmed/22964331.

Ding, Y. *et al.* (2008) 'Beta-catenin stabilization extends regulatory T cell survival and induces anergy in nonregulatory T cells.', *Nature medicine*, 14(2), pp. 162–9. doi: 10.1038/nm1707.

Dranoff, G. (2004) 'Cytokines in cancer pathogenesis and cancer therapy.', *Nature reviews. Cancer*, 4(1), pp. 11–22. doi: 10.1038/nrc1252.

Driessens, G. *et al.* (2011) 'Beta-catenin inhibits T cell activation by selective interference with linker for activation of T cells-phospholipase C-γ1 phosphorylation.', *Journal of immunology (Baltimore, Md. : 1950)*, 186(2), pp. 784–90. doi: 10.4049/jimmunol.1001562.

Dunn, G. P. *et al.* (2002) 'Cancer immunoediting: from immunosurveillance to tumor escape.', *Nature immunology*, 3(11), pp. 991–8. doi: 10.1038/ni1102-991.

Eberl, G. (2016) 'Immunity by equilibrium.', *Nature reviews. Immunology*, 16(8), pp. 524–32. doi: 10.1038/nri.2016.75.

Elzi, D. J. *et al.* (2012) 'Wnt antagonist SFRP1 functions as a secreted mediator of senescence.', *Molecular and cellular biology*, 32(21), pp. 4388–99. doi: 10.1128/MCB.06023-11.

Emmanuel, A. O. *et al.* (2018) 'TCF-1 and HEB cooperate to establish the epigenetic and transcription profiles of CD4+CD8+ thymocytes.', *Nature immunology*, 19(12), pp. 1366–1378. doi: 10.1038/s41590-018-0254-4.

Evans, J. a (2007) 'Diaphragmatic defects and limb deficiencies - taking sides.', *American journal of medical genetics. Part A*, 143A(18), pp. 2106–2112. doi: 10.1002/ajmg.a.

Fouad, Y. A. and Aanei, C. (2017) 'Revisiting the hallmarks of cancer.', *American journal of cancer research*, 7(5), pp. 1016–1036. Available at: http://www.ncbi.nlm.nih.gov/pubmed/28560055.

Francois, B. *et al.* (2018) 'Interleukin-7 restores lymphocytes in septic shock: the IRIS-7 randomized clinical trial.', *JCI insight*, 3(5). doi: 10.1172/jci.insight.98960.

Fulop, T. *et al.* (2017) 'Immunosenescence and Inflamm-Aging As Two Sides of the Same Coin: Friends or Foes?', *Frontiers in immunology*, 8, p. 1960. doi: 10.3389/fimmu.2017.01960.

Fülöp, T. *et al.* (2017) 'Cellular Senescence, Immunosenescence and HIV.', *Interdisciplinary topics in gerontology and geriatrics*, 42, pp. 28–46. doi: 10.1159/000448542.

Gasteiger, G. *et al.* (2017) 'Cellular Innate Immunity: An Old Game with New Players.', *Journal of innate immunity*, 9(2), pp. 111–125. doi: 10.1159/000453397.

Geiger, T. L. and Sun, J. C. (2016) 'Development and maturation of natural killer cells.', *Current opinion in immunology*, 39, pp. 82–9. doi: 10.1016/j.coi.2016.01.007.

Genet, C. (2005) 'Analysis of CRELD1 as a candidate 3p25 atrioventicular septal defect locus (AVSD2)', pp. 526–528. doi: 10.1111/j.1399-0004.2005.00435.x.

Gerberick, G. F. *et al.* (1997) 'Selective modulation of T cell memory markers CD62L and CD44 on murine draining lymph node cells following allergen and irritant treatment.', *Toxicology and applied pharmacology*, 146(1), pp. 1–10. doi: 10.1006/taap.1997.8218.

Germain, R. N. (2002) 'T-cell development and the CD4-CD8 lineage decision.', *Nature reviews. Immunology*, 2(5), pp. 309–322. doi: 10.1038/nri798.

Gett, A. V and Hodgkin, P. D. (1998) 'Cell division regulates the T cell cytokine repertoire, revealing a mechanism underlying immune class regulation.', *Proceedings of the National Academy of Sciences of the United States of America*, 95(16), pp. 9488–93. doi: 10.1073/pnas.95.16.9488.

Ghosh, P. *et al.* (2012) 'Polymorphic Haplotypes of CRELD1 Differentially Predispose Down Syndrome and Euploids Individuals to Atrioventricular Septal Defect', (September), pp. 2843–2848. doi: 10.1002/ajmg.a.35626.

Godfrey, D. I. *et al.* (1993) 'A developmental pathway involving four phenotypically and functionally distinct subsets of CD3-CD4-CD8- triple-negative adult mouse thymocytes defined by CD44 and CD25 expression.', *Journal of immunology (Baltimore, Md. : 1950)*, 150(10), pp. 4244–52. Available at: http://www.ncbi.nlm.nih.gov/pubmed/8387091.

Goel, H. L. and Mercurio, A. M. (2013) 'VEGF targets the tumour cell.', *Nature reviews. Cancer*, 13(12), pp. 871–82. doi: 10.1038/nrc3627.

Görgens, A. *et al.* (2013) 'Revision of the human hematopoietic tree: granulocyte subtypes derive from distinct hematopoietic lineages.', *Cell reports*, 3(5), pp. 1539–52. doi: 10.1016/j.celrep.2013.04.025.

Graef, I. A., Chen, F. and Crabtree, G. R. (2001) 'NFAT signaling in vertebrate development.', *Current opinion in genetics & development*, 11(5), pp. 505–12. Available at: http://www.ncbi.nlm.nih.gov/pubmed/11532391.

Gunasekaran, U. and Gannon, M. (2011) 'Type 2 diabetes and the aging pancreatic beta cell.', *Aging*, 3(6), pp. 565–75. doi: 10.18632/aging.100350.

Guo, Y. *et al.* (2010) 'Novel CRELD1 gene mutations in patients with atrioventricular septal defect', *World Journal of Pediatrics*, 6(4), pp. 348–352. doi: 10.1007/s12519-010-0235-7.

Hamilton, J. A. (2008) 'Colony-stimulating factors in inflammation and autoimmunity.', *Nature reviews. Immunology*, 8(7), pp. 533–44. doi: 10.1038/nri2356.

Hanahan, D. and Weinberg, R. A. (2011) 'Hallmarks of cancer: the next generation.', *Cell*,

144(5), pp. 646–74. doi: 10.1016/j.cell.2011.02.013.

Hoffmeyer, K. *et al.* (2012) 'Wnt/β-catenin signaling regulates telomerase in stem cells and cancer cells.', *Science (New York, N.Y.)*, 336(6088), pp. 1549–54. doi: 10.1126/science.1218370.

Hogan, P. G. *et al.* (2003) 'Transcriptional regulation by calcium, calcineurin', *and NFAT. Genes Dev.*, 17(18), pp. 2205–2232. doi: 10.1101/gad.1102703.GENES.

Höhne, M. *et al.* (2018) 'Single-nephron proteomes connect morphology and function in proteinuric kidney disease.', *Kidney international*, 93(6), pp. 1308–1319. doi: 10.1016/j.kint.2017.12.012.

Ter Horst, R. *et al.* (2016) 'Host and Environmental Factors Influencing Individual Human Cytokine Responses.', *Cell*, 167(4), p. 1111–1124.e13. doi: 10.1016/j.cell.2016.10.018.

Hu, Z., Ott, P. A. and Wu, C. J. (2018) 'Towards personalized, tumour-specific, therapeutic vaccines for cancer.', *Nature reviews. Immunology*, 18(3), pp. 168–182. doi: 10.1038/nri.2017.131.

Hurez, V. *et al.* (2012) 'Mitigating age-related immune dysfunction heightens the efficacy of tumor immunotherapy in aged mice.', *Cancer research*, 72(8), pp. 2089–99. doi: 10.1158/0008-5472.CAN-11-3019.

Huttlin, E. L. *et al.* (2017) 'Architecture of the human interactome defines protein communities and disease networks.', *Nature*. Nature Publishing Group, 545(7655), pp. 505–509. doi: 10.1038/nature22366.

Huttlin, E. L. L. *et al.* (2015) 'The BioPlex Network: A Systematic Exploration of the Human Interactome.', *Cell*, 162(2), pp. 425–440. doi: 10.1016/j.cell.2015.06.043.

De Jager, P. L. *et al.* (2015) 'ImmVar project: Insights and design considerations for future studies of "healthy" immune variation.', *Seminars in immunology*, 27(1), pp. 51–7. doi: 10.1016/j.smim.2015.03.003.

Jensen, C. T., Strid, T. and Sigvardsson, M. (2016) 'Exploring the multifaceted nature of the common lymphoid progenitor compartment.', *Current opinion in immunology*, 39, pp. 121–6. doi: 10.1016/j.coi.2016.01.009.

Jiang, X. *et al.* (2019) 'Role of the tumor microenvironment in PD-L1/PD-1-mediated tumor immune escape.', *Molecular cancer*, 18(1), p. 10. doi: 10.1186/s12943-018-0928-4.

Johnson, J. L. *et al.* (2018) 'Lineage-Determining Transcription Factor TCF-1 Initiates the Epigenetic Identity of T Cells.', *Immunity*, 48(2), p. 243–257.e10. doi: 10.1016/j.immuni.2018.01.012.

Jose, S. S. *et al.* (2017) 'Chronic Inflammation in Immune Aging: Role of Pattern Recognition Receptor Crosstalk with the Telomere Complex?', *Frontiers in immunology*, 8, p. 1078. doi: 10.3389/fimmu.2017.01078.

K. Redig, J. *et al.* (2014) 'Allelic Interaction between CRELD1 and VEGFA in the Pathogenesis of Cardiac Atrioventricular Septal Defects.', *AIMS genetics*, 1(1), pp. 1–19. doi: 10.3934/genet.2014.1.1#sthash.jksuJTeC.dpuf.

Kaplan, M. H., Hufford, M. M. and Olson, M. R. (2015) 'The development and in vivo function of T helper 9 cells.', *Nature reviews. Immunology*, 15(5), pp. 295–307. doi: 10.1038/nri3824.

Kawakami, F., Suzuki, K. and Ohtsuki, K. (2008) 'A novel consensus phosphorylation motif in sulfatide- and cholesterol-3-sulfate-binding protein substrates for CK1 in vitro.', *Biological & pharmaceutical bulletin*, 31(2), pp. 193–200. doi: JST.JSTAGE/bpb/31.193 [pii].

Kiani, A. *et al.* (2004) 'Expression and regulation of NFAT (nuclear factors of activated T cells) in human CD34+ cells: down-regulation upon myeloid differentiation.', *Journal of leukocyte biology*, 76(5), pp. 1057–65. doi: 10.1189/jlb.0404259.

Kim, S. J., Cho, S.-R. and Yoo, G. E. (2017) 'Age-Related Changes in Bimanual Instrument Playing with Rhythmic Cueing.', *Frontiers in psychology*, 8, p. 1569. doi: 10.3389/fpsyg.2017.01569.

Klein, L. *et al.* (2014) 'Positive and negative selection of the T cell repertoire: what thymocytes see (and don't see).', *Nature reviews. Immunology*, 14(6), pp. 377–91. doi: 10.1038/nri3667.

Kneidinger, N. *et al.* (2011) 'Activation of the WNT/β-catenin pathway attenuates experimental emphysema.', *American journal of respiratory and critical care medicine*, 183(6), pp. 723–33. doi: 10.1164/rccm.200910-1560OC.

Koch, S., Reppert, S. and Finotto, S. (2015) 'NFATc1 deletion in T lymphocytes inhibits the allergic trait in a murine model of asthma', *Clinical & Experimental Allergy*, 45(8), p. n/a-n/a. doi: 10.1111/cea.12493.

Kotake, S. *et al.* (2017) 'The Plasticity of Th17 Cells in the Pathogenesis of Rheumatoid Arthritis.', *Journal of clinical medicine*, 6(7). doi: 10.3390/jcm6070067.

Kovalovsky, D. *et al.* (2009) 'Beta-catenin/Tcf determines the outcome of thymic selection in response to alphabetaTCR signaling.', *Journal of immunology (Baltimore, Md. : 1950)*, 183(6), pp. 3873–84. doi: 10.4049/jimmunol.0901369.

Krueger, A., Ziętara, N. and Łyszkiewicz, M. (2017) 'T Cell Development by the Numbers.', *Trends in immunology*, 38(2), pp. 128–139. doi: 10.1016/j.it.2016.10.007.

Kurosaki, T., Kometani, K. and Ise, W. (2015) 'Memory B cells.', *Nature reviews. Immunology*, 15(3), pp. 149–59. doi: 10.1038/nri3802.

Lambrecht, B. N., Hammad, H. and Fahy, J. V (2019) 'The Cytokines of Asthma.', *Immunity*, 50(4), pp. 975–991. doi: 10.1016/j.immuni.2019.03.018.

Laurenti, E. and Göttgens, B. (2018) 'From haematopoietic stem cells to complex differentiation landscapes.', *Nature*, 553(7689), pp. 418–426. doi: 10.1038/nature25022.

Lee, J.-U., Kim, L.-K. and Choi, J.-M. (2018) 'Revisiting the Concept of Targeting NFAT to Control T Cell Immunity and Autoimmune Diseases.', *Frontiers in immunology*, 9, p. 2747. doi: 10.3389/fimmu.2018.02747.

Lee, P. P. *et al.* (2001) 'A critical role for Dnmt1 and DNA methylation in T cell development, function, and survival.', *Immunity*, 15(5), pp. 763–774. doi: 10.1016/S1074-7613(01)00227-8.

Li, Y. *et al.* (2016) 'A Functional Genomics Approach to Understand Variation in Cytokine Production in Humans.', *Cell*, 167(4), p. 1099–1110.e14. doi: 10.1016/j.cell.2016.10.017.

Li, Z. *et al.* (2019) 'Copy number variations in the GATA4, NKX2-5, TBX5, BMP4 CRELD1, and 22q11.2 gene regions in Chinese children with sporadic congenital heart disease', *Journal of Clinical Laboratory Analysis*, 33(2), pp. 1–6. doi: 10.1002/jcla.22660.

Liang, X. *et al.* (2017) 'Silencing of Armadillo Repeat-Containing Protein 8 (ARMc8) Inhibits TGF-β-Induced EMT in Bladder Carcinoma UMUC3 Cells.', *Oncology research*, 25(1), pp. 99–105. doi: 10.3727/096504016X14719078133609.

Liang, X. *et al.* (2019) 'PAX3 Promotes Proliferation of Human Glioma Cells by WNT/β-Catenin Signaling Pathways.', *Journal of molecular neuroscience : MN*. doi: 10.1007/s12031-019-01283-2.

Libro, R., Bramanti, P. and Mazzon, E. (2016) 'The role of the Wnt canonical signaling in neurodegenerative diseases.', *Life sciences*, 158, pp. 78–88. doi: 10.1016/j.lfs.2016.06.024.

Liu, Z. *et al.* (2009) 'WNT signaling promotes Nkx2.5 expression and early cardiomyogenesis via downregulation of Hdac1.', *Biochimica et biophysica acta*, 1793(2), pp. 300–11. doi: 10.1016/j.bbamcr.2008.08.013.

van Loosdregt, J. and Coffer, P. J. (2018) 'The Role of WNT Signaling in Mature T Cells: T Cell Factor Is Coming Home.', *Journal of immunology (Baltimore, Md. : 1950)*, 201(8), pp. 2193–2200. doi: 10.4049/jimmunol.1800633.

López-Otín, C. *et al.* (2013) 'The hallmarks of aging.', *Cell*, 153(6), pp. 1194–217. doi: 10.1016/j.cell.2013.05.039.

Lorenz, H. *et al.* (2006) 'The fluorescence protease protection (FPP) assay to determine protein localization and membrane topology.', *Nature Protocols*, 1(1), pp. 276–279. doi: 10.1038/nprot.2006.42.

Ma, B. and Hottiger, M. O. (2016) 'Crosstalk between Wnt/β-Catenin and NF-κB Signaling Pathway during Inflammation.', *Frontiers in immunology*, 7, p. 378. doi: 10.3389/fimmu.2016.00378.

Ma, J. *et al.* (2011) 'Critical role of TCF-1 in repression of the IL-17 gene.', *PloS one*, 6(9), p. e24768. doi: 10.1371/journal.pone.0024768.

Ma, J. *et al.* (2012) 'β-catenin/TCF-1 pathway in T cell development and differentiation.', *Journal of neuroimmune pharmacology : the official journal of the Society on NeuroImmune Pharmacology*, 7(4), pp. 750–62. doi: 10.1007/s11481-012-9367-y.

MacDonald, B. T. and He, X. (2012) 'Frizzled and LRP5/6 receptors for Wnt/β-catenin signaling.', *Cold Spring Harbor perspectives in biology*, 4(12). doi: 10.1101/cshperspect.a007880.

Macian, F. (2005) 'NFAT proteins: key regulators of T-cell development and function.', *Nature reviews. Immunology*, 5(June), pp. 472–484. doi: 10.1038/nri1632.

Malladi, S. *et al.* (2016) 'Metastatic Latency and Immune Evasion through Autocrine Inhibition of WNT.', *Cell*, 165(1), pp. 45–60. doi: 10.1016/j.cell.2016.02.025.

Mami-Chouaib, F. and Tartour, E. (2019) 'Editorial: Tissue Resident Memory T Cells.', *Frontiers in immunology*, 10, p. 1018. doi: 10.3389/fimmu.2019.01018.

Martin, J., Afouda, B. A. and Hoppler, S. (2010) 'Wnt/beta-catenin signalling regulates cardiomyogenesis via GATA transcription factors.', *Journal of anatomy*, 216(1), pp. 92–107. doi: 10.1111/j.1469-7580.2009.01171.x.

Maslen, C. L. *et al.* (2006) 'CRELD2: gene mapping, alternate splicing, and comparative genomic identification of the promoter region.', *Gene*, 382, pp. 111–20. doi: 10.1016/j.gene.2006.06.016.

Mass, E. *et al.* (2014) 'Murine Creld1 Controls Cardiac Development through Activation of Calcineurin / NFATc1 Signaling Mass Figure S1', *Developmental Cell*, 28, pp. 711–726. doi: 10.1016/j.devcel.2014.02.012.

Matsumoto, K. and Ema, M. (2014) 'Roles of VEGF-A signalling in development, regeneration, and tumours.', *Journal of biochemistry*, 156(1), pp. 1–10. doi: 10.1093/jb/mvu031.

Meikle, P. J. and Summers, S. A. (2017) 'Sphingolipids and phospholipids in insulin resistance and related metabolic disorders.', *Nature reviews. Endocrinology*, 13(2), pp. 79–91. doi: 10.1038/nrendo.2016.169.

Menk, A. V *et al.* (2018) 'Early TCR Signaling Induces Rapid Aerobic Glycolysis Enabling Distinct Acute T Cell Effector Functions.', *Cell reports*, 22(6), pp. 1509–1521. doi: 10.1016/j.celrep.2018.01.040.

Merkenschlager, M. *et al.* (1997) 'How many thymocytes audition for selection?', *The Journal of experimental medicine*, 186(7), pp. 1149–58. doi: 10.1084/jem.186.7.1149.

Meyer Zu Horste, G. *et al.* (2018) 'Fas Promotes T Helper 17 Cell Differentiation and Inhibits T Helper 1 Cell Development by Binding and Sequestering Transcription Factor STAT1.', *Immunity*. Elsevier Inc., 48(3), p. 556–569.e7. doi: 10.1016/j.immuni.2018.03.008.

Miyamoto, T. *et al.* (2002) 'Myeloid or lymphoid promiscuity as a critical step in hematopoietic lineage commitment.', *Developmental cell*, 3(1), pp. 137–47. Available at: http://www.ncbi.nlm.nih.gov/pubmed/12110174.

Momozawa, Y. *et al.* (2018) 'IBD risk loci are enriched in multigenic regulatory modules encompassing putative causative genes.', *Nature communications*, 9(1), p. 2427. doi: 10.1038/s41467-018-04365-8.

Monticelli, S. and Rao, A. (2002) 'NFAT1 and NFAT2 are positive regulators of IL-4 gene transcription.', *European journal of immunology*, 32(10), pp. 2971–8. doi: 10.1002/1521-4141(2002010)32:10<2971::AID-IMMU2971>3.0.CO;2-G.

Mukai, T., Fujita, S. and Morita, Y. (2019) 'Tankyrase (PARP5) Inhibition Induces Bone Loss through Accumulation of Its Substrate SH3BP2.', *Cells*, 8(2). doi: 10.3390/cells8020195.

Murphy, K. & Weaver, C. (2016) *Janeway's Immunobiology,*. 9th editio. Garland Science.

Naito, T. *et al.* (2011) 'Transcriptional control of T-cell development.', *International immunology*, 23(11), pp. 661–8. doi: 10.1093/intimm/dxr078.

Narita, M. and Lowe, S. W. (2005) 'Senescence comes of age.', *Nature medicine*, 11(9), pp. 920–2. doi: 10.1038/nm0905-920.

Netea, M. G. *et al.* (2016) 'Trained immunity: A program of innate immune memory in health and disease.', *Science (New York, N.Y.)*, 352(6284), p. aaf1098. doi: 10.1126/science.aaf1098.

Netea, M. G. and van der Meer, J. W. M. (2017) 'Trained Immunity: An Ancient Way of Remembering.', *Cell host & microbe*, 21(3), pp. 297–300. doi: 10.1016/j.chom.2017.02.003.

Nguyen, V., Mendelsohn, A. and Larrick, J. W. (2017) 'Interleukin-7 and Immunosenescence.', *Journal of immunology research*, 2017, p. 4807853. doi: 10.1155/2017/4807853.

Niccoli, T. and Partridge, L. (2012) 'Ageing as a risk factor for disease.', *Current biology : CB*, 22(17), pp. R741-52. doi: 10.1016/j.cub.2012.07.024.

Nikolich-Žugich, J. (2014) 'Aging of the T cell compartment in mice and humans: from no naive expectations to foggy memories.', *Journal of immunology (Baltimore, Md. : 1950)*, 193(6), pp. 2622–9. doi: 10.4049/jimmunol.1401174.

Nikolich-Žugich, J. (2018) 'The twilight of immunity: emerging concepts in aging of the immune system.', *Nature immunology*, 19(1), pp. 10–19. doi: 10.1038/s41590-017-0006-x.

Noguchi, T. *et al.* (2017) 'Temporally Distinct PD-L1 Expression by Tumor and Host Cells Contributes to Immune Escape.', *Cancer immunology research*, 5(2), pp. 106–117. doi: 10.1158/2326-6066.CIR-16-0391.

Notani, D. *et al.* (2010) 'Global regulator SATB1 recruits beta-catenin and regulates T(H)2 differentiation in Wnt-dependent manner.', *PLoS biology*, 8(1), p. e1000296. doi:

10.1371/journal.pbio.1000296.

Nusse, R. and Clevers, H. (2017) 'Wnt/β-Catenin Signaling, Disease, and Emerging Therapeutic Modalities.', *Cell*, 169(6), pp. 985–999. doi: 10.1016/j.cell.2017.05.016.

Nusse, R. and Varmus, H. E. (1982) 'Many tumors induced by the mouse mammary tumor virus contain a provirus integrated in the same region of the host genome.', *Cell*, 31(1), pp. 99–109. Available at: http://www.ncbi.nlm.nih.gov/pubmed/6297757.

Nutt, S. L. *et al.* (2015) 'The generation of antibody-secreting plasma cells.', *Nature reviews. Immunology*, 15(3), pp. 160–71. doi: 10.1038/nri3795.

O'Sullivan, T. E., Sun, J. C. and Lanier, L. L. (2015) 'Natural Killer Cell Memory.', *Immunity*, 43(4), pp. 634–45. doi: 10.1016/j.immuni.2015.09.013.

Okamura, H. *et al.* (2000) 'Concerted dephosphorylation of the transcription factor NFAT1 induces a conformational switch that regulates transcriptional activity.', *Molecular cell*, 6(3), pp. 539–50. Available at: http://www.ncbi.nlm.nih.gov/pubmed/11030334.

Ongrádi, J. *et al.* (2009) 'Immunosenescence and vaccination of the elderly, I. Age-related immune impairment.', *Acta microbiologica et immunologica Hungarica*, 56(3), pp. 199–210. doi: 10.1556/AMicr.56.2009.3.1.

Oukka, M. *et al.* (1998) 'The transcription factor NFAT4 is involved in the generation and survival of T cells', *Immunity*, 9(3), pp. 295–304. doi: 10.1016/S1074-7613(00)80612-3.

Pachulec, E., Neitzke-Montinelli, V. and Viola, J. P. B. (2016) 'NFAT2 Regulates Generation of Innate-Like CD8+ T Lymphocytes and CD8+ T Lymphocytes Responses.', *Frontiers in immunology*, 7, p. 411. doi: 10.3389/fimmu.2016.00411.

Pawelec, G. *et al.* (2009) 'Impact of aging on cancer immunity and immunotherapy.', *Cancer immunology, immunotherapy : CII*, 58(12), pp. 1907–8. Available at: http://www.ncbi.nlm.nih.gov/pubmed/19787858.

Pawelec, G. (2017) 'Immunosenescence and cancer.', *Biogerontology*, 18(4), pp. 717–721. doi: 10.1007/s10522-017-9682-z.

Pawelec, G. (2018) 'Age and immunity: What is "immunosenescence"?', *Experimental gerontology*, 105, pp. 4–9. doi: 10.1016/j.exger.2017.10.024.

Peng, S. *et al.* (2001) 'NFATc1 and NFATc2 together control both T and B cell activation and differentiation', *Immunity*, 14(1), pp. 13–20. doi: 10.1016/S1074-7613(01)00085-1.

Pollak, M. (2008) 'Insulin and insulin-like growth factor signalling in neoplasia.', *Nature reviews. Cancer*, 8(12), pp. 915–28. doi: 10.1038/nrc2536.

Posch, M. G. *et al.* (2008) 'Are Infrequently Found in Patients With Congenital Cardiac Septal Defects', 253, pp. 251–253. doi: 10.1002/ajmg.a.

Pui, J. C. *et al.* (1999) 'Notch1 expression in early lymphopoiesis influences B versus T lineage determination.', *Immunity*, 11(3), pp. 299–308. Available at: http://www.ncbi.nlm.nih.gov/pubmed/10514008.

Qu, J. *et al.* (2019) 'Perspectives on Wnt Signal Pathway in the Pathogenesis and Therapeutics of Chronic Obstructive Pulmonary Disease.', *The Journal of pharmacology and experimental therapeutics*, 369(3), pp. 473–480. doi: 10.1124/jpet.118.256222.

Querfurth, H. W. and LaFerla, F. M. (2010) 'Alzheimer's disease.', *The New England journal of medicine*, 362(4), pp. 329–44. doi: 10.1056/NEJMra0909142.

Raisz, L. G. (1988) 'Local and systemic factors in the pathogenesis of osteoporosis.', *The*

New England journal of medicine, 318(13), pp. 818–28. doi: 10.1056/NEJM198803313181305.

Ranger, a M. *et al.* (1998) 'Inhibitory function of two NFAT family members in lymphoid homeostasis and Th2 development.', *Immunity*, 9, pp. 627–635. doi: 10.1016/S1074-7613(00)80660-3.

Ranger, A. M. *et al.* (1998) 'Delayed lymphoid repopulation with defects in IL-4-driven responses produced by inactivation of NF-ATc', *Immunity*, 8(1), pp. 125–134. doi: 10.1016/S1074-7613(00)80465-3.

Ranger, A. M. *et al.* (1998) 'The transcription factor NF-ATc is essential for cardiac valve formation.', *Nature*, 392(6672), pp. 186–90. doi: 10.1038/32426.

Rengarajan, J., Tang, B. and Glimcher, L. H. (2002) 'NFATc2 and NFATc3 regulate T(H)2 differentiation and modulate TCR-responsiveness of naïve T(H)cells.', *Nature immunology*, 3(1), pp. 48–54. doi: 10.1038/ni744.

Robey, E. and Fowlkes, B. J. (1994) 'Selective events in T cell development.', *Annual review of immunology*, 12, pp. 675–705. doi: 10.1146/annurev.iy.12.040194.003331.

Robinson, S. W. *et al.* (2003) 'Missense mutations in CRELD1 are associated with cardiac atrioventricular septal defects.', *American journal of human genetics*, 72(4), pp. 1047–52. doi: 10.1086/374319.

Rothenberg, E. V (2014) 'Transcriptional control of early T and B cell developmental choices.', *Annual review of immunology*, 32, pp. 283–321. doi: 10.1146/annurev-immunol-032712-100024.

Rowshanravan, B., Halliday, N. and Sansom, D. M. (2018) 'CTLA-4: a moving target in immunotherapy.', *Blood*, 131(1), pp. 58–67. doi: 10.1182/blood-2017-06-741033.

Rupp, P. a. *et al.* (2002) 'Identification, genomic organization and mRNA expression of CRELD1, the founding member of a unique family of matricellular proteins', *Gene*, 293, pp. 47–57. doi: 10.1016/S0378-1119(02)00696-0.

Schilham, M. W. *et al.* (1998) 'Critical involvement of Tcf-1 in expansion of thymocytes.', *Journal of immunology (Baltimore, Md. : 1950)*, 161(8), pp. 3984–91. Available at: http://www.ncbi.nlm.nih.gov/pubmed/9780167.

Schmiedel, B. J. *et al.* (2018) 'Impact of Genetic Polymorphisms on Human Immune Cell Gene Expression.', *Cell*, 175(6), p. 1701–1715.e16. doi: 10.1016/j.cell.2018.10.022.

Schreiber, K. *et al.* (2012) 'Spleen cells from young but not old immunized mice eradicate large established cancers.', *Clinical cancer research : an official journal of the American Association for Cancer Research*, 18(9), pp. 2526–33. doi: 10.1158/1078-0432.CCR-12-0127.

Shaw, J. P. *et al.* (1988) 'Identification of a putative regulator of early T cell activation genes.', *Science (New York, N.Y.)*, 241(4862), pp. 202–5. doi: 10.1126/science.3260404.

Shim, J. W. and Madsen, J. R. (2018) 'VEGF Signaling in Neurological Disorders.', *International journal of molecular sciences*, 19(1). doi: 10.3390/ijms19010275.

Shukla, U. *et al.* (2009) 'Tyrosine phosphorylation of 3BP2 regulates B cell receptor-mediated activation of NFAT.', *The Journal of biological chemistry*, 284(49), pp. 33719–28. doi: 10.1074/jbc.M109.049999.

De Silva, N. S. and Klein, U. (2015) 'Dynamics of B cells in germinal centres.', *Nature reviews. Immunology*, 15(3), pp. 137–48. doi: 10.1038/nri3804.

Sprent, J. and Surh, C. D. (2011) 'Normal T cell homeostasis: the conversion of naive cells into memory-phenotype cells.', *Nature immunology*, 12(6), pp. 478–84. doi: 10.1038/ni.2018.

Staal, F. J. *et al.* (2001) 'Wnt signaling is required for thymocyte development and activates Tcf-1 mediated transcription.', *European journal of immunology*, 31(1), pp. 285–93. doi: 10.1002/1521-4141(200101)31:1<285::AID-IMMU285>3.0.CO;2-D.

Staal, F. J. T., Luis, T. C. and Tiemessen, M. M. (2008) 'WNT signalling in the immune system: WNT is spreading its wings.', *Nature reviews. Immunology*, 8(8), pp. 581–93. doi: 10.1038/nri2360.

Steinke, F. C. *et al.* (2014) 'TCF-1 and LEF-1 act upstream of Th-POK to promote the CD4(+) T cell fate and interact with Runx3 to silence Cd4 in CD8(+) T cells.', *Nature immunology*, 15(7), pp. 646–656. doi: 10.1038/ni.2897.

Su, D.-M., Aw, D. and Palmer, D. B. (2013) 'Immunosenescence: a product of the environment?', *Current opinion in immunology*, 25(4), pp. 498–503. doi: 10.1016/j.coi.2013.05.018.

Takaba, H. and Takayanagi, H. (2017) 'The Mechanisms of T Cell Selection in the Thymus.', *Trends in immunology*, 38(11), pp. 805–816. doi: 10.1016/j.it.2017.07.010.

Takeuchi, O. and Akira, S. (2010) 'Pattern recognition receptors and inflammation.', *Cell*, 140(6), pp. 805–20. doi: 10.1016/j.cell.2010.01.022.

Tang, H. *et al.* (2019) 'SDF-1/CXCR4 induces epithelial-mesenchymal transition through activation of the Wnt/β-catenin signaling pathway in rat chronic allograft nephropathy.', *Molecular medicine reports*, 19(5), pp. 3696–3706. doi: 10.3892/mmr.2019.10045.

Teh, H. S. *et al.* (1988) 'Thymic major histocompatibility complex antigens and the alpha beta T-cell receptor determine the CD4/CD8 phenotype of T cells.', *Nature*, 335(6187), pp. 229–33. doi: 10.1038/335229a0.

Thrasivoulou, C., Millar, M. and Ahmed, A. (2013) 'Activation of intracellular calcium by multiple Wnt ligands and translocation of β-catenin into the nucleus: A convergent model of Wnt/Ca2+and Wnt/β-catenin pathways', *Journal of Biological Chemistry*, 288(50), pp. 35651–35659. doi: 10.1074/jbc.M112.437913.

Tran, F. H. and Zheng, J. J. (2017) 'Modulating the wnt signaling pathway with small molecules.', *Protein science : a publication of the Protein Society*, 26(4), pp. 650–661. doi: 10.1002/pro.3122.

Truong, A. *et al.* (2016) 'Dynamics of internalization and recycling of the prometastatic membrane type 4 matrix metalloproteinase (MT4-MMP) in breast cancer cells.', *The FEBS journal*, 283(4), pp. 704–22. doi: 10.1111/febs.13625.

Tung, E. K.-K. *et al.* (2012) 'Upregulation of the Wnt co-receptor LRP6 promotes hepatocarcinogenesis and enhances cell invasion.', *PloS one*, 7(5), p. e36565. doi: 10.1371/journal.pone.0036565.

Uekita, T. *et al.* (2001) 'Cytoplasmic tail-dependent internalization of membrane-type 1 matrix metalloproteinase is important for its invasion-promoting activity.', *The Journal of cell biology*, 155(7), pp. 1345–56. doi: 10.1083/jcb.200108112.

Ushach, I. and Zlotnik, A. (2016) 'Biological role of granulocyte macrophage colony-stimulating factor (GM-CSF) and macrophage colony-stimulating factor (M-CSF) on cells of the myeloid lineage.', *Journal of leukocyte biology*, 100(3), pp. 481–9. doi: 10.1189/jlb.3RU0316-144R.

Ventura, M. T. *et al.* (2017) 'Immunosenescence in aging: between immune cells depletion

and cytokines up-regulation.', *Clinical and molecular allergy : CMA*, 15, p. 21. doi: 10.1186/s12948-017-0077-0.

Voorneveld, P. W. *et al.* (2015) 'The BMP pathway either enhances or inhibits the Wnt pathway depending on the SMAD4 and p53 status in CRC.', *British journal of cancer*, 112(1), pp. 122–30. doi: 10.1038/bjc.2014.560.

Weiskopf, K. *et al.* (2016) 'Myeloid Cell Origins, Differentiation, and Clinical Implications.', *Microbiology spectrum*, 4(5). doi: 10.1128/microbiolspec.MCHD-0031-2016.

Wertheimer, A. M. *et al.* (2014) 'Aging and cytomegalovirus infection differentially and jointly affect distinct circulating T cell subsets in humans.', *Journal of immunology (Baltimore, Md. : 1950)*, 192(5), pp. 2143–55. doi: 10.4049/jimmunol.1301721.

Wiehagen, K. R. *et al.* (2010) 'Loss of tonic T-cell receptor signals alters the generation but not the persistence of CD8+ memory T cells.', *Blood*, 116(25), pp. 5560–70. doi: 10.1182/blood-2010-06-292458.

Xanthoudakis, S. *et al.* (1996) 'An enhanced immune response in mice lacking the transcription factor NFAT1.', *Science (New York, N.Y.)*, 272(May), pp. 892–895.

Xia, S. *et al.* (2016) 'An Update on Inflamm-Aging: Mechanisms, Prevention, and Treatment.', *Journal of immunology research*, 2016, p. 8426874. doi: 10.1155/2016/8426874.

Xu, Y. *et al.* (2003) 'Deletion of beta-catenin impairs T cell development.', *Nature immunology*, 4(12), pp. 1177–82. doi: 10.1038/ni1008.

Yang, Y. and Mlodzik, M. (2015) 'Wnt-Frizzled/planar cell polarity signaling: cellular orientation by facing the wind (Wnt).', *Annual review of cell and developmental biology*, 31, pp. 623–46. doi: 10.1146/annurev-cellbio-100814-125315.

Ye, X. *et al.* (2007) 'Downregulation of Wnt signaling is a trigger for formation of facultative heterochromatin and onset of cell senescence in primary human cells.', *Molecular cell*, 27(2), pp. 183–96. doi: 10.1016/j.molcel.2007.05.034.

Yoshida, H. *et al.* (1998) 'The transcription factor NF-ATc1 regulates lymphocyte proliferation and Th2 cytokine production.', *Immunity*, 8(1), pp. 115–24. doi: 10.1016/S1074-7613(00)80464-1.

Yu, Q. *et al.* (2009) 'T cell factor 1 initiates the T helper type 2 fate by inducing the transcription factor GATA-3 and repressing interferon-gamma.', *Nature immunology*, 10(9), pp. 992–9. doi: 10.1038/ni.1762.

Yu, Q. *et al.* (2011) 'T cell factor-1 negatively regulates expression of IL-17 family of cytokines and protects mice from experimental autoimmune encephalomyelitis.', *Journal of immunology (Baltimore, Md. : 1950)*, 186(7), pp. 3946–52. doi: 10.4049/jimmunol.1003497.

Yu, S. *et al.* (2012) 'The TCF-1 and LEF-1 transcription factors have cooperative and opposing roles in T cell development and malignancy.', *Immunity*. Elsevier Inc., 37(5), pp. 813–26. doi: 10.1016/j.immuni.2012.08.009.

Zanoni, I. *et al.* (2009) 'CD14 regulates the dendritic cell life cycle after LPS exposure through NFAT activation.', *Nature*, 460(7252), pp. 264–8. doi: 10.1038/nature08118.

Zatyka, M. *et al.* (2005) 'Analysis of CRELD1 as a candidate 3p25 atrioventicular septal defect locus (AVSD2).', *Clinical genetics*, 67(6), pp. 526–8. doi: 10.1111/j.1399-0004.2005.00435.x.

Zeng, F. and Harris, R. C. (2014) 'Epidermal growth factor, from gene organization to bedside.', *Seminars in cell & developmental biology*, 28, pp. 2–11. doi:

10.1016/j.semcdb.2014.01.011.

Zerrahn, J., Held, W. and Raulet, D. H. (1997) 'The MHC reactivity of the T cell repertoire prior to positive and negative selection.', *Cell*, 88(5), pp. 627–36. doi: 10.1016/s0092-8674(00)81905-4.

Zhan, T., Rindtorff, N. and Boutros, M. (2017) 'Wnt signaling in cancer.', *Oncogene*, 36(11), pp. 1461–1473. doi: 10.1038/onc.2016.304.

Zhang, Y. *et al.* (2018) 'Hematopoietic Hierarchy - An Updated Roadmap.', *Trends in cell biology*, 28(12), pp. 976–986. doi: 10.1016/j.tcb.2018.06.001.

Zhao, Y. *et al.* (2016) 'Armc8 regulates the invasive ability of hepatocellular carcinoma through E-cadherin/catenin complex.', *Tumour biology : the journal of the International Society for Oncodevelopmental Biology and Medicine*, 37(8), pp. 11219–24. doi: 10.1007/s13277-016-5006-1.

Zhian, S., Belmont, J. and Maslen, C. L. (2012) 'Specific association of missense mutations in CRELD1 with cardiac atrioventricular septal defects in heterotaxy syndrome', *American Journal of Medical Genetics, Part A*, 158 A(8), pp. 2047–2049. doi: 10.1002/ajmg.a.35457.

Zhu, J. and Paul, W. E. (2008) 'CD4 T cells: fates, functions, and faults.', *Blood*, 112(5), pp. 1557–69. doi: 10.1182/blood-2008-05-078154.

Zook, E. C. and Kee, B. L. (2016) 'Development of innate lymphoid cells.', *Nature immunology*, 17(7), pp. 775–82. doi: 10.1038/ni.3481.